博士論文

Study of the active species and effect of CO_2 bubbling in the electrochemical reduction of CO_2 in aqueous solutions

（水溶液中の二酸化炭素の電気化学還元における二酸化炭素通気の影響と化学的活性種に関する研究）

鍾　恒 (しょう　はん)

博士論文

Study of the active species and effect of CO_2 bubbling in the electrochemical reduction of CO_2 in aqueous solutions

（水溶液中の二酸化炭素の電気化学還元における二酸化炭素通気の影響と化学的活性種に関する研究）

A dissertation submitted to the Graduated School of Engineering
The University of Tokyo
in partial fulfillment of the requirements for the degree of
Doctor of Philosophy

鍾　恒

Heng Zhong

Under the supervision of
Professor Dr. Katsushi Fujii
Professor Dr. Yoshiaki Nakano

March 2015

Acknowledgements

I still remember clearly the first day I came to the University of Tokyo to take the entrance exam. But now, 3 years have passed, and I will soon finish my phD study. Looking back at these three years, I received so many kind helps and advices not only during my research but also during my life living in Japan. I can hardly finish this dissertation without their kind helps. Here, I would like to acknowledge all the people those who helped me during my studying in Tokyo.

First and foremost, I would like to express my gratitude to my supervisor Professor Katsushi Fujii, who gave me great support and guidance during my phD study. I can always obtain excellent ideas and understand my research results more profoundly after discussion with Professor Fujii. I would also like to sincerely appreciate another supervisor of mine, Professor Yoshiaki Nakano, who accepted me as a phD student in his lab and provided me with excellent experiment equipments to carry out my research. Without their kind help and support, I could not have this precious opportunity to study in the University of Tokyo, let along finishing my phD dissertation.

I want to convey my appreciation to Associate Professor Masakazu Sugiyama who gave me lots of extraordinary advices to improve my research, doctoral dissertation, and presentation. I also want to thank Associate Professor Takuo Tanemura and Assistant Professor Kentarou Watanabe for their suggestion to my research.

I sincerely appreciate Professor Fangming Jin from Shanghai Jiao Tong University in China, who let me carry out my experiments in her lab and gave me wonderful suggestions. I also want to thank Dr. Guodong Yao and Dr. Jun Yun from Professor Jin's lab for their kind help with my experiments during my staying in Professor Jin's lab.

I would like to thank Professor Tetsu Tatsuma from IIS of the University of Tokyo and Professor Takaya Kubo from RCAST of the University of Tokyo for reviewing this dissertation and suggesting great advices to improve this dissertation.

Thanks to Dr. Cai Liu, Yuxiao Zeng from Nakano-lab for helping me settle down in Tokyo when I first came here. I would like to thank Akihiro Nakamura, Yuya Taki, Kayo Koike, and Futami Sano for teaching me how to use the experimental instruments, and all the

Abstract

Solar energy is regarded as one of the most promising renewable energies to replace the fossil fuels in the 21st century. However, the solar energy is not stable and not available at night. Therefore, energy conversion, storage and transportation systems are needed for better utilizing the solar energy. Photoelectrochemical and electrochemical CO_2 reduction combining with solar energy to produce hydrocarbons and other organic chemicals, such as CH_3OH and $HCOOH$, are promising ways to transform and store solar energy into chemical energy. In these methods, CO_2 bubbling into the aqueous electrolytes ($KHCO_3$, KCl, etc.) is used and generally regarded as the active species. Since CO_2 can react with water to generate H_2CO_3, which further decomposes into HCO_3^- and CO_3^{2-}, the effect of CO_2 bubbling on the electrolyte and CO_2 reduction needs to be studied. Meanwhile, in the electrochemical reduction of $KHCO_3$ without CO_2 bubbling, formation of $HCOOH$ was reported. However, both CO_2 and HCO_3^- were reported as the active species for the $HCOOH$ production. The real active species is still not clear. Therefore, the active species in the electrochemical reduction of $KHCO_3$ and the effect of CO_2 bubbling in different solutions were studied and presented in this dissertation.

This dissertation is divided into 7 chapters, and the details are as follow:

Chap 1 is the general introduction. The background of the solar energy conversion, storage and transportation were first presented. Then, technologies and previous reports of electrochemical reduction of CO_2 in aqueous solutions were introduced. Finally, the motivations and objects of this research were given, which included investigating the active species and effect of CO_2 bubbling in the electrochemical reduction of CO_2 in aqueous solutions.

Chap 2 is the experimental section, in which the electrochemical cells, experimental setups, experimental materials and procedures, and analysis methods were presented.

Chap 3 studied the electrochemical reduction of $NaHCO_3$ and $KHCO_3$ without CO_2 bubbling using I-V measurement (products analysis is discussed in Chap 4). Voltammograms were obtained at various $NaHCO_3$ and/or $KHCO_3$ concentrations, and different temperatures on Cu working electrode. Reasons for why current density was increased by the high

temperature and high HCO_3^- concentration were also thermodynamically studied.

Chap 4 analyzed the products in the electrochemical reduction of $KHCO_3$ without CO_2 bubbling and studied the active species in this reaction. Results showed that H_2 was the main products (over 90%) after 1 hour's reaction. The current increase caused by the high concentration of HCO_3^- and elevated temperature was mainly contributed by the H_2 evolution. However, the CO, CH_4 and C_2H_4 were also detected in the gas products, which had not been reported before. After examining the decomposition of HCO_3^-, results revealed that high concentration and elevated temperature strongly promoted the decomposition of the HCO_3^- into CO_2. The active species in the electrochemical reduction of $KHCO_3$ is probably the CO_2 rather than the HCO_3^-. The chemical reaction pathway of the decomposition of HCO_3^- into CO_2 was also discussed.

Chap 5 studied the electrochemical reduction of CO_2 in different electrolytes ($KHCO_3$, KCl, and KOH) under CO_2 bubbling at various conditions. The effects of CO_2 bubbling, temperature, electrolyte, applied potential, reaction time, stirring, and geometrical shape of the working electrode on the faradaic efficiency of CO_2 reduction were investigated. Results showed that the HCO_3^- concentration and the applied potential strongly affected the CO_2 reduction and product selectivity. Lower concentration (0.1 mol/L) of HCO_3^- had better performance for the CO_2 reduction than higher concentrations (0.5, 1.0, and 1.5 mol/L). The best faradaic efficiency of CO_2 reduction of 55.1% was obtained in 0.1 mol/L $KHCO_3$ at applied potential of -2.1 V (vs Ag/AgCl) on a Cu wire working electrode.

Chap 6 examined the effect of CO_2 bubbling into different solutions ($KHCO_3$, KCl, KOH, K_2CO_3 etc.) by measuring the pH changes and total carbon concentrations. The concentrations of different carbonaceous species (CO_2, H_2CO_3, HCO_3^-, CO_3^{2-}) in these solutions before and after bubbling with CO_2 were calculated according to the experimental data. Results showed that much higher ratio of dissolved CO_2 to total dissolved carbon ($[H_2CO_3^*]$/TC) was contained in 0.1 mol/L $KHCO_3$ (23.6%) than that in 1.5 mol/L $KHCO_3$ (2.8%), which possibly promoted the CO_2 reduction.

Chap 7 summarized the results above and discussed the progresses made in this dissertation. The limitations in this dissertation and suggestions to the future works were also given in chapter 7.

Contents

Chapter 1

Introduction

1.1 Background

1.1.1 Energy crisis

Human beings have used the fossil fuels as the major energy source for over 300 years since the industrial revolution. Human society becomes more and more relying on the fossil fuels for its developing. Fig. 1.1 shows the composition of world energy consumption in 2013 by energy source (data from ref [1]). It can be seen that fossil fuels (including petroleum, natural gas and coal) contributed up to 86% of the world's total annual energy consumption in 2013. The fossil fuels formed by the anaerobic decomposition of buried ancient organisms contain so high energy density that strongly promoted the developing of human civilization. Meanwhile, fossil fuels especially for petroleum are crucial raw materials for making many important chemicals, such as pesticides, pharmaceuticals, solvents, fertilizers, and plastics. These chemicals extremely improve the living condition of human society.
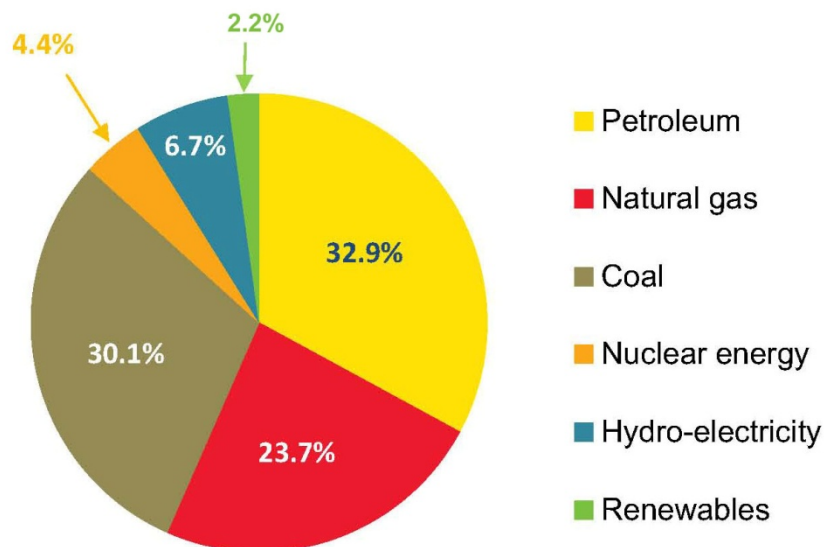
Fig. 1.1 Composition of world annual energy consumption of 2013 by energy source (data source: BP report 2014 [1]).

However, unfortunately, this great boom of human civilization relying on the fossil fuels will not last long. The utilization rate of the fossil fuels is far beyond the generation rate of the fossil fuels. It took millions of years for buried ancient organisms finally became the fossil fuels through complicated and delicate natural process [2]. However, the utilization rate of the fossil fuels by humankind is ten thousand times faster than their formation rate. Moreover, this utilization rate is keeping rising rapidly. The total world annual energy consumption in 1850 was only about 30 EJ. However, this number greatly increased nearly 18 times to about 530 EJ in 2008 [3]. As a result, the fossil fuels are believed to be soon run out in the next century. It is reported that the global proved storage of petroleum and natural gas can be used for only 53.3 and 55.1 more years, respectively, at current production rate [1]. Situation for coal is a bit better (113 more years), but is still not optimism [1].

1.1.2 Global warming

Since fossil fuels are organic materials, the main products for combusting fossil fuels are carbon dioxide (CO_2) and water (H_2O). As huge amount of fossil fuels are combusted by human being to supply energies, large quantities CO_2 have been released to the atmosphere, which severely destroy the natural carbon cycle [4,5]. Approximately 960kg/MWh of CO_2 emitted during the generation of electricity from coal fired power plants [6]. As a result, the concentration of CO_2 in the atmosphere increased sharply from ca. 280 ppm in 18th century to nearly 400 ppm in the 21st century as shown in Fig. 1.2 [7]. CO_2, as well as CH_4, N_2O, H_2O and O_3, are known as the greenhouse gas (GHG) which absorb and emit radiation within the thermal infrared range and hence affect the temperature of the earth. As the concentration of atmospheric CO_2 increasing, the earth is gradually warming up due to the greenhouse gas keep the heat from discharging. This process is known as the greenhouse effect. It is reported that the annual average temperature of the earth increased about 0.5 ^{o}C during the last 50 years [8]. The global warming caused by the increasing atmospheric CO_2 can cause a series of serious environmental problems, such as iceberg melting, sea level rising, extreme weather frequency and severity increasing, which will greatly affect the ecosystem and/or threaten human existence. Ice reflects solar radiation much more effective than water, therefore, as the

iceberg melting to water caused by the global warming, the trends for earth's temperature rising will become irreversible.
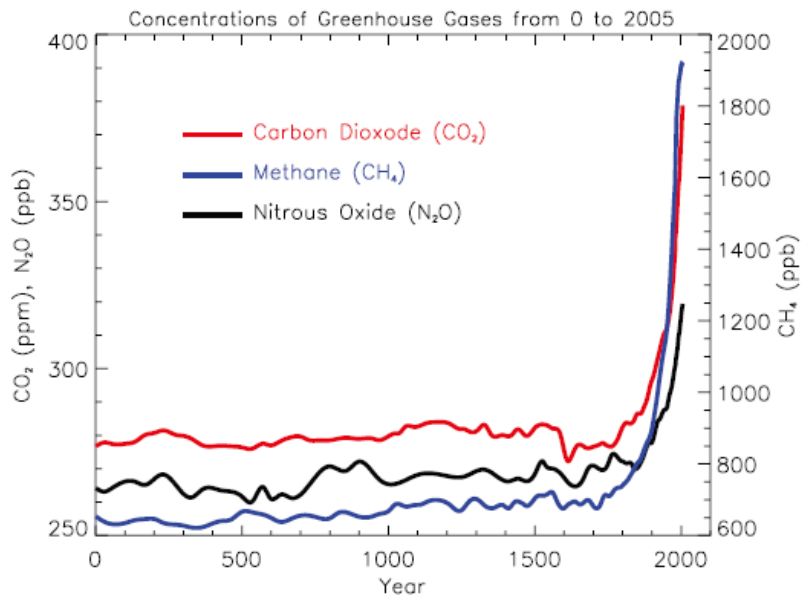
Fig. 1.2 Atmospheric concentrations of important long-lived greenhouse gases over the last 2,000 years (presented by IPCC report 2007 [7]).

1.1.3 Alternative energies

Since the problems of fossil fuels are so serious and urgent, finding alternative sources to replace the fossil fuels to supply not only reliable energy source but also raw materials for chemical synthesis are in urgent need. Renewable energies, such as solar energy, hydropower, wind and biomass, and nuclear energy are two possible selections.

1.1.3.1 **Nuclear energy**

Nuclear energy uses the exothermic nuclear process to generate useful heat and electricity [9,10]. The utilization of nuclear energy to generate electricity begun in the middle

of 20th century and then has been used worldwide now [11]. The extraordinarily high energy density of nuclear fuel makes it able to satisfy the energy requirement of human society. The CO_2 emission from a nuclear power plant is lower than the traditional fossil fuels plants by two orders of magnitude [9]. It can be seen in Fig. 1.1 that nuclear energy contributed 4.4% of the total world energy consumption in 2013. However, it is still not high. The safety, Uranium reserves, and the management of nuclear waste are typical problems that limit the utilization of nuclear energy. Therefore, there is still a long way to go for a better utilization of the nuclear energy.

1.1.3.2 **Renewable energy**

Renewable energy, which can be naturally replenished on a human time scale, is one of the most potential ways to replace the fossil fuels. Typical renewable energy includes solar, biomass, wind, geothermal, hydropower and tide *etc*.

Biomass has been used as the energy source by human beings for a very long time in the human history since we learnt how to use fire. Combustion biomass such as woods provided our ancient ancestors with heat, helped avoiding from danger and finally made the human civilization thrive on the earth. Modern methods transform the biomass into value added biofuels, such as biohydrogen, bioethanol, biomethanol and fatty acid (m)ethylester, *etc*, using thermochemical and biochemical conversion technologies to generate not only heat but also electricity [12-14]. Advantages for biomass derived energy includes: (1) easily available from common biomass source; (2) bio-fuels are potentially environmental friendly; (3) biodegradable and sustainable. However, the problem of CO_2 emission through the combustion of biofuels still exists. Furthermore, most of the traditional biofuels such as bioethanol and biodiesel are produced from agricultural food crops such as corn, wheat and sugar seeds which demand high-quality agricultural lands for growing [12]. The production of biofuels from such food crops might cause the world food crisis more severe, especially in poor countries.

Hydropower derived from the falling and/or running water is mainly used for electricity generating. Hydropower energy is the most widely used renewable energy nowadays. As shown in Fig. 1.1, the hydro-electricity constituted 6.7% of the world total energy

consumption in 2013, which is more than three times than the sum of other renewable energies. However, the environmental problems caused by the hydro-electricity generation should be taken into account carefully. Constraint in a river system will lead to multiple modifications of its metabolism and its environmental fabric [15]. Sediment generation and local precipitation pattern changing caused by the hydro-electricity generation system, especially for a large scale, are critical problems which are still not easy to predict precisely so far [15,16]. Since most of world biggest rivers run across multi countries, the geopolitical contention is another intractable issue. Most importantly, it is reported that the world's hydropower available in readily accessible locations is only 2TW [17]. The world's energy consumption in 2013 was 41.1 TW [1], which is far beyond the total capacity of hydropower. Therefore, other renewable energies should be considered for a 100% replacing fossil fuels.

Wind power mainly indicates using wind energy extracted from wind using wind turbines to generate electricity. Wind power is the largest developed and commercially used renewable energies except hydro-power, which hold about 60% of the world renewable power capacities except hydro-power [6,18]. The utilization of wind power divided into onshore and offshore according to its location. The onshore wind farm is usually restricted by land availability. Wind turbine noise and their visual impact on the natural environment are main problems for building onshore wind turbines [19]. Offshore wind farm installed at sea has dozens of advantages: (1) more available spaces and fewer effects of the noise and visual intrusion; (2) stronger, smoother and more consistent wind can be obtained [19]. Therefore, offshore wind farm are much more concerned during the developing of wind energy. However, offshore wind turbines are more expensive and difficult to install and maintenance which inevitably increase the cost of the wind power. The capital cost of offshore wind-electricity is around 3760–5870 USD/kW, which is higher than that of rooftop photovoltaics (PV) (2480–3270 USD/kW) and ground-mounted PV (1830–2350 USD/kW) [6]. Therefore, how to decrease the cost is the main problem for further enlarging the utilization of wind energy.

Solar energy is regarded as one of the most promising renewable energy to replace the fossil fuels because of its huge potential resource. The annual energy capacity growing rate of solar energy is the fastest among all the renewable energies [18]. The major solar energy utilization is divided into solar thermal and solar photovoltaics. The utilization of solar

thermal has two categories: (1) solar thermal non-electric and (2) solar thermal electric [20]. Solar thermal non-electric method is mainly used for water heating and space heating and cooling [21,22]. Solar thermal electric technologies use lens or mirrors to concentrate solar heat to produce water steam and then generate electricity. This process is also known as concentrated solar power (CSP). Typical technologies for CSP include Parabolic Trough, Fresnel Mirror, Power Tower and Solar Dish Collector according to different concentrating systems [20]. The capacity of solar hot water (non-electric) utilization was 326 GW in 2013, which is much higher than the capacity CSP (3.4 GW) [23]. The strict requirement for the concentrating system and relatively high cost limited the utilization of CSP. Photovoltaic method converts the solar energy into electricity directly by using the ingenious properties of semiconductors, which is called as photovoltaic effect. Photovoltaic is one of the fastest growing technologies in the world with a growth rate of 35–40% per year [24]. The total solar PV capacity of the world in 2013 was 139 GW, which increased 39% than 2012 [23]. Crystalline silicon-based PV cells and thin film technologies made out of series of different semi-conductors, such as amorphous silicon, cadmium-telluride and copper indium gallium diselenide, are two main PV technologies currently available in market [20].

Fig 1.3 shows the estimated long-term technical and economical potentials of the main renewable energy sources except hydro power. Although the installed total wind power capacity of 2013 was two times higher than the solar PV capacity [23], the estimated available energy potential of solar is much higher than that of wind power (>10 times). The estimated energy potential of wind power at production cost less than 10 ¢/kWh is only 38 PWh/year. However, the total world energy consumption was 148 PWh in 2013 [1], which means wind energy cannot satisfy the energy requirement of human beings. The estimated energy potential of solar power at production cost less than 10 ¢/kWh is 603 PWh/year. This suggests that the energy requirement of human society can be solely satisfied by the solar energy. Therefore, it is crucial to develop solar energy to achieve the human society without fossil fuels.
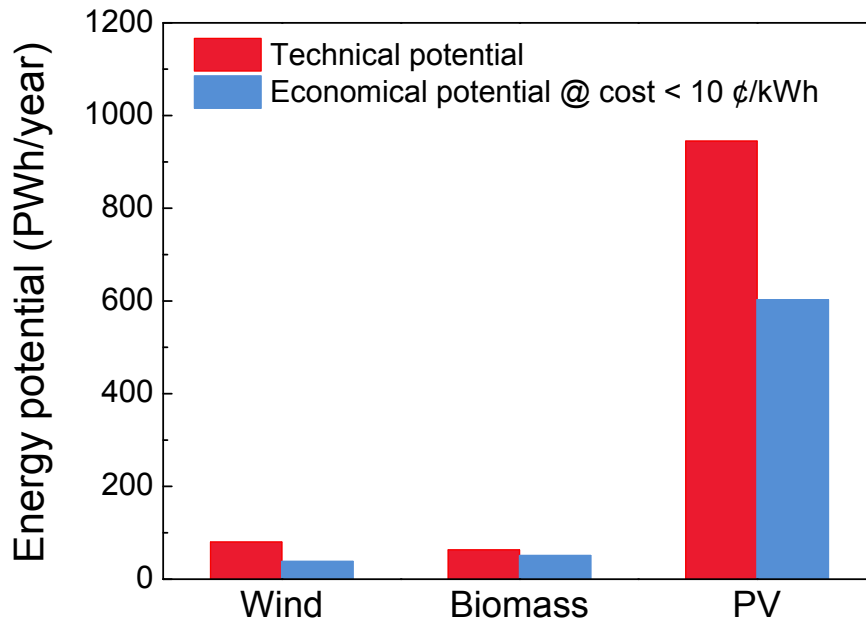
Fig. 1.3 Estimated long-term technical and economical potentials of renewable energy sources (data source: Vries et al. 2007 [25]).

1.2 Solar energy conversion and storage

1.2.1 Necessities of solar energy conversion and storage

Although solar energy is one of the most promising renewable energies to replace the fossil fuels due to its huge potential resource, several innate disadvantages need to be solved for a better utilizing of the solar energy. First, solar energy is only available at daytime without clouds blocking the sunlight. Second, density of solar energy strongly depends on the sun position which is strongly affected by the time and geographic coordinates on earth. The solar energy density fluctuates with time and varies from place to palace. Effective solar irradiance reaching the earth's surface ranges from about 0.06 to 0.25 kW/m^2 at the highest and lowest latitudes, respectively [20]. As a result, the solar energy is mainly concentrated in equatorial area and lack in high latitude areas in north and south hemisphere. However, most of the developed countries which have a large energy requirement lie in the north hemisphere,

where are lack of solar energy. As a result, solar energy conversion, storage and transportation systems are indispensible to stabilize the solar power and make it available at night and areas lack of solar energy

1.2.2 Methods for solar energy conversion and storage in large scale

Mechanical methods. Electricity generated from solar energy can be used to lift water to higher location or compress air by using electromotor. As a result, solar energy is stored into potential energy. So far, most of the electrical energy storages are using mechanical methods. Pumped hydroelectric system accounts for 99 % of a worldwide storage capacity of 127,000 MW of discharge power and compressed air storage with a capacity of 440 MW is a distant second [26]. However, these mechanical methods can only store the electrical energy in a specific location. The issue of energy transportation requires new technologies.

Rechargeable batteries. Using Rechargeable batteries is another promising method for the energy storage and transportation because it is easy to use and can transform and store the electrical energy into a chemical energy with a very high conversion efficiency and can output electricity directly. Typical rechargeable batteries used for large scale energy storage include lead-acid batteries, sodium-sulfur batteries, redox-flow batteries and lithium-ion batteries etc [26,27]. However, the energy density and cost of the rechargeable batteries cannot be satisfied together. A typical lifetime of 10 to 20 years of the battery exists, which lead to an environmental problem of disposal the waste batteries.

Chemical products. Chemical products, such as H_2, CH_4 and EtOH, produced from water splitting and CO_2 reduction using solar energy or electricity generated from the renewable energies could be another promising way for the energy storage. The energy density of H_2 on a mass basis is 141.9 MJ/kg for both liquid and gaseous forms, which is much higher than the batteries [28]. Meanwhile, H_2 is a clean energy source because only H_2O is generated after its combustion, which means no environmental problems need to be concerned. Hence, chemical products could be a better intermediate than batteries for the energy storage and transportation.

1.2.3 H_2 production from photoelectrochemical water splitting

Electricity generated from the solar energy can be used for the electrochemical water splitting to produce H_2, which has been invented more than one hundred years [29]. Based on different electrolytes, the water electrolysis can be divided into alkaline electrolysis, acid electrolysis and proton exchange membrane (PEM) electrolysis [30]. Common industrial electrolyzers for H_2 production have a nominal energy conversion efficiency of around 70% [31]. By combining with photovoltaics with electrolyzers, a solar to H_2 overall energy conversion efficiency over 12% was reported [32].

H_2 can be produced directly from the solar energy by using semiconductor photoelectrodes, which is called as photoelectrochemical (PEC) method. Photo-induced electrons generated on the semiconductor after absorbing photons can transferred to the H^+ in the water solution through the semiconductor or some co-catalyst (such as Pt) and finally produce H_2. The photoelectrochemical effect was firstly found by Fujishima and Honda in 1972 [33]. As shown in Fig. 1.4, by connecting a TiO_2 electrode with a Pt black electrode through an external load, O_2 and H_2 were formation on TiO_2 electrode and Pt electrode respectively after shining with light [33]. However, due to the large band gap of TiO_2, very small amount of solar energy can be used, which is not good for improving the energy conversion efficiency. Fig. 1.5 shows the band structures of typical semiconductors and the redox potentials of water splitting. There is a strict requirement for the band structure of the semiconductor used for water splitting. The conduction band edge of the semiconductor must be more negative than the H^+/H_2 redox potential and the valence band edge of the semiconductor must be more positive than the O_2/H_2O redox potential to achieve the PEC water splitting. The more negative of the conduction band edge and more positive of the valence band edge are the easier of the water splitting achieves. This leads to a larger band gap semiconductor is more favorable for the water splitting. However, large band gap is not good for the light absorption. As a result, the band structure of the semiconductor should be large enough to satisfy the redox potential requirement of water splitting and small enough to absorb solar light as much as possible. There isn't so many natural materials can fulfill such a strict requirement. Hence the band engineering of semiconductors is required. By delicately

control the synthesis of multi-junction semiconductors, a 12.4% energy conversion efficiency from solar to H_2 was achieved by using a $GaInP_2/GaAs$ photocathode [34].
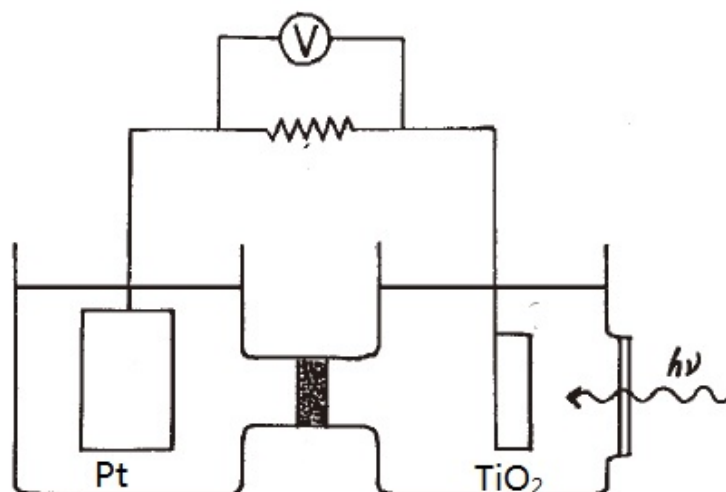
Fig. 1.4 Electrochemical cell for photoelectrochemical water splitting and H_2 production using TiO_2 photoanode (presented by Fujishima et al. 1972 [33]).
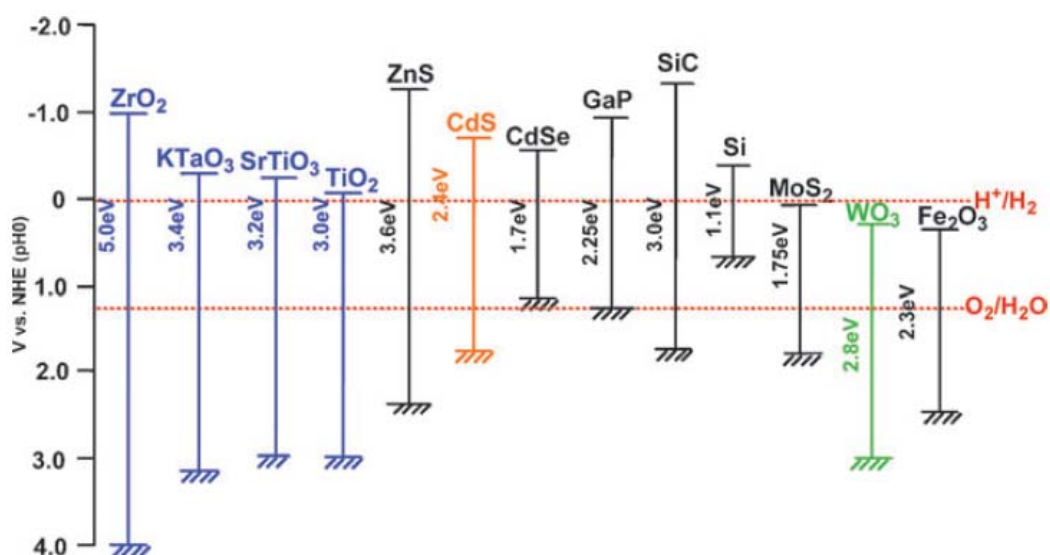
Fig. 1.5 Relationship between band structures of typical semiconductors and redox potentials of water splitting (presented by Kudo et al. 2009 [35]).

1.2.4 Photoelectrochemical CO$_2$ reduction

As discussed above, H$_2$ has much higher energy density than batteries which could be a better material for energy storage than batteries. However, H$_2$ is very hard to liquefy. The H$_2$ needs to be cooled below its critical point of 33 K (-240.15^{o}C) to be liquefy. Commercial used H$_2$ usually stored as compressed gas state. As a result, the energy density of H$_2$ decreased tremendously from 141.9 MJ/kg on a mass basis to only 5.6 MJ/L on a volume basis. Comparison of energy density of different energy storage materials on a volume basis were depicted in Fig. 1.6. The energy density of Li-ion battery ranges from 0.9 to 2.63 MJ/L, which is slightly lower than the energy density of H$_2$. Liquid organic materials, such as methanol and ethanol have much higher energy density than H$_2$ and Li-ion battery. The energy densities of methanol and ethanol are 15.6 and 24 MJ/L, respectively, which are much higher than the H$_2$. Therefore, liquid chemical fuels are more suitable for energy storage and transportation than H$_2$.
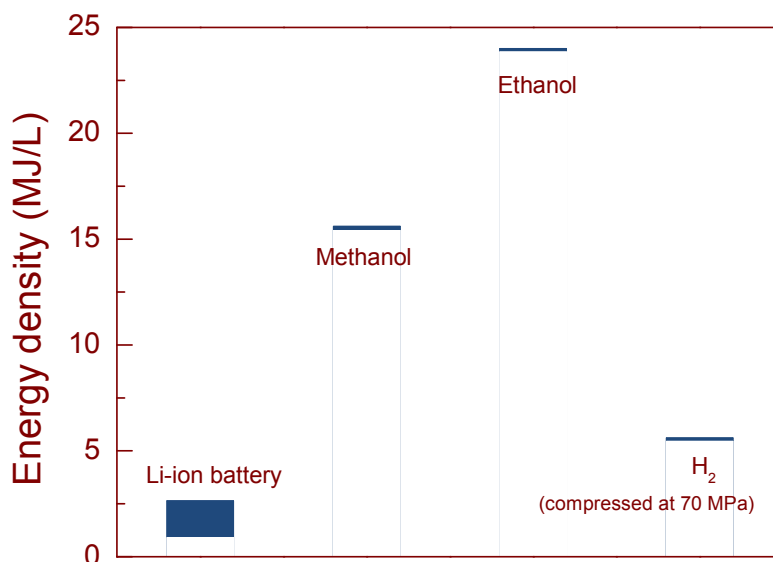
Fig. 1.6 Energy densities on a volume basis of typical energy storage materials (data source: Wiki [36]).

In the photoelectrochemical water splitting system, by introducing CO_2 source and using proper electrode materials and/or co-catalysts, CO_2 can be directly reduced into CO, CH_4, CH_3OH, EtOH and HCOOH etc, using solar energy [37]. However, the situation in the photoelectrochemical reduction of CO_2 is more complicated than in H_2. Typical CO_2 reduction products with its redox potentials (vs. SHE (standard hydrogen electrode)) and half-electrochemical thermodynamic equations at 1atm and 25°C are shown in Table 1.1 [38]. It can be seen that a series of different products can be produced during the reduction of CO_2. The standard potentials of these reactions are very close to each other as well as the H_2 evolution. Therefore, a mix of CO_2 reduction products together with H_2 is usually generated in the photoelectrochemical reduction of CO_2. As a result, the product selectivity becomes another serious problem besides the energy conversion efficiency.

Table 1.1 Standard potentials of typical CO_2 reduction reactions and H_2 evolution in aqueous solutions at 1.0 atm and 25°C[a]

Entry	Half-electrochemical thermodynamic reactions	Electrode potentials (V vs. SHE) under standard conditions
1	$CO_2 (g) + 4H^+ + 4e^- = C (s) + 2H_2O (l)$	0.210
2	$CO_2 (g) + 2H^+ + 2e^- = HCOOH (l)$	-0.250
3	$CO_2 (g) + 2H^+ + 2e^- = CO (g) + H_2O (l)$	-0.106
4	$CO_2 (g) + 4H^+ + 4e^- = HCHO (l) + H_2O (l)$	-0.070
5	$CO_2 (g) + 6H^+ + 6e^- = CH_3OH (l) + H_2O (l)$	0.016
6	$CO_2 (g) + 8H^+ + 8e^- = CH_4 (g) + 2H_2O (l)$	0.169
7	$2CO_2 (g) + 2H^+ + 2e^- = HOOC\text{-}COOH (aq)$	-0.500
8	$2CO_2 (g) + 12H^+ + 12e^- = CH_2CH_2 (g) + 4H_2O (l)$	0.064
9	$2CO_2 (g) + 12H^+ + 12e^- = CH_3CH_2OH (l) + 3H_2O (l)$	0.084
10	$2H^+ + 2e^- = H_2 (g)$	0.000

[a]data source: Qiao et al. (2014) [38].

To improve the product selectivity and energy conversion efficiency, co-catalysts are often used in the photoelectrochemical reduction of CO_2. There are four different schemes of photoelectrochemical reduction of CO_2 according to the catalyst applying method as shown in Fig. 1.7 [37]. Fist one is heterogeneous catalysis on a semiconductor electrode. Some semiconductors have the innate ability to catalyze the photoelectrochemical reduction such as p-Si and p-InP for CO production, p-GaP for CH_3OH and HCOOH production [39-43]. Transition metals such as Ni, Cu, Zn, Ag, Pb decorated semiconductor electrodes including p-InP, p-GaP and p-CdTe etc can also improve the product selectivity [44-46]. Homogeneous catalysts such as Re(bpy)(CO)$_3$Cl and Re(bipy-But)(CO)$_3$Cl were reported to catalyze the reduction of CO_2 into CO with a selectivity over 90% [47,48]. More complicated methods using both heterogeneous catalysis and homogeneous catalysis for the photoelectrochemical reduction of CO_2 have been also reported. It is reported that the homogeneous catalyst of pyridine combining with the heterogeneous photocathodes of p-GaP or $CuInS_2$ achieved the selectively reduction of CO_2 into CH_3OH with a faradaic efficiency over 96% [49,50].

Although the selectivity of the photoelectrochemical reduction of CO_2 can be relatively high as long as using proper co-catalysts, the overall energy conversion efficiency from solar energy to chemical energy is still very low. Actually, very few report discussed the energy conversion efficiency because it is so low. The band structure dilemma, which is the band edge of the semiconductor must satisfy both requirements of solar energy absorption and CO_2 reduction, is the main reason that limits the energy conversion efficiency. Therefore, like the suggestion in photoelectrochemical water splitting, separating the photoelectrochemical process into photovoltaic and electrolysis parts could be a much more available way because the CO_2 reduction is so complicated. Then the problems of solar energy absorption and CO_2 reduction efficiency could be solved separately, which greatly simplify this problem. In this dissertation, only electrochemical reduction of CO_2 is discussed.
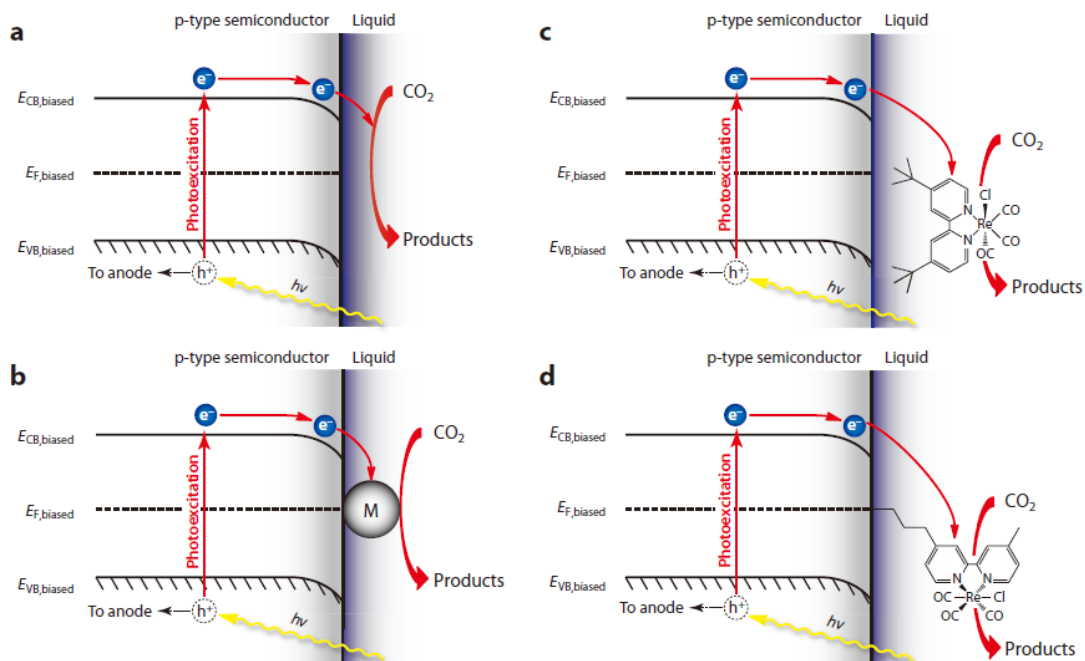
Fig. 1.7 Four schemes of photoelectrochemical reduction of CO_2 according to the catalyst applying method: (a) heterogeneous catalysis on a semiconductor electrode, (b) heterogeneous catalysis on a metal-decorated semiconductor electrode, (c) homogeneous catalysis through a semiconductor/molecular catalyst junction, and (d) heterogeneous catalysis through a molecular catalyst–decorated semiconductor electrode (presented by Kumar et al. 2012 [37]).

1.3 Electrochemical reduction of CO_2

1.3.1 History of electrochemical CO_2 reduction

Fundamental studies of electrochemical reduction of CO_2 began as early as in the 19th century by Royer, in which the main product obtained was formic acid by using a Zinc cathode [51,52]. Due to the oil embargoes in 1970s, the studies of electrochemical reduction of CO_2 were intensified in 1980s because chemicals and fuels could be produced through this method [53-58]. Products of CO, CH_4, C_2H_4, HCOOH, EtOH (ethanol) etc were found at

various metal electrodes [59]. Since the energy crisis become more and more serious recently, researches on electrochemical reduction of CO_2 have been further promoted, which are mainly focus on decreasing the over potential, improving product selectivity and current density [36,60-62].

Compared with the traditional CO_2 reduction method such as hydrogenation, which reduce CO_2 gas by using H_2 at 300-400°C [63,64], electrochemical method is more convenient and can be operated at ambient conditions. More importantly, there is no gaseous H_2 needed during the electrochemical CO_2 reduction. Water, as the most abundant source in our planet, provides the hydrogen source during the reaction. As a result, there is no need for H_2 production, storage and transformation, which are high energy consumption processes.

1.3.2 Electrolytes in the electrochemical CO_2 reduction

Electrochemical reduction of CO_2 can be divided by aqueous and non-aqueous according to the electrolyte used. Aqueous electrolyte is the most common used in the electrochemical reduction of CO_2. Various inorganic chemicals can be used as the aqueous electrolyte. Potassium (K) and/or sodium (Na) cation with different anions such as bicarbonate, carbonate, chloride, sulphpate, etc. are frequently used in the electrochemical reduction of CO_2 [54,65-67]. It is reported that different anions and cations in the electrolyte can affect the product selectivity. Thorson et al. reported that cations with a large atomic radius such as Cs and Rb promoted the CO production, while small cations such as Na promoted the H_2 generation on Ag electrode, which could be explained by the interplay between the level of cation hydration and the extent of cation adsorption on Ag electrodes [68]. Schizodimou et al. investigated a series of cations with different valences and found that the electrochemical reaction rate increases with the surface charge of the cation in the order of $Na^+ < Mg^{2+} < Ca^{2+} < Ba^{2+} < Al^{3+} < Zr^{4+} < Nd^{3+} < La^{3+}$ in the acid solutions on a $Cu_{88}Sn_6Pb_6$ alloy cathode. The acceleration effect was attributed to the participation of the radical anion ($CO_2 \bullet^-$) in the rate determining step [69]. Hori et al. studied the effect of different anions and found that HCO_3^-, Cl^-, ClO_4^- and SO_4^{2-} had better performance on the CO_2 reduction than HPO_4^- on a Cu working electrode at 5 mA/cm^2 [54].

Although Propylene Carbonate and Bmim-PF$_6$ (1-Butyl-3-methylimidazolium hexafluorophosphate) were reported [70,71], methanol was the most common used solvent in the non-aqueous electrochemical reduction of CO$_2$ [72-74]. The main product obtained in the electrochemical reduction of CO$_2$ in non-aqueous solutions is CO. Due to the low solubility of CO$_2$ in water (about 35 mmol/L at CO$_2$ partial pressure of 1 atm), current density in the electrochemical reduction of CO$_2$ in aqueous solutions usually smaller than 10 mA/cm^2 [37]. The solubility of CO$_2$ in methanol is more than 4 times higher than in water at ambient conditions [75]. Therefore, much higher current density could be achieved in non-aqueous solutions in general. However, from the literature results, the current density showed no advantage in non-aqueous solutions at ambient pressure. Most of the electrochemical reduction of CO$_2$ in non-aqueous solutions were conducted in high pressure to further increase the solubility of CO$_2$ (5 to 40 atm), which then led to a current density increase to as high as 300 mA/cm^2 [74]. However, high current density achieved by high pressure usually leads to a high over potential, which is not good for energy conversion [36].

1.3.3   Electrodes in the electrochemical CO$_2$ reduction

Metal electrodes have been widely used as the working electrodes in the electrochemical reduction of CO$_2$. Effect of the metal working electrodes on the product selectivity have been intensively studied in 1980s, and their results are summarized in Fig. 1.8. It can be seen that, most of the transition metals from group 4 to 9 have no catalytic activity for CO$_2$ reduction. Only H$_2$ was produced when these metals were used as working electrode. However, transition metals from group 10 to 12 have an innate catalytic activity to catalyze the CO$_2$ into different products. In, Sn, Tl and Pb from group 13 and 14 also have the ability to reduce CO$_2$ mainly into HCOOH. The detail of the mechanism of product selectivity on different metal electrodes will be introduced in the next section.
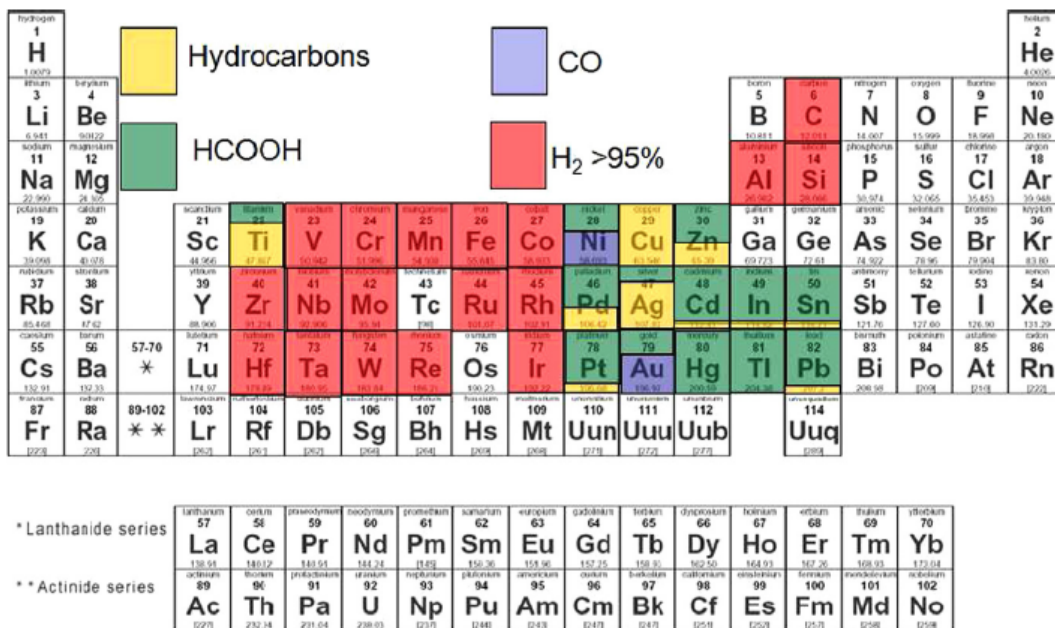
Fig. 1.8 Product distribution on different metal based cathodes in the electrochemical reduction of CO_2 in $KHCO_3$ based media (presented by Ganesh [76]).

Although many metal electrodes can be used as the cathode to catalyze the CO_2 reduction, the over potential for CO_2 reduction are very high. Therefore, methods for using nano-particle decorated electrodes and metal oxides were presented recently to reduce the CO_2 reduction over potential. The research results are summarized in Table 1.2. Au nanoparticles was reported to achieve a CO_2 reduction into CO with a faradaic efficiency over 60% at an overpotential as low as 140 mV, in which increased stabilization of the $CO_2^{\bullet-}$ intermediate on the surfaces of the Au electrodes was regarded as the main reason [77]. Nano-SnO_2 load carbon and grapheme, and annealed Cu_2O film showed the ability to decrease the over potential of formate generation to 340 and 250 mV, respectively [78,79]. Although the faradaic efficiencies of CO_2 reduction were not high at low over potential in these reports, it still suggested that nano-particles could be the future direction to improve the energy conversion efficiency of electrochemical reduction of CO_2.

Table 1.2 Recent progresses in the electrochemical reduction of CO_2 for decreasing over potential

Electrode	product	faradaic efficiency	over potential	Year	Ref
Nano-Au (Oxide dereived)	CO	>60%	140 mV	2012	[77]
		>98%	240 mV		
Annealed Cu_2O film (~ 3μm)	formate	33%	250~450 mV	2012	[78]
	CO	45%	190~390 mV		
Nano-SnO_2 loaded graphene or carbon black	formate	~10%	340 mV	2014	[79]
		~90%	~1140 mV		

1.3.4 Reaction mechanism in the electrochemical CO_2 reduction

It is reported that different catalytic activity and product selectivity of the metal electrodes mainly depend on the CO_2 and H_2 adsorption and intermediate desorption abilities on the metals. Fig. 1.9 shows the relationship between the electrode adsorption properties and the reaction paths. Although the reaction mechanism of CO_2 is still not clear, the first step of CO_2 reduction is generally accepted as the adsorption of CO_2 on the metal electrode and form a $CO_2^{\bullet-}$ radical, which further reduced into different products. It can be seen from Fig. 1.9, the product selectivity in different metal electrodes started in the very first step. If the metal electrode is weak in adsorbing CO_2, $CO_2^{\bullet-}$ radical cannot generated, and then the main product of the electrochemical reaction is H_2. Since H_2 evolution always competes with CO_2 reduction, the ability to adsorb H and CO_2 of the metal electrode becomes the second determine point of the product selectivity. After metal electrodes adsorbing the $CO_2^{\bullet-}$ radical, if $CO_2^{\bullet-}$ is easy to desorb, formate or oxalate are easy to form. If the adsorbed $CO_2^{\bullet-}$ allows OH⁻ group to be removed, CO and further reduced products are possible to generate. Or else, H_2, CO_2 or formate is formed. As a result, high hydrogen overvoltage electrodes with negligible CO adsorption (such as Hg, Cd, Pb, Tl, In and Sn) can reduce CO_2 into formate

with a high current efficiency. At the low hydrogen overvoltage metals with a high CO adsorption strength (such as Pt, Ni, and Fe), CO_2 is reduced to form tightly adsorbed CO, then H_2 is produced. The electrode materials with a medium hydrogen overvoltage and a weak CO adsorption (such as Au, Ag, Zn and Cu) catalyze the breaking of the carbon–oxygen bond in CO_2 and produce more reduced product [62].

Although the reaction pathways of CO_2 reduction is so complicated and still not clear so far. A relatively detailed pathway for $HCOO^-$, CH_4, CH_3OH and C_2H_4 production from electrochemical reduction of CO_2 on Cu electrode was proposed recently by Schouten et al. as shown in Fig. 1.10 [80]. Besides the overall rate determine step of CO_2 adsorption onto the Cu surface, a proton coupled electron transfer step and a electron transfer step account for another rate determine step in the CH_4 and C_2H_4 production process, respectively. Therefore, the production of CH_4 was reported to be affected by the pH since the proton is required in the rate determine step while C_2H_4 synthesis was independent with the pH [81].

CO$_2$(g)

Electrode adsorption properties ? — *Poor* → Main product is hydrogen

Good ↓

M-H is dominant adsorbed species ? — *Yes* → Main product is hydrogen

No ↓
Significant M-CO$_2$, M-CO$_2$H or M-CO levels also present

Metal readily desorbs M-CO$_2^-$ species ? — *Yes* → Formate/oxalate

Desorption from the form M-CO$_3^-$ → Disproportionation

No ↓
Significant M-CO$_2$H, M-OCOH, M-CO or further reduced species

M-CO$_2$H stabilised and desorbed in the formate form ? — *Yes* → Formate

↓

Do adsorbed species allow OH$^-$ groups to be removed ? (metal has a basic nature) — *No* / *Unreactive MCO$_2$H / MOCOH* → CO$_2$, H$_2$ or formate

Yes ↓
M-CO and further reduced species

CO readily desorbed — *Yes* → CO gas given off

No ↓
M-C and M-COH species

Do adsorbed species allow removal of OH$^-$ groups ? — *No* → M-COH species leading to products such as alcohols, aldehydes and ethylene.

Yes ↓

M-C species leading to production of products such as methane

Fig. 1.9 Reaction paths as a function of electrode adsorption properties (presented by Chaplin et al. 2003 [82])
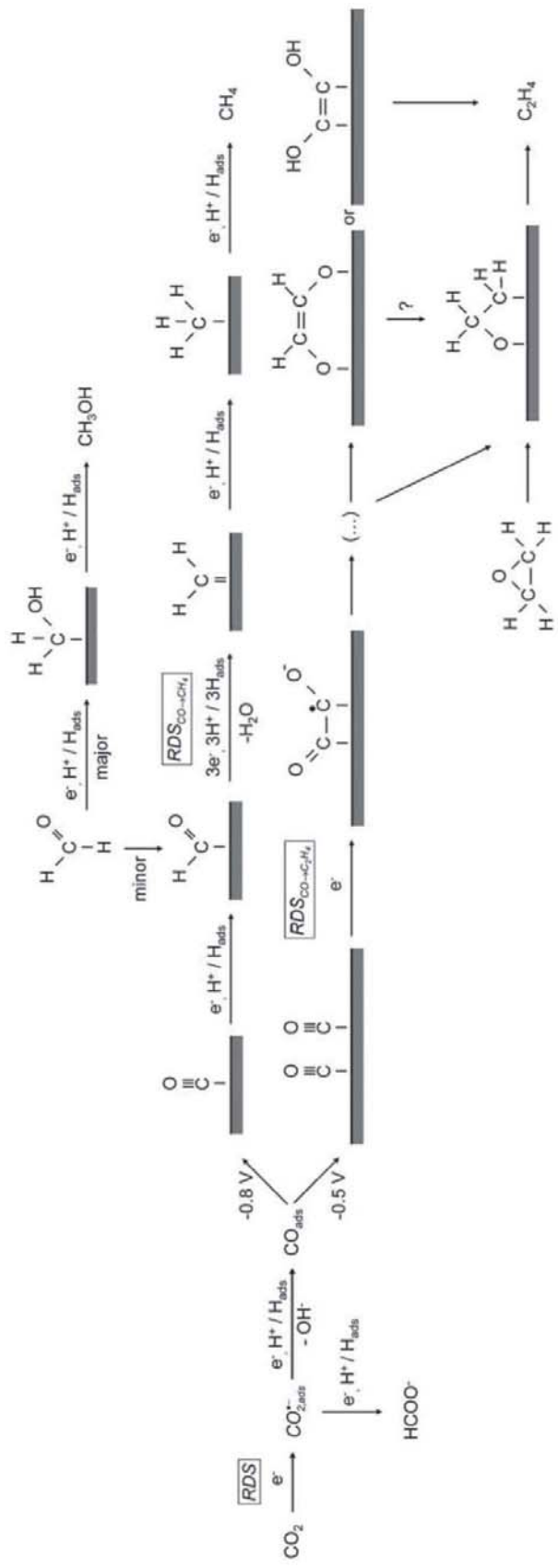
Fig. 1.10 Proposed mechanism for the electrochemical reduction of carbon dioxide on copper (presented by Schouten et al. 2011 [80]).

1.4 Research motivation and purpose

Although the detailed reaction mechanism of CO_2 reduction is still not clear, CO_2 is generously regarded as the active species, which is always bubbled into the electrolyte to supply the carbon source. However, it is also reported that CO_2 reduction can be achieved without CO_2 bubbling.

In 1983, Hori reported that $HCOO^-$ was found in the electrochemical reduction of HCO_3^- without CO_2 bubbling at room temperature on a Hg electrode [83]. The CO_2 dissociated from HCO_3^- was suggested as the active species for $HCOO^-$ production [83]. However, HCO_3^- rather than CO_2 was recently reported as the active species for $HCOO^-$ production in the electrochemical reduction of HCO_3^- with or without CO_2 bubbling at Pb or Cu electrodes, respectively [67,84]. Therefore, the active species are probably CO_2 and/or HCO_3^- according to these reports. However, the actual active species is still not clear. Therefore, the active species in the electrochemical reduction of CO_2 is studied in this research to help further studying the mechanism of CO_2 reduction and improving the efficiency.

Although various chemicals can be used as supporting electrolytes, $KHCO_3$ and $NaHCO_3$ are two most used electrolytes in the electrochemical reduction of CO_2 [77,85-90]. It is known that CO_2 can dissolve in and react with H_2O to form H_2CO_3, which further decomposes into HCO_3^- and CO_3^{2-}, as shown as follow [91].

$$CO_2 \text{ (g)} \rightleftarrows CO_2 \text{ (aq)} \tag{1.1}$$

$$CO_2 \text{ (aq)} + H_2O \text{ (l)} \rightleftarrows H_2CO_3 \text{ (aq)} \tag{1.2}$$

$$H_2CO_3 \text{ (aq)} \rightleftarrows H^+ \text{ (aq)} + HCO_3^- \text{ (aq)} \tag{1.3}$$

$$HCO_3^- \text{ (aq)} \rightleftarrows H^+ \text{ (aq)} + CO_3^{2-} \text{ (aq)} \tag{1.4}$$
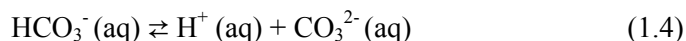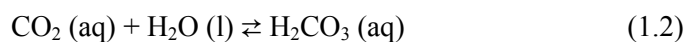
These processes are strongly pH dependent. At pH between 7.5-8.5, HCO_3^- is the dominant anion, at the pH above 11.5, CO_3^{2-} becomes the major anion, and only H_2CO_3 exists at pH below 5 [91]. H_2 evolution reaction (HER) is an unavoidable side reaction in the electrochemical reduction of CO_2. HER is prevalent in acidic solutions, whereas CO_2 does not

exist in a basic solution. This could be the reason why CO_2 reduction experiments are normally conducted in 0.05–0.5 mol/L $NaHCO_3$ or $KHCO_3$ supporting electrolyte which is close to neutral pH [76]. On the other hand, effect of the concentration of HCO_3^- on the CO_2 reduction has been rarely studied. Only Hori et al. studied the effect of 0.03 to 1.5 mol/L HCO_3^- on the electrochemical CO_2 reduction on a Cu electrode using a galvanostatic method in 1980s [54]. It is reported that the best faradaic efficiency of CO_2 reduction was obtained only when the concentration of HCO_3^- was 0.1 mol/L, lower or higher concentrations led to a faradaic efficiency decrease [54]. However, the reason was not discussed. Possible reason could be the HCO_3^- concentration affected the CO_2 absorption and led to a decrease in the active species in the electrolytes. Therefore, how much CO_2 was absorbed in different electrolytes after CO_2 bubbling needs to be studied to verify the real amount of active species in different electrolytes. However, the amount of dissolved CO_2 in typical electrolytes under CO_2 bubbling has not been reported before. Since this could be an important data to reveal the reason of why low $KHCO_3$ concentration promoting the CO_2 reduction faradaic efficiency, the concentrations of CO_2 in different solutions before and after CO_2 bubbling were studied. The effect of CO_2 bubbling into different solutions were also discussed in this research.

1.5 Outline of this thesis

This dissertation is divided into 7 chapters, and the details are as follow:

Chap 1 is the general introduction. The background of the solar energy conversion, storage and transportation were first presented. Then, technologies and previous reports of electrochemical reduction of CO_2 in aqueous solutions were introduced. Finally, the motivations and objects of this research, including investing the active species and effect of CO_2 bubbling in the electrochemical reduction of CO_2 in aqueous solutions, were given.

Chap 2 is the experimental section, in which the electrochemical cells, experimental setups, experimental materials and procedures, and analysis methods were introduced.

Chap 3 studied the electrochemical reduction of $NaHCO_3$ and $KHCO_3$ without CO_2 bubbling using I-V measurement (products analysis is studied in Chap 4). Voltammograms were obtained at various $NaHCO_3$ and/or $KHCO_3$ concentrations and different temperatures

on Cu working electrode. Reasons for why current density was increased by the high temperature and high HCO_3^- concentration were also thermodynamically studied.

Chap 4 studied the active species in the electrochemical reduction of $KHCO_3$ without CO_2 bubbling at elevated temperature by using very high $KHCO_3$ concentration solution. The reaction pathway of HCO_3^- decomposing into CO_2 was also examined.

Chap 5 studied the electrochemical reduction of CO_2 in different electrolytes ($KHCO_3$, KCl, and KOH) under CO_2 bubbling at various conditions. The effects of CO_2 bubbling, temperature, electrolyte, applied potential, reaction time, stirring, and geometrical shape of the working electrode on the faradaic efficiency of CO_2 reduction were investigated.

Chap 6 examined the effect of CO_2 bubbling in different solutions ($KHCO_3$, KCl, KOH, K_2CO_3 etc.) by measuring the pH changes and total carbon concentrations. The concentrations of different carbonaceous species (CO_2, H_2CO_3, HCO_3^-, CO_3^{2-}) in these solutions before and after bubbling with CO_2 were calculated according to the experimental data.

Chap 7 summarized the results above and gave the conclusions.

Chapter 2

Experimental

2.1 Experimental method

2.1.1 Electrochemical measurement

Electrochemical reduction of CO_2 was conducted in two different electrochemical cells. A normal one compartment three electrodes electrochemical cell with a diameter of 28 mm and height of 50 mm purchased from ALS Company (SVC-3 Voltammetry cell, ALS Co., Ltd) was used for the I-V study (Fig. 2.1). This cell is not leak-tight, therefore, gas products generated during the experiments were directly released to the atmosphere. A copper wire (Φ 0.5 mm, 99.999%, Nilaco), a Pt coil (Φ 0.5 mm, ALS Co., Ltd) and a standard Ag/AgCl (3.0 mol/L NaCl) electrode (RE-1B, ALS Co., Ltd) were used as the working, counter, and reference electrodes, respectively. 17-20 mL electrolyte was filled in the cell during the reaction. A Solartron 1280C electrochemical system was used to conduct all the electrochemical experiments. For the I-V measurement, a typical potential scan is started from the open circuit potential and negatively increased to -2.0 V (vs Ag/AgCl) with a scan rate of 20 mV/s.

A home-made H-type leak-tight electrochemical cell was used for CO_2 bubbling and gas products collection for further analysis. The schematic of this cell is shown in Fig. 2.2. A three electrodes system was used in this electrochemical cell. The working and reference electrodes were put in the same compartment and separated from the counter electrode by a Nafion film (DuPont: N117). Since CO_2 reduction is a redox reaction. During the reduction of CO_2, OH^- is oxidized into O_2. By separating the working and counter electrodes, the recombination of generated products on these two electrodes can be effectively prohibited. The gas sample could be either sampled manually through syringe or directly connected to the gas chromatographer (GC) for online analysis. Both gas in and out route can be totally closed by valves when not use. A typical experimental procedure for using the H-type cell is as follow. Same amount (35 mL) of electrolyte was added into both WE and CE chambers of the electrochemical cell. Then CO_2 gas was bubbled into the WE chamber for 30 min when necessary. The pH values of both chambers were measured. Working, counter and reference electrodes were placed in the electrochemical cell. The outlet gas tube was either directly

connected to gas chromatographer or closed by valve. A Solartron 1280C electrochemical system was used to conduct the electrochemical experiments. Both I-V and potentiostatic method were used.
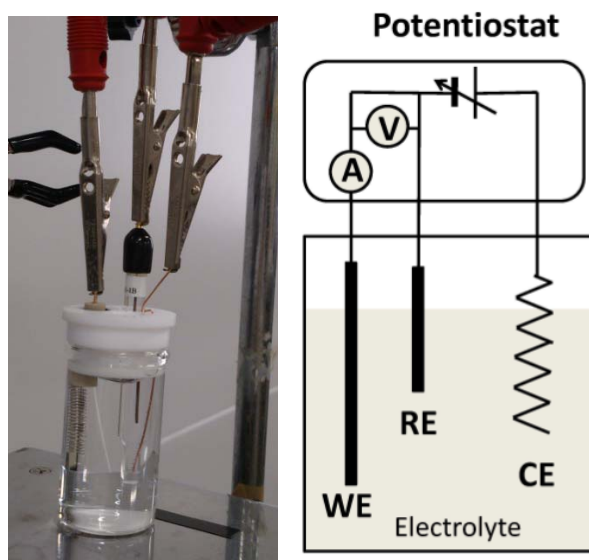
Fig. 2.1 One compartment three electrode electrochemical cell (SVC-3 Voltammetry cell, ALS Co., Ltd).
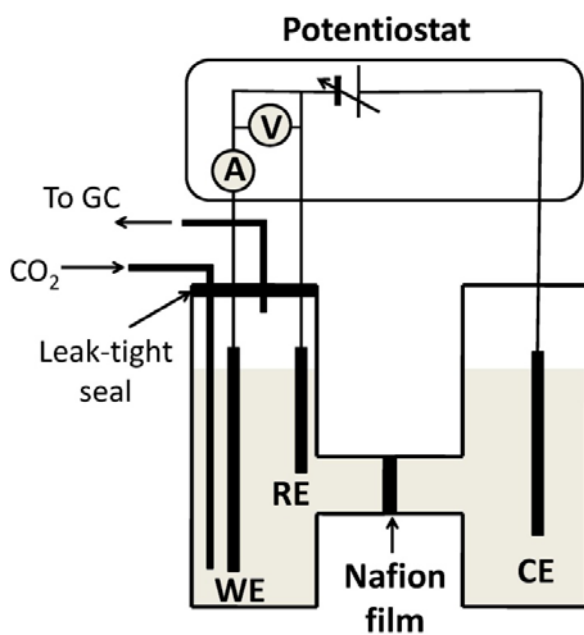
Fig. 2.2 H-type electrochemical cell used for experiments with CO_2 bubbling and gas collection.

2.1.2 Dissolved CO_2 measurement

For the measurement of dissolved CO_2 in different solutions, CO_2 was continuously bubbled into 30-mL solutions contained in a 40-mL TOC sample vial with a controlled flow rate as shown in Fig. 2.3. The pHs of the solutions were measured continuously. An obvious pH decrease in the solutions could be observed during the CO_2 bubbling due to the dissolved CO_2 transformed into H_2CO_3 and further dissociated to generate H^+. When the pH remained stable for over 30 min, the total carbon concentrations (TC) of these solutions were measured immediately by a Shimadzu TOC analyzer (TOC-V CPH). The TCs of different solutions before bubbling were also measured for comparison.
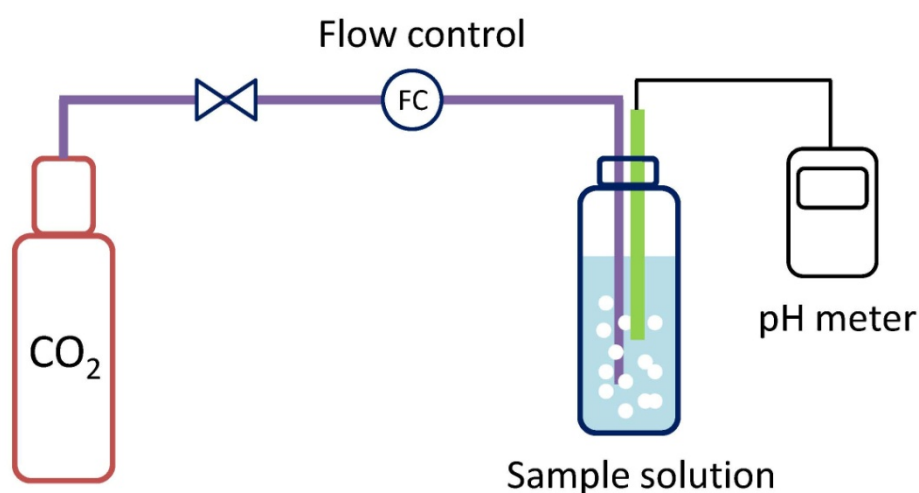
Fig. 2.3 Schematic of CO_2 bubbling setup for dissolved CO_2 measurement.

2.2 Analysis method

2.2.1 Gas analysis

Gas chromatographer equipped with a thermal conductivity detector (GC/TCD) was

widely used for the qualitatively and quantitatively analysis of gas samples. By sweeping through a series of columns of the GC, different gas molecules can be separated and determined from different retention time which was caused by the adsorption strength differences between different gas molecules and the column walls or packing materials in the column. A thermal conductivity detector (TCD) was used to monitor the outlet stream from the column. By sensing the changes in the thermal conductivities between the gas sample and carrier gas, the amount of specific gas products can be quantified.

An Agilent 7890A GC/TCD was used in this study to analysis the gas products. The gas sample can be either manually sampled and injected by using a syringe or directly connected to the GC for online measurement. This GC system allows the sample gas flow through five different columns and hence can analyze H_2, CO, CO_2, CH_4, C_2H_4, C_2H_6, O_2 and N_2 within one test. The schematic of the valves and columns system of the GC/TCD is shown in Fig. 2.4. The detailed analysis method of the GC/TCD are summarized in Table 2.1. There are two sample loops in this system, each has a volume of 2 mL. The total volume of the sample route is about 10 mL, which means that at least 10 mL of sample needs to be injected to fill the sample route. If the sample amount was not enough for the measurement, sample diluting was used. 0.1 – 0.3 mL sample was collected by a syringe. Then, it was injected into another syringe, which was pre-filled with 20 mL Ar gas, through a silicone placed Luer connector. The mixed gas sample was then sealed in the syringe and waited for 10 minutes before being finally injected into the GC. According to the oven temperature program, a typical analysis process lasted about 10 min.
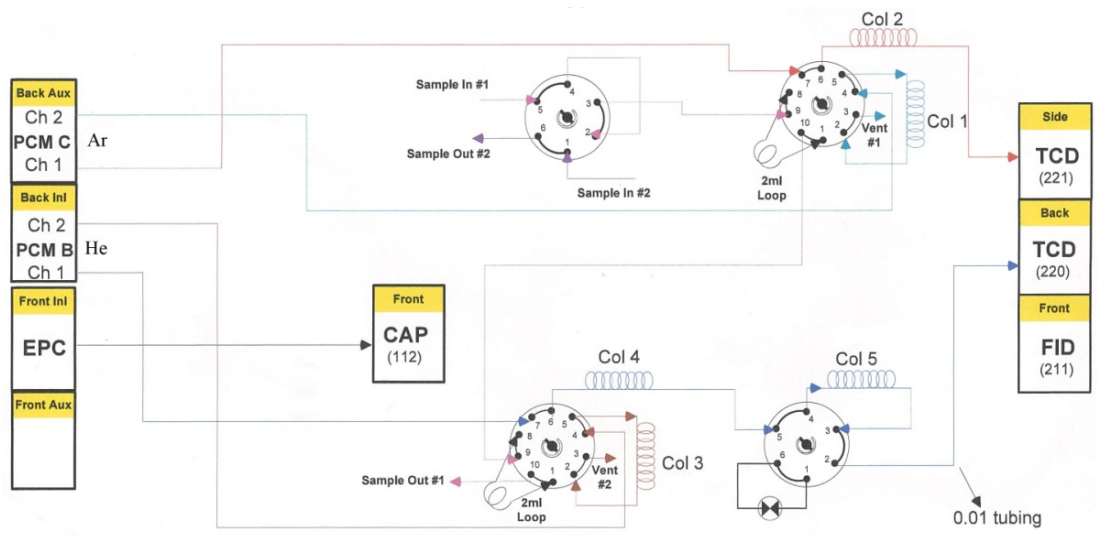
Fig. 2.4 Schematic of valve and column system of GC/TCD.

Table 2.1 Analysis method of GC/TCD

Detectors	Thermal Conductivity Detector (TCD)
	(Back TCD & Side TCD)
Column	Column #1: MS5A 8ft
	Column #2: HAYASEP Q 3ft
	Column #3: HAYASEP Q 0.5m
	Column #4: HAYASEP Q 6ft
	Column #5: MS5A 8ft
Carrier gas	Side TCD: Ar (99.9999%) (for: H_2)
	Back TCD: He (99.99995%) (for: CO, CO_2, CH_4, C_2H_4,
	C_2H_6,)
Reference flow rate	Side TCD: 30 mL/min
	Back TCD: 45 mL/min
Inlet temperature	120 °C
Detector temperature	200 °C
Oven temperature	60 °C for 1 min
	then 20 °C/min to 150 °C for 0 min
	then 12 °C/min to 170 °C for 0 min
	then 30 °C/min to 190 °C for 2 min

2.2.2 Total organic carbon (TOC) analysis

Carbon is existed in both organic (hydrocarbons, proteins, lipids etc) and inorganic (CO_2, bicarbonate and carbonate) materials. The total organic carbon (TOC) analyzer can measure and calculate the concentration of the TOC in solutions, which are frequently used as an indicator of water quality. Actually, the TOC analyzer cannot detect the TOC directly. It can only detect CO_2 by a non-dispersive infrared sensor. Therefore, there are two main methods for the TOC measurement. First one is catalytically transform all the IC (inorganic carbon) and TOC (total organic carbon) in the sample into CO_2 at 600~900°C, and then analyze the CO_2 amount to determine the total carbon (TC) concentration. And then another sample was extracted and added with acid (HCl) until pH below 3. All the IC reacts with HCl and releases CO_2. By analyzing this amount of CO_2, IC is known. Finally, the TOC was derived from TC minus IC. Another method for TOC calculation is called Non-Purgeable Organic Carbon (NPOC) method, which is not related to this research and will not introduce here.

Since the TC in the water solution can be directly measured by using the TOC analyzer, the TCs in different solutions before and after bubbling with CO_2 were analyzed.

2.2.3 Efficiency calculation

The faradaic efficiencies (FE) of different products were calculated as follow:

$$FE = \frac{n_{product} \times n_{electron} \times F}{Q} \times 100\% \tag{2.1}$$

where, $n_{product}$ means the molar amount of target product, $n_{electron}$ represents electron transfer number per molecule (for CO, n = 2; CH_4, n = 8; C_2H_4, n = 12; H_2, n = 2), F is the faradaic constant (96485.3 C/mol), Q is the total electron transferred during the whole reaction. The number of Q can be obtained from the electrochemical software used for conducting the experiment. According to this equation, faradaic efficiency represents the efficiency of current utilization, or in other words, the product selectivity.

Chapter 3

I-V study of the electrochemical reduction of KHCO$_3$ and/or NaHCO$_3$ at elevated temperatures without CO$_2$ bubbling

3.1 Introduction

It was reported that formate was produced in the electrochemical reduction of $KHCO_3$ without CO_2 bubbling [67,83,84]. Both CO_2 and HCO_3^- were reported as the active species. However, the real active species in this reaction is still not clear. Since that there is no CO_2 bubbling used in the electrochemical reaction, the possibility of the HCO_3^- as the active species is higher than the CO_2. Then the concentration of HCO_3^- should affect the CO_2 reduction. Therefore, the effect of electrochemical reduction of high concentration HCO_3^- solutions without CO_2 bubbling were studied in this chapter.

Fig 3.1 showed the solubility of $NaHCO_3$ and $KHCO_3$ in water as a function of temperature. The solubility of both $NaHCO_3$ and $KHCO_3$ increases with temperature. Therefore, an elevated temperature up to 60 ^{o}C was used to improve the solubility of HCO_3^- in water solution and make the preparing of high concentration $KHCO_3$ solution easier.
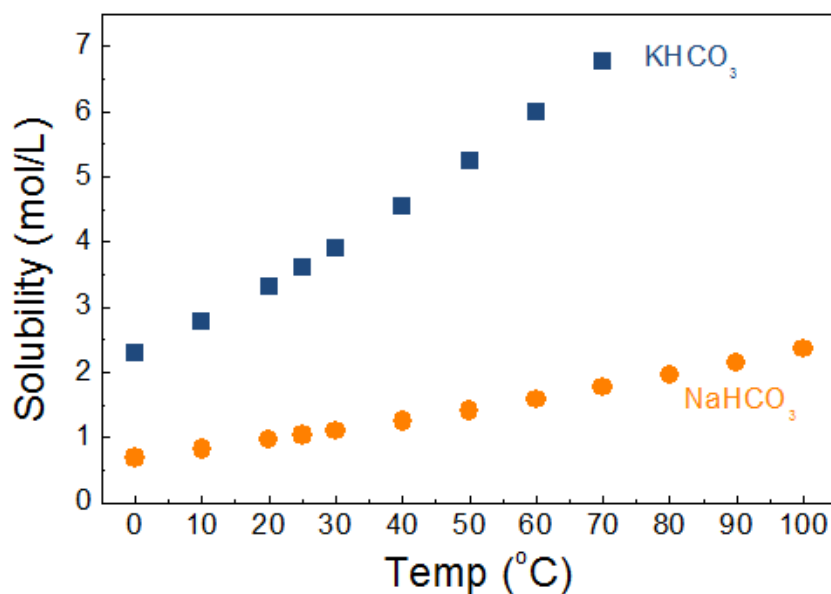
Fig. 3.1 Solubility of $KHCO_3$ and $NaHCO_3$ in the water as a function of temperature (data source: CRC Handbook of Chemistry and Physics (90th Edition) [92]).

In this chapter, the I-V characteristic is used because of the first order checking of the reaction process. Since the current in the electrochemical reactions is often used to indicate the chemical redox reaction. The effect of the HCO_3^- on the electrochemical reduction of

$KHCO_3$ without CO_2 bubbling were mainly studied by I-V analysis in this chapter for a preliminary study.

3.2 Experimental

It has been widely reported that Cu has the ability to effectively reduce the CO_2 into CO, CH_4, C_2H_4 and HCOOH in water solutions [54,62]. Therefore, the Cu wire was chosen as the working electrode in here. A copper wire (Φ 0.5 mm, 99.999%, Nilaco) was used as the working electrode. The length of the working electrode was 22 or 30 mm at different conditions, which gave a surface area of *ca.* 0.35 or 0.47 cm^2, respectively. The native copper oxide was removed from the wires by etching for 60 s in 0.1 mol/L aqueous HCl. The reference electrode was a standard Ag/AgCl (3 mol/L NaCl) electrode (RE-1B, ALS Co., Ltd). A Pt coil (Φ 0.5 mm, ALS Co., Ltd) was selected as the counter electrode. All the potentials mentioned in this research were referred to Ag/AgCl unless otherwise specified. $NaHCO_3$ (99.5%) and $KHCO_3$ (99.5%) (Kanto chemical Co., Inc) were used directly without any further treatment. The chemicals used in this chapter are shown in Table 3.1. All electrochemical experiments were conducted in a one compartment electrochemical cell which was introduced in chapter 2 (Fig. 2.1) through a Solartron 1280C electrochemical system. A water bath (EWS-100RD, AS ONE Corporation) was used for the temperature control.

Table 3.1 Materials used in Chapter 3

Entry	Item	Specification	Producer
1	Cu wire	99.999%, Φ 0.5 mm	The Nilaco Corporation
2	Pt wire	99.999%, Φ 0.5 mm	The Nilaco Corporation
3	$KHCO_3$	99.5%	Kanto chemical Co., Inc
4	$NaHCO_3$	99.5%	Kanto chemical Co., Inc
5	HCl	0.1 mol/L	Kanto chemical Co., Inc
6	Deionized water	18.2 MΩ,	Organo Corporation (PRA-0015)

3.3 Effect of NaHCO$_3$ and KHCO$_3$ concentrations at room temperature

Since the HCO$_3^-$ is assumed as the active species, high concentration of the HCO$_3^-$ should facilitate the CO$_2$ reduction especially for the case without CO$_2$ bubbling. Fig. 3.2 illustrated the voltammograms obtained in the electrochemical reduction of various concentrations of NaHCO$_3$ and/or KHCO$_3$ solutions at room temperature without CO$_2$ bubbling. The current density increased with the electrolyte concentration when KHCO$_3$ or NaHCO$_3$ solution was used solely as the electrolyte. Due to the solubility of NaHCO$_3$ in the water, the highest concentration of NaHCO$_3$ used here was 0.5 mol/L. When the concentration of KHCO$_3$ increased to 1.5 mol/L, the highest current density was obtained. This suggested that the HCO$_3^-$ concentration can strongly improve the current density which means that the reaction was promoted. On the other hand, the current density was very similar when NaHCO$_3$ or KHCO$_3$ solution was used in the same concentration (0.1 and 0.5 mol/L). In Fig. 3.2 (b), the current density obtained in the electrolytes with 0.1 mol/L NaHCO$_3$ plus 0.5 mol/L KHCO$_3$, and 0.5 mol/L NaHCO$_3$ plus 0.1 mol/L KHCO$_3$ showed no big difference. These results suggested that the K$^+$ and Na$^+$ in the solution showed no obvious effect on the electrochemical reaction. The electrochemical reaction was strongly related with the HCO$_3^-$ concentration. High concentration of HCO$_3^-$ was favorable for obtaining high current density.
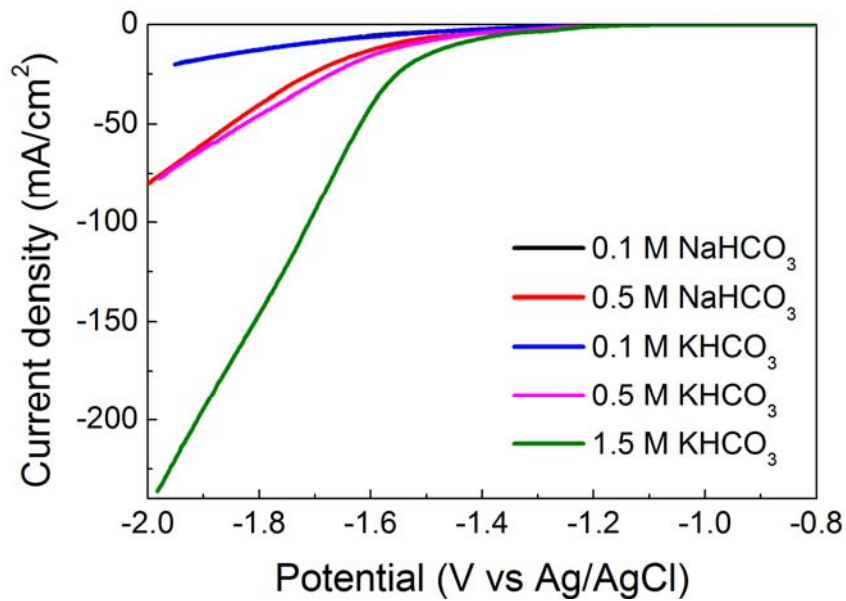
(a)
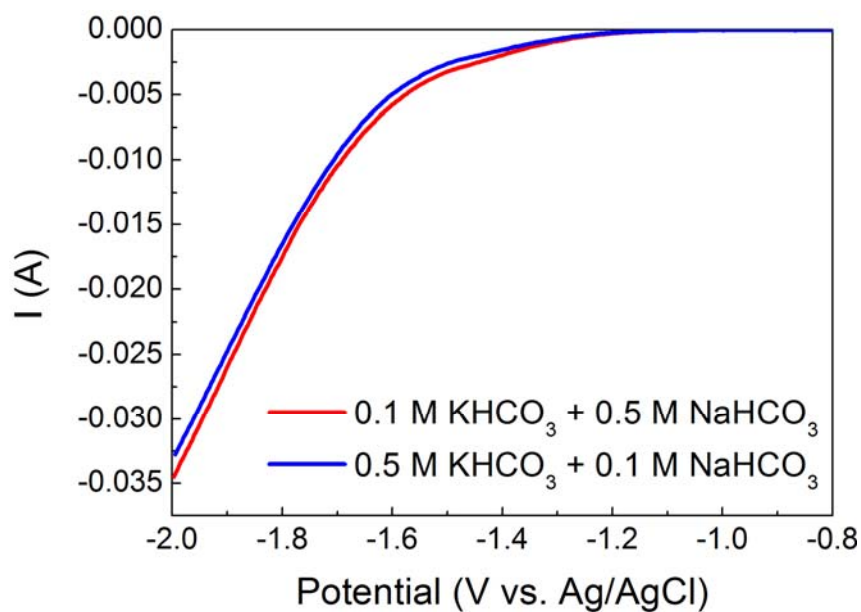
(b)

Fig. 3.2 Voltammograms obtained in (a) various concentrations of $NaHCO_3$ or $KHCO_3$ solutions and (b) solutions contain both $NaHCO_3$ and $KHCO_3$ at a Cu working electrode (M: mol/L, scan rate: 20 mV/s, temperature: room temperature (20 ^{o}C); length of WE: (a): 30 mm, (b): 22 mm).

3.4 Effect of temperature

Results in section 3.3 showed that the high concentration of HCO_3^- could effectively improve the current density, which suggested that a further increase in the HCO_3^- concentration would probably lead to a further increase in the current density. However, this is hard to achieve at room temperature due to the solubility limit of the bicarbonate salts. Therefore, the temperature elevated experiments using different concentration of $KHCO_3$ with or without $NaHCO_3$ were carried out to study the effect of temperature and the higher concentration of the electrolyte. Fig. 3.3 showed the voltammograms obtained in different concentrations of $KHCO_3$ solutions at temperature ranges from 20 to 60 ^{o}C. When the temperature increased from 20 to 60 ^{o}C, the current densities increased with the temperature in both 1.5 and 3.0 mol/L $KHCO_3$ solutions. However, compared with the temperature, the HCO_3^- concentration had a stronger effect on the current density. This suggested that the HCO_3^- concentration was a more important factor to affect the current density than the temperature.
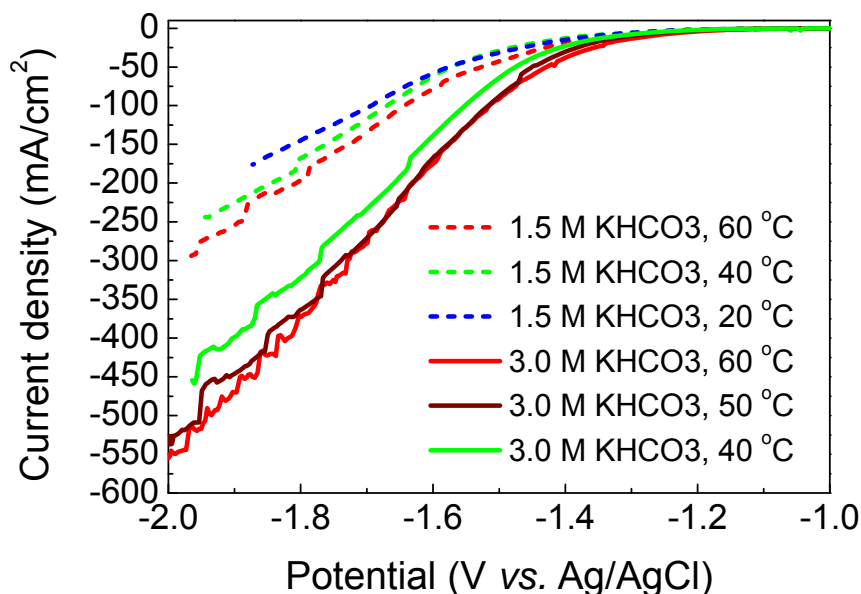
Fig. 3.3 Voltammograms obtained in various concentrations of $KHCO_3$ solutions at elevated temperatures on a Cu working electrode (scan rate: 20 mV/s, length of WE: 30 mm).

It is reported that C_2H_4, CH_4, CO, HCOOH, and H_2 are the most common products found in the electrochemical reduction of CO_2 on Cu working electrode [54]. Actually the current density increase might not relate to the increase of the CO_2 reduction, it could be caused by the enhancement of H_2 evolution. However, according to the literature, H_2 production is markedly prohibited at the potential from -1.5V to -1.6 V (vs. Ag/AgCl) when the Cu was used as the working electrode in $KHCO_3$ electrolyte, and hydrocarbons such as CH_4 and C_2H_4 becomes the dominant products [54]. Therefore, the current density obtained at -1.5 V at various concentrations of $KHCO_3$ and/or $NaHCO_3$ in the I-V studies were recorded and showed in Fig 3.4. It can be seen in Fig 3.4 (a), the current density increased with the temperature in different HCO_3^- concentration solutions. The current density increased about 40 mA/cm^2 when the temperature increased from 20 to 60 ^{o}C in the solution with 1.5 mol/L $KHCO_3$ plus 0.5 mol/L $NaHCO_3$. Compared with the temperature, HCO_3^- concentration had a much higher effect on promoting the current density. The current density increased about 70 mA/cm^2 when the HCO_3^- concentration increased from 1.5 to 4.0 mol/L at 60 ^{o}C (Fig. 3.4 (b)). The highest current density of -114.2 mA/cm^2 was obtained at 60 ^{o}C in the solution with 4.0 mol/L HCO_3^-.

In a general electrode redox reaction of

$$O + ne \underset{k_b}{\overset{k_f}{\rightleftharpoons}} R$$

(3.1)

the cathodic current density of i_c can be given as [93]

$$i_c = nFk_f C_o(0.t)$$

(3.2)

where

i_c is the cathodic current density, A/m^2

n is the electron transfer number per molecule

F is the faradaic constant, 96485 C/mol

k_f is the forward reaction rate constant, s^{-1} for a one order reaction

$C_o(0,t)$ is the concentration of reactant O at the electrode surface as a function of time, mol/L.
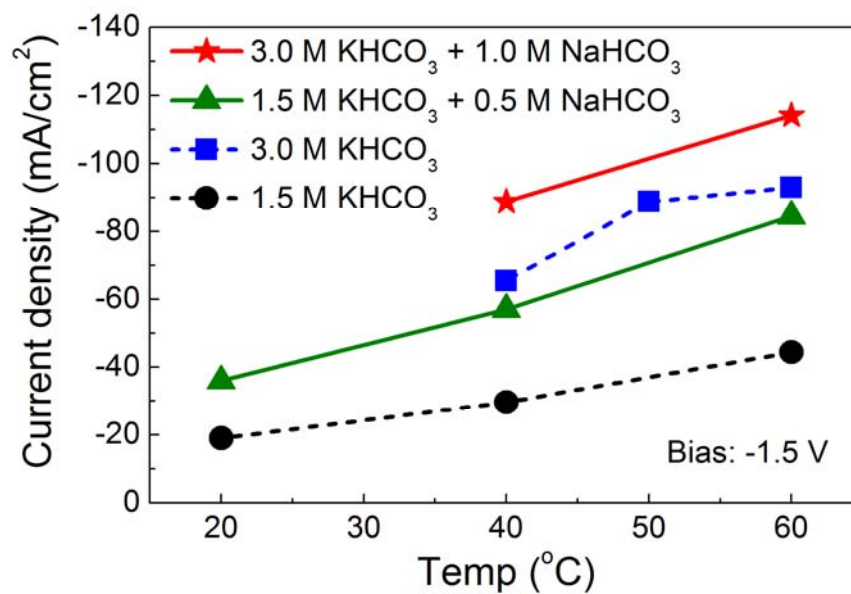
(a)
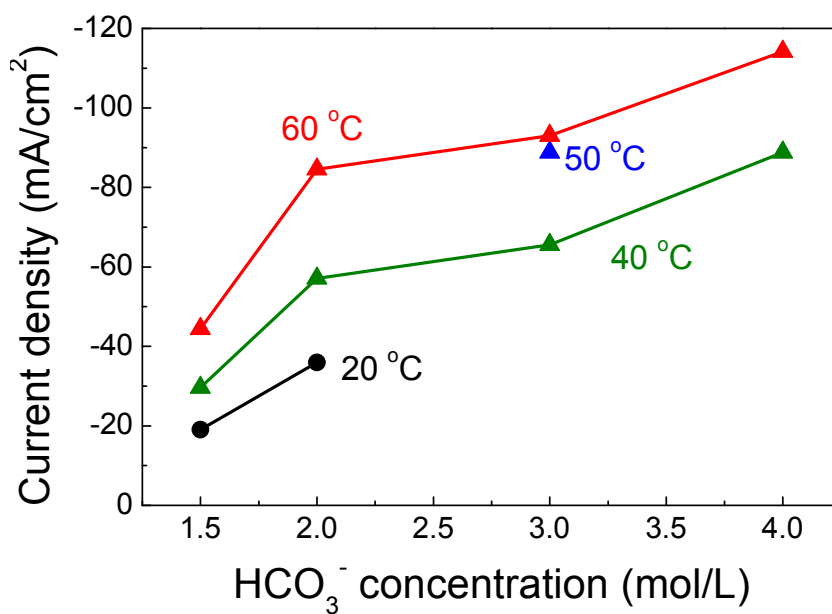
(b)

Fig. 3.4 Current densities obtained in the electrochemical reduction of various concentrations of $KHCO_3$ and/or $NaHCO_3$ solutions without CO_2 bubbling at -1.5 V as a function of (a) temperature and (b) HCO_3^- concentration (M: mol/L).

Meanwhile the reaction rate constant k_f is related to the temperature as follow,

$$k_f = Ae^{-E_a/RT} \tag{3.3}$$

where, A is the pre-exponential factor, E_a is the activation energy, R is the ideal gas constant, and T is the absolute temperature. Insert Eq. 3.3 into Eq. 3.2, one can obtain

$$i_c = nFC_o(0,t)Ae^{-E_a/RT} \tag{3.4}$$

Although the reaction of electrochemical CO_2 reduction should be much more complicated that reaction 3.1 (see Table 1.1), and the $C_o(0,t)$ should be different from the bulk concentration of the electrolytes (especially at a high current density), the Eq. (3.4) still can be used to explain the relationship of current density, HCO_3^- concentration, and temperature roughly. As a result, the temperature increase led to a rate constant increase and then caused the current density increase. Since the factors of n, $C_0(0,t)$, and E_a, are difficult to measure, assuming they are constants in Eq. (3.4), then one can obtain,

$$i_c = Me^{N/T} \tag{3.5}$$

in which,

$$M = nFC_o(0,t)A \tag{3.6}$$

$$N = -E_a/R \tag{3.7}$$

Therefore, using two knowing experimental data (current density at given temperature), one can obtain the factors M and N. Then the $i_c - t$ curve can be plotted, which is shown in Fig. 3.5. The calculation results showed that the experimental data were in accordance with the calculation except the current density obtained in 3.0 mol/L $KHCO_3$ at 50 °C, which could be attributed to some experimental error.

It can be seen from Table 1.1, the production of H_2, CO and HCOOH are all two electron transfer reactions. It is hard to distinguish the real reaction happened in the electrochemical reduction of $KHCO_3$ from the voltammetry studies. Therefore, the product analysis is required, which will be discussed in the next chapters.
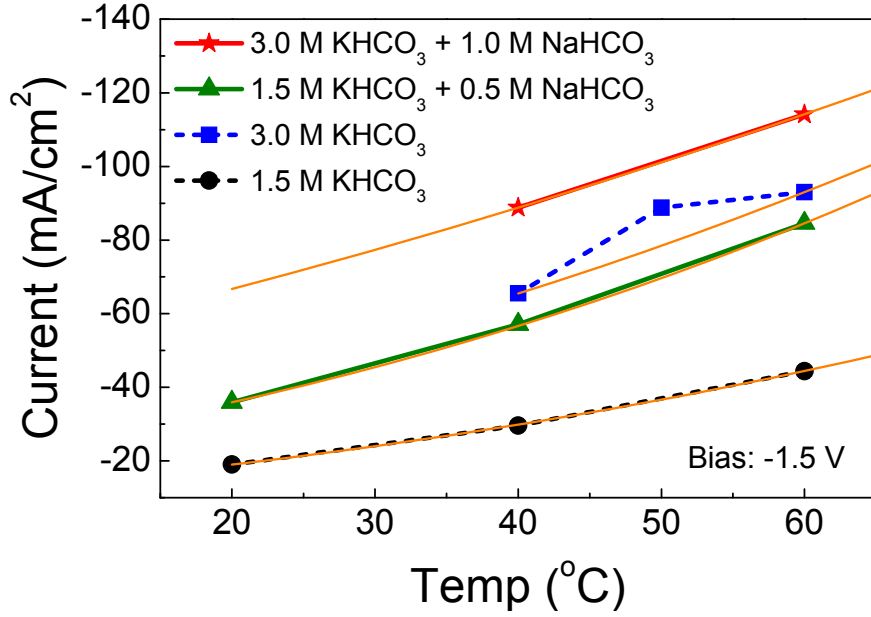
Fig. 3.5 Calculated current densities (orange line) and experimental data (red star, green triangle, blue square, black dot) as a function of temperature (applied potential: -1.5 V).

3.5 Thermodynamic study

The relationship between the standard enthalpy of formation and the temperature at constant pressure can be described as [94]

$$\mathrm{d}H = Cp\,\mathrm{d}T \tag{3.8}$$

where, C_p is the heat capacity at constant pressure. Usually, the variation of heat capacity with the temperature can be omitted if the temperature range is small. However, if it is necessary to calculate the C_p at different temperature, an empirical equation can be used as follow,

$$Cp = a + bT + c/T^2 \tag{3.9}$$

where, a, b, and c are empirical parameters that are independent of temperature, T is the absolute temperature. Insert Eq. 3.9 into Eq. 3.8, and integrate the obtained equation, one can get,

$$\Delta_f H^0 (T_2) = \Delta_f H^0 (T_1) + a\,(T_2 - T_1) + 1/2\,b\,(T_2^2 - T_1^2) - c\,(1/T_2 - 1/T_1) \tag{3.10}$$

Therefore, the standard enthalpy of formation of chemicals at different temperature can be

calculated if a, b, c, and $\Delta_f H^0(T_1)$ are known. Table 3.2 listed the empirical parameters of the heat capacities of typical CO_2 reduction products and their standard enthalpy of formation at 298.15 K and 333.15 K. The $\Delta_f H^0$(298.15 K), a, b, and c in Table 3.2 are obtained directly from reference book [95,96], $\Delta_f H^0$(333.15 K) is calculated from Eq. 3.10. It can be seen that the standard enthalpies of all the chemicals increased slightly when the temperature increased from 298.15 to 333.15 K. This suggests that the temperature does not obviously affect the standard enthalpies of these chemicals at this temperature ranges. Using the data obtained in Table 3.2, the standard enthalpies of possible reactions in the electrochemical CO_2 reduction at 298.15 and 333.15 K can be calculated, and the results are shown in Table 3.3. The standard enthalpies of all the reactions are not changed too much as the temperature increase. All the standard enthalpies of the CO_2 reduction reactions are negative. However, the standard enthalpy of H_2 evolution changes from 0 to 1.02 kJ/mol when the temperature increased from 298.15 to 333.15 K. These results suggest that the reactions of CO_2 reduction are exothermic while the H_2 evolution at elevated temperature is endothermic. Therefore, elevated temperature should benefit the H_2 evolution but prohibit the CO_2 reduction. According to these results, the current density increase in the electrochemical reduction of $KHCO_3$ at elevated temperature could be attributed to the enhancement of H_2 evolution. Therefore, the gas products analysis is necessary.

Table 3.2 Standard enthalpies of formation of typical chemicals in the CO_2 reduction and their empirical parameters of heat capacity

| | Δ_fH^0 (298.15 K)[a] | Δ_fH^0 (333.15 K)[a] | C_p^0 (J K^{-1} mol^{-1}) = a + bT + c/T^2 | | |
	(kJ/mol)	(kJ/mol)	a[b]	b/(10^{-3} K^{-1})[b]	c/(10^5 K^2)[b]
CO_2 (g)	-393.5	-392.2	44.22	8.79	-8.62
C_2H_4 (g)	52.4	53.9	39.29	57.13	-13
CO (g)	-110.53	-109.5	30.96	2.44	-2.8
CH_4 (g)	-74.6	-73.3	11.93	77.65	1.4
HCOOH (l)	-425	-421.5	99.16	N/A	N/A
H_2O (l)	-285.83	-283.2	20.36	109.2	20.3
H^+ (aq)	0	0	0[a]	N/A	N/A
H_2 (g)	0	1.0	26.88	3.59	1.1

[a]Data source: Lange's Handbook of Chemistry [95];

[b]Data source: Thermochemical Data of Elements and Compounds [96].

Table 3.3 Calculated standard enthalpies of possible reactions in the electrochemical CO_2 reduction at 298.15 and 333.15 K

Reactions	Δ_rH^0 (298.15 K) (kJ/mol)	Δ_rH^0 (333.15 K) (kJ/mol)	Δ_rH^0 changes[a] (kJ/mol)
CO_2 (g) + 2H$^+$ + 2e$^-$ = CO (g) + H_2O (l)	-2.86	-0.55	2.31
CO_2 (g) + 8H$^+$ + 8e$^-$ = CH_4 (g) + 2H_2O (l)	-252.76	-247.51	5.25
2CO_2 (g) + 12H$^+$ + 12e$^-$ = C_2H_4 (g) + 4H_2O (l)	-303.92	-294.52	9.4
CO_2 (g) + 2H$^+$ + 2e$^-$ = HCOOH (l)	-31.5	-29.37	2.13
2H$^+$ + 2e$^-$ = H_2 (g)	0	1.02	1.02

[a]Δ_rH^0 changes from Δ_rH^0 (298.15 K) to Δ_rH^0 (333.15 K).

3.6 Summary

The electrochemical reductions of $KHCO_3$ and/or $NaHCO_3$ with very high HCO_3^- concentrations (up to 4.0 mol/L) at elevated temperatures were investigated. Summaries of these results were given as follow:

1. The voltammetry studies showed that the current density in the electrochemical reduction of $KHCO_3$ and/or $NaHCO_3$ was strongly affected by the HCO_3^- concentration. Increasing the HCO_3^- concentration remarkably enhanced the current density.

2. There is no big difference in the voltammograms obtained in the solutions with same HCO_3^- concentration but different Na^+ and K^+ concentration, which suggested that the Na^+ and K^+ did not obviously affect the electrochemical reaction.

3. Temperature increase can also promote the current density. However, compared with the HCO_3^- concentration, temperature increase had a less effect on the current density enhancement. This probably because the temperature did not change too much compared with the HCO_3^- concentration variation.

4. H_2 evolution reaction often companies the electrochemical CO_2 reduction in aqueous solutions. Results from the calculation of standard enthalpies of possible reactions in the electrochemical CO_2 reduction showed that the reactions of CO_2 reduction were exothermic while the H_2 evolution was endothermic at elevated temperature. This suggested that elevated temperature should benefit the H_2 evolution while prohibit the CO_2 reduction. Therefore, whether the current density increase was attributed to the CO_2 reduction or H_2 evolution should be investigated by the products analysis.
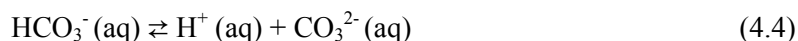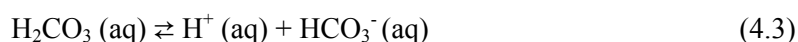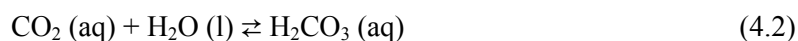
Chapter 4

Study of the active species in the electrochemical reduction of KHCO$_3$ without CO$_2$ bubbling

4.1 Introduction

In Chapter 3, the electrochemical reduction of $KHCO_3$ and/or $NaHCO_3$ without CO_2 bubbling was studied by the I-V measurement. Although the current density was strongly promoted by the high HCO_3^- concentration, the products analysis is required to distinguish whether the CO_2 reduction was promoted. Since there was no CO_2 bubbling used during the electrochemical reaction, the active species for the CO_2 reduction also needed to be studied.

In photoelectrochemical or electrochemical reduction of CO_2 in aqueous solutions, CO_2 bubbling is always used during these reactions and regarded as a carbon source [54,65,78,87]. However, CO_2 can dissolve in and react with H_2O to form H_2CO_3, which further decomposes into HCO_3^- and CO_3^{2-}, as shown in reactions 4.1 to 4.4 [91].

$$CO_2 \text{ (g)} \rightleftarrows CO_2 \text{ (aq)} \tag{4.1}$$

$$CO_2 \text{ (aq)} + H_2O \text{ (l)} \rightleftarrows H_2CO_3 \text{ (aq)} \tag{4.2}$$

$$H_2CO_3 \text{ (aq)} \rightleftarrows H^+ \text{ (aq)} + HCO_3^- \text{ (aq)} \tag{4.3}$$

$$HCO_3^- \text{ (aq)} \rightleftarrows H^+ \text{ (aq)} + CO_3^{2-} \text{ (aq)} \tag{4.4}$$

Therefore, there are four different carbonaceous species in aqueous solutions, which are dissolved CO_2, H_2CO_3, HCO_3^-, and CO_3^{2-}. The actual active species in the electrochemical or photoelectrochemical reduction of CO_2 need to be clarified to further study the mechanism of CO_2 reduction and improve reduction efficiency. However, there have been very few studies on the active species in the electrochemical reduction of CO_2.

In 1983, Hori reported that $HCOO^-$ was found in the electrochemical reduction of HCO_3^- without CO_2 bubbling at room temperature with an Hg electrode [83]. The CO_2 dissociated from HCO_3^- was suggested as the active species for the $HCOO^-$ production [83]. However, recently, HCO_3^- rather than CO_2 was reported as the active species for $HCOO^-$ production in the electrochemical reduction of HCO_3^- with or without CO_2 bubbling at Pb or Cu electrodes [67,84]. Therefore, the active species are probably CO_2 and/or HCO_3^- according to these reports. However, the actual active species is still not clear.

If HCO_3^- is the active species in the electrochemical reduction of CO_2/HCO_3^- without CO_2 bubbling, increasing the concentration of HCO_3^- should promote CO_2 reduction. Therefore, we investigated the gas products after the electrochemical reduction of very high concentration of $KHCO_3$ electrolyte without CO_2 bubbling, and studied the active species in this reaction. The temperature increase reduces the solubility of CO_2 gas while improving the solubility of $KHCO_3$ in water, as shown in Fig 4.1[92]. Therefore, an elevated temperature (up to 60^oC) was used to decrease the effect of dissolved CO_2 and make high-concentration $KHCO_3$ electrolyte easier to prepare.
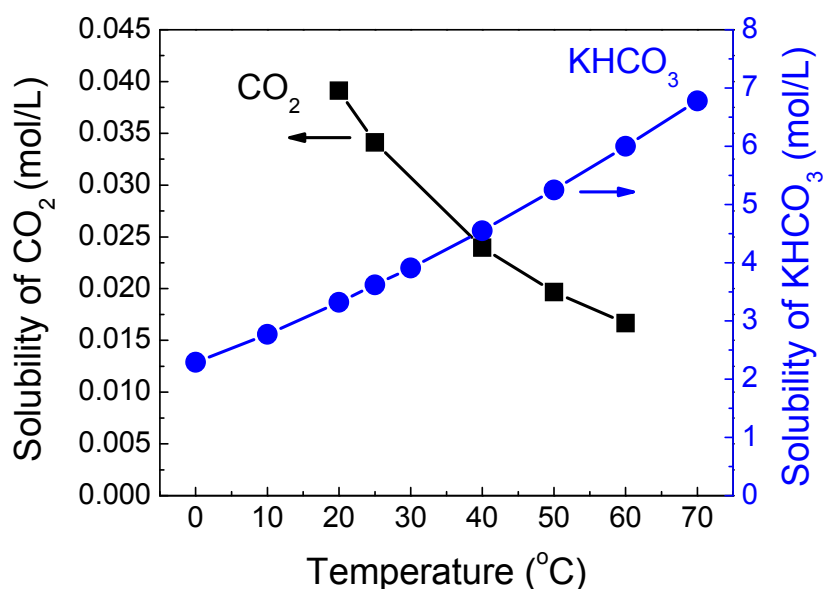
Fig. 4.1 Solubility of CO_2 and $KHCO_3$ in water as function of temperature (partial pressure of CO_2: 100 kPa) (data source: CRC Handbook of Chemistry and Physics (90th Edition) [92])**.**

4.2 Experimental

Schematic drawing of the home-made leak-tight H-type glass electrochemical cell used in this chapter is shown in Fig. 4.2. The working electrode and counter electrode were

separated with a Nafion film (DuPont: N117) in the H-type cell. A copper wire (Φ 0.5 mm, 99.999%, Nilaco) was used as the working electrode. The length of the working electrode was 44 mm. Thus, the surface area of the working electrode was 0.69 cm^2. The native copper oxide was removed from the wire by etching for 60 s in 0.1 mol/L aqueous HCl solution. The reference electrode was a standard Ag/AgCl (3.0 mol/L NaCl) electrode (RE-1B, ALS Co., Ltd). All the potentials in this research are referred to Ag/AgCl unless otherwise specified. A Pt wire (Φ 0.5 mm, Nilaco) with the same length as the working electrode was selected as the counter electrode. Chemical of KHCO$_3$ (99.5%, Kanto chemical Co., Inc) was used directly without any purification. The electrolytes were produced by mixing the chemicals with deionized water (18.2 MΩ, Organo Corporation, PRA-0015). The volume of the electrolytes was 35 mL in both compartments of H-type cell. We did not use CO$_2$ bubbling in this research. The chemicals used in this chapter were summarized in Table 4.1.
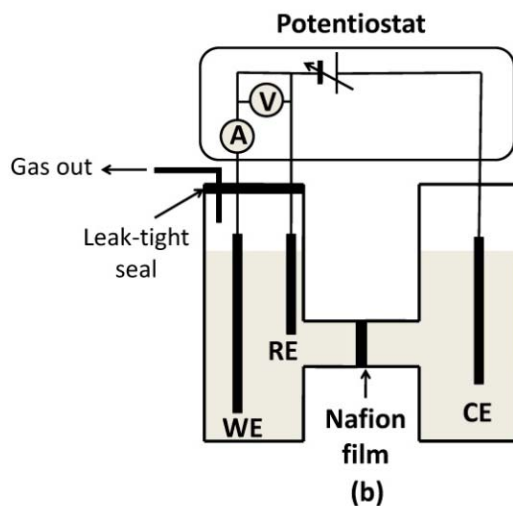
Fig. 4.2 Schematics of the H-type leak-tight electrochemical reaction cell.

Table 4.1 Materials used in Chapter 4

Entry	Item	Specification	Producer
1	Cu wire	99.999%, Φ 0.5 mm	The Nilaco Corporation
2	Pt wire	99.999%, Φ 0.5 mm	The Nilaco Corporation
3	$KHCO_3$	99.5%	Kanto chemical Co., Inc
4	HCl	0.1 mol/L	Kanto chemical Co., Inc
5	Deionized water	18.2 MΩ,	Organo Corporation (PRA-0015)
6	Ar gas	99.9999%	Taiyo Nippon Sanso Corporation

All the electrochemical experiments were conducted using a Solartron 1280C electrochemical system. A water bath (EWS-100RD, AS ONE Corporation) was used for temperature control. After the reactions, the gas samples were collected and analyzed using a customized Agilent 7890A gas chromatographer equipped with a thermal conductivity detector (GC/TCD). This GC system can be used for both online and offline test. In this chapter, an offline mode was used. Due to the special design of this GC analysis system, over 20 mL sample gas is required for one measurement in the offline mode. H_2, CO, CH_4, C_2H_4, and CO_2 can be detected in one measurement, which is usually not available for normal GC/TCDs. If the gas production was less than 20 mL after the reaction, the gas sample was collected and diluted into 20 mL with Ar gas using two syringes. The mixed gas sample was then sealed in the syringe and waited for 10 minutes before being finally injected into the GC. The gas analysis method used in the GC/TCD is shown in Table 4.2.

Table 4.2 Analysis method of GC/TCD

Detectors	Thermal Conductivity Detector (TCD)
	(Back TCD & Side TCD)
Column	Column #1: MS5A 8ft
	Column #2: HAYASEP Q 3ft
	Column #3: HAYASEP Q 0.5m
	Column #4: HAYASEP Q 6ft
	Column #5: MS5A 8ft
Carrier gas	Side TCD: Ar (99.9999%) (for: H_2)
	Back TCD: He (99.99995%) (for: CO, CO_2, CH_4, C_2H_4,
	C_2H_6,)
Reference flow rate	Side TCD: 30 mL/min
	Back TCD: 45 mL/min
Inlet temperature	120 °C
Detector temperature	200 °C
Oven temperature	60 °C for 1 min,
	then 20 °C/min to 150 °C for 0 min,
	then 12 °C/min to 170 °C for 0 min,
	then 30 °C/min to 190 °C for 2 min
Sample injection amount	20~40 mL

The faradaic efficiency (FE) was used to evaluate the product selectivity. The faradaic efficiency is calculated as follow:

$$FE = \frac{n_{product} \times n_{electron} \times F}{Q} \times 100\% \qquad (4.5)$$

where, $n_{product}$ means the molar amount of target product, $n_{electron}$ represents electron transfer number per molecule (for CO, n = 2; CH_4, n = 8; C_2H_4, n = 12; H_2, n = 2), F is the faradaic constant (96485.3 C/mol), Q is the total electron transferred during the whole reaction.

4.3 Effect of KHCO₃ concentration, temperature and applied potential on the product selectivity

Gas products after the electrochemical reduction of 0.1 and 3.0 mol/L $KHCO_3$ for 60 min at -1.6 V and various temperatures were analyzed to study the effect of $KHCO_3$ concentration and temperature. The volumes of the gas generated after the reactions are listed in Table 4.3. Results showed that H_2 was the main product after the reactions no matter what temperature or $KHCO_3$ concentration were used. The volume of H_2 increased nearly 10 times as the $KHCO_3$ concentration increased from 0.1 to 3.0 mol/L. Although the temperature increase also improved H_2 production, the effect was much smaller compared with that of $KHCO_3$ concentration. This was possibly because the change of temperature was small compared with the $KHCO_3$ concentration. As a result, the high current density obtained at high $KHCO_3$ concentration and temperature discussed in chapter 3 was mainly attributed to H_2 evolution. However, CO, CH_4, and C_2H_4 were detected in the gas phase after the electrochemical reduction of 3.0 mol/L $KHCO_3$ at 40 and 60°C even without CO_2 bubbling. It should be noted that only formate production was reported in previous studies of electrochemical reduction of HCO_3^- without CO_2 bubbling [83,84]. Faradaic efficiencies of these gas products after the electrochemical reactions were calculated and listed in Table 4.4. The faradaic efficiency of CO_2 reduction represents the sum of CO, CH_4, and C_2H_4. In the 3.0 mol/L $KHCO_3$, there was no CO_2 reduction observed at 20 °C. However, when the temperature increased to 40 and 60 °C, the faradaic efficiencies of CO_2 reduction increased to 0.51% and 0.66%, respectively. This suggested that elevated temperature can promote the reduction of CO_2 (or HCO_3^-). When the concentration of $KHCO_3$ decreased from 3.0 to 0.1 mol/L and the temperature remained at 60 °C, the CO_2 reduction was not detected. This suggests that high $KHCO_3$ concentration is necessary in the electrochemical reduction of $KHCO_3$ without CO_2 bubbling.

The liquid samples after the electrochemical reduction of 3.0 mol/L $KHCO_3$ at -1.6 V for 60 min without CO_2 bubbling was measured by ion chromatography for HCOOH. However, there was no HCOOH detected in the liquid phase.

Table 4.3 Volumes of different products after the electrochemical reactions at various temperatures and $KHCO_3$ concentrations[a]

$KHCO_3$ (mol/L)	Temp (^oC)	Volume (mL)			
		CO	CH_4	C_2H_4	H_2
3.0	20	N/D[b]	N/D	N/D	24.49
3.0	40	0.039	0.010	0.008	25.16
3.0	60	0.038	N/D	0.024	26.7
0.1	60	N/D	N/D	N/D	2.89

[a]Reaction condition: Potential: -1.6 V (vs. Ag/AgCl), time: 60 min.

[b]N/D: not detected (detect limitation: 10 ppm).

Table 4.4 Faradaic efficiencies of different products after the electrochemical reactions at various temperatures and $KHCO_3$ concentrations[a]

$KHCO_3$ (mol/L)	Temp (^oC)	Faradaic efficiency (%)					
		CO	CH_4	C_2H_4	CO_2 reduction[b]	H_2	Total
3.0	20	N/D[c]	N/D	N/D	N/D	93.1	93.1
3.0	40	0.16	0.16	0.19	0.51	104.9	105.4
3.0	60	0.14	N/D	0.52	0.66	96.7	97.4
0.1	60	N/D	N/D	N/D	N/D	97.0	97.0

[a]Reaction condition: Potential: -1.6 V (vs. Ag/AgCl), time: 60 min.

[b]CO_2 reduction is the sum of CO, CH_4 and C_2H_4.

c N/D: not detected (detect limitation: 10 ppm).

It is reported that the applied potential strongly affects the product selectivity in the electrochemical reduction of CO_2 [54,97]. Therefore, the effect of applied potential on product selectivity was investigated by conducting the electrochemical reactions in 3.0 mol/L $KHCO_3$ without CO_2 bubbling at 60 ^oC for 60 min at various potentials. The faradaic efficiencies of the products after the reactions are shown in Fig. 4.3. The main product was H_2, which composed over 90% of the faradaic efficiency at the applied potential ranged from -1.4 to -1.8 V. The faradaic efficiency of H_2 increased with negative applied potential, which means more negative potential promotes hydrogen evolution and prohibits CO_2 reduction. The faradaic efficiency of CO was 5.1% at -1.4 V and reduced greatly with the negative increase in potential. The faradaic efficiency of C_2H_4 first increased with negative potential

and then decreased when the applied potential exceeded -1.6 V. For CH_4 production, there was no CH_4 detected at -1.4 and -1.6 V, and very few amount of CH_4 (faradaic efficiency: approx. 0.07%) was detected at -1.8 V. The highest faradaic efficiency of CO_2 reduction (CO + CH_4 + C_2H_4) of 5.2% was achieved at -1.4 V and 60 ^{o}C in 3.0 mol/L $KHCO_3$.
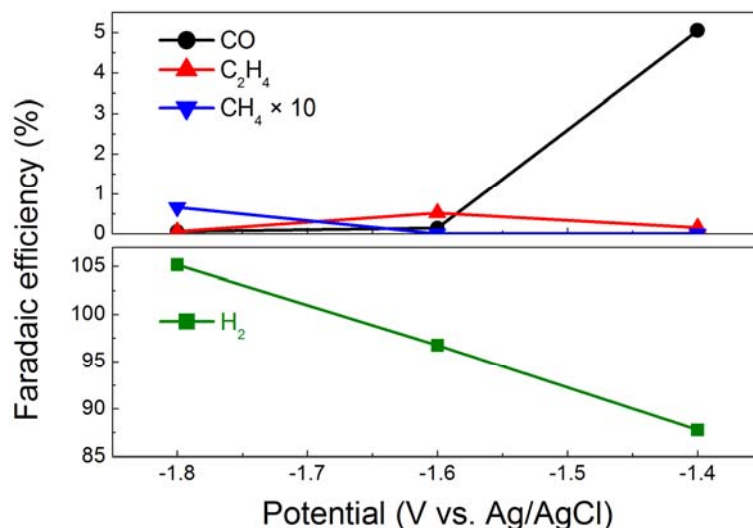
Fig. 4.3 Faradaic efficiencies of gas products after electrochemical reactions at various applied potentials (reaction condition: electrolyte: 3.0 mol/L $KHCO_3$, temp: 60 ^{o}C, reaction time: 60 min).

4.4 Study of active species

According to the discussion in Section 4.3, CO_2 reduction can be achieved in the electrochemical reduction of $KHCO_3$ even without CO_2 bubbling, however, the production and faradaic efficiencies are very low. If assuming that HCO_3^- is the active species, high $KHCO_3$ concentration should lead to high CO_2 reduction. However, results in Table 4.3 showed that increasing the $KHCO_3$ concentration strongly promoted the H_2 evolution rather than CO_2 reduction. Therefore, the active species in the electrochemical reduction of $KHCO_3$ without CO_2 bubbling was probably not HCO_3^-. Then, the active species was probably the

dissolved CO_2, which was generated from the decomposition of HCO_3^-, since it is the only carbon source. Possible reaction pathway for the decomposition of HCO_3^- into CO_2 was the HCO_3^- first reacting with H_2O to generate H_2CO_3 and OH^- as shown in reaction 4.6.

$$HCO_3^- \text{ (aq)} + H_2O \text{ (l)} \rightleftarrows H_2CO_3 \text{ (aq)} + OH^- \text{ (aq)} \qquad (4.6)$$
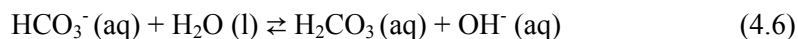
It is well known that very few H_2CO_3 exists in the water solutions because it is easy to transform to dissolved CO_2 as shown in reaction 4.7 [91].

$$H_2CO_3 \text{ (aq)} \rightleftarrows H_2O \text{ (l)} + CO_2 \text{ (aq)} \qquad (4.7)$$
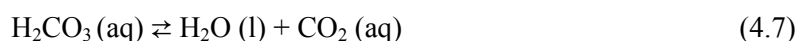
Therefore, the overall reaction for the decomposition HCO_3^- (aq) into CO_2 should be the sum of reaction 4.6 and 4.7, which is

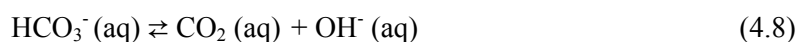$$HCO_3^- \text{ (aq)} \rightleftarrows CO_2 \text{ (aq)} + OH^- \text{ (aq)} \qquad (4.8)$$

To confirm the reaction 4.8, spontaneous gas generation from the decomposition of HCO_3^- in different concentrations of $KHCO_3$ solutions (35 mL) at various temperatures were measured. The gas volumes were always measured at room temperature (25^oC), even the temperature of $KHCO_3$ solution was different. The gas chromatography (GC) quantitative analysis showed that only CO_2 was generated during the experiments. The results of CO_2 generation are shown in Fig. 4.4. In 0.1 mol/L $KHCO_3$ at 25 ^oC, very few CO_2 was produced. The volume of the CO_2 gas was only *ca* 2 mL after 50 min. When the $KHCO_3$ concentration increased to 3.0 mol/L, the CO_2 generation slightly increased to about 3.5 mL after 50 min. This suggested that high HCO_3^- concentration could promote the decomposition of HCO_3^- into CO_2, however, the effect was not strong. When the temperature of 3.0 mol/L $KHCO_3$ solution ascended to 60 ^oC, a sharp increase in the CO_2 generation was observed. Over 45 mL CO_2 was generated after 50 min. These results showed that elevated temperature strongly promoted CO_2 generation due to the decomposition of HCO_3^-, this probably due to the solubility of CO_2 decreased as the temperature increasing (Fig. 4.1). The reaction of dissolved CO_2 transforming into gaseous CO_2 was shown below,

$$CO_2 \text{ (aq)} \rightleftarrows CO_2 \text{ (g)} \qquad \Delta_r H^0(298.15) = 19.76 \text{ kJ/mol} \qquad (4.9)$$
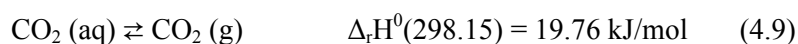
The calculated standard enthalpy of this reaction at 298.15 K is 19.76 kJ/mol. Meanwhile, the standard enthalpy of reaction 4.8 is calculated to be 46.6 kJ/mol. These results indicate that reaction 4.8 and 4.9 are endothermic, which means increasing the temperature enhance the decomposition of HCO_3^- into gaseous CO_2. As a result, high temperature promotes the decomposition of HCO_3^- into CO_2. Compared with $KHCO_3$ concentration, temperature had a much stronger effect.
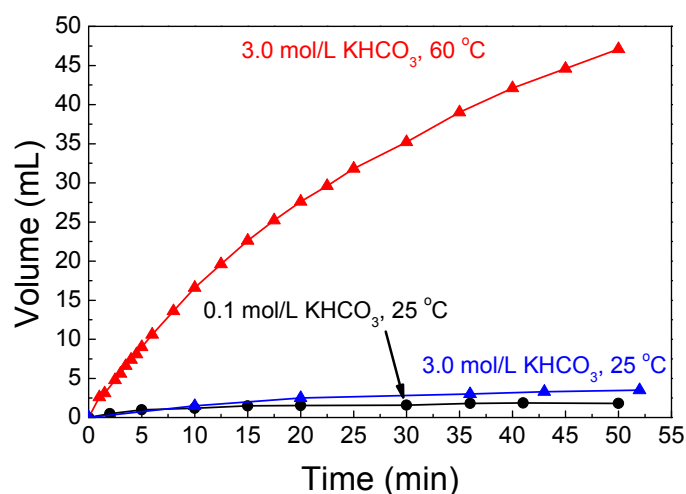
Fig. 4.4 CO_2 generation from the decomposition of different concentrations of 35 mL $KHCO_3$ at various temperatures as function of time (gas volumes were measured at $25^\circ C$, 1 atm).

In reaction 4.8, the reaction rate of HCO_3^- decomposition can be written as

$$v = -\frac{d[HCO_3^-]}{dt} = k[HCO_3^-]^n \qquad (4.10)$$

where,

v is the reaction rate,

$[HCO_3^-]$ is the concentration of HCO_3^- in the solution,

k is the reaction rate constant at given temperature,

n is the reaction order.

If the reaction order n is 0, $[HCO_3^-]$ should vary linearly with time. If the reaction order n is 1 or 2, $Ln[HCO_3^-]$ or $1/[HCO_3^-]$ should change linearly with time, respectively. Therefore, the

reaction order of reaction 4.8 can be determined by checking the linearity of $[HCO_3^-]$ – t, $Ln[HCO_3^-]$ – t, and $1/[HCO_3^-]$ – t. Since the volume of CO_2 production was measured, if assuming 1 mol CO_2 production requires 1 mol HCO_3^-, which means there is no other reactions, the change of $[HCO_3^-]$ versus time can be calculated using the CO_2 production data. Then the reaction order n of reaction 4.8 can be investigated. The relationships of $[HCO_3^-]$ – t, $Ln[HCO_3^-]$ – t, and $1/[HCO_3^-]$ – t obtained in 0.5 mol/L $KHCO_3$ at 60 ^{o}C were plotted in Fig. 4.5. However, from these results, it is hard to distinguish which relationship is more linear, which means the reaction order can hardly be determined here. This was probably because the $[HCO_3^-]$ variation was so small compared with the original $[HCO_3^-]$. Therefore, all the relationships showed a relatively good linearity.
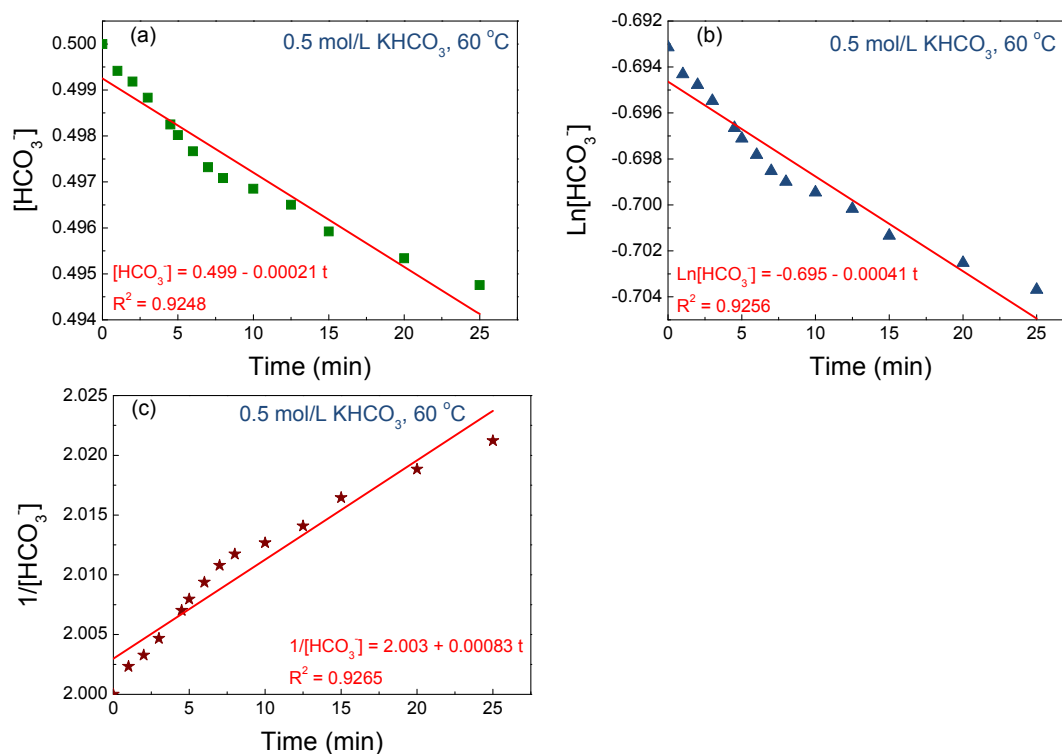
Fig. 4.5 $[HCO_3^-]$ (a), $Ln[HCO_3^-]$ (b), and $1/[HCO_3^-]$ (c) variations as function of time obtained in 0.5 mol/L $KHCO_3$ at 60 ^{o}C.

If assuming the decomposition of HCO_3^- into CO_2 is a one order reaction, the rate

equation can be written as

$$v = -\frac{d[HCO_3^-]}{dt} = k[HCO_3^-] \quad\quad (4.11)$$

Integrate this equation, one can obtain

$$Ln[HCO_3^-] = -kt + C \quad\quad (4.12)$$

where C is the constant of integration. Therefore, the rate constant k at different temperatures can be obtained from the slope of the $Ln[HCO_3^-]$ – t plot at different temperatures. The $Ln[HCO_3^-]$ – t plots with their linear fitting curves in 3.0 mol/L $KHCO_3$ solutions at 25, 40, 50, and 60 ^oC were depicted in Fig. 4.6. From the linear fitting curves obtained from the experimental data, the reaction rate constant of the decomposition of HCO_3^- into CO_2 (reaction 4.8) were 0.3163×10^{-4}, 1.0909×10^{-4}, 1.7417×10^{-4}, and $4.9885\times10^{-4}\,s^{-1}$ at 25, 40, 50, and 60 ^oC, respectively.
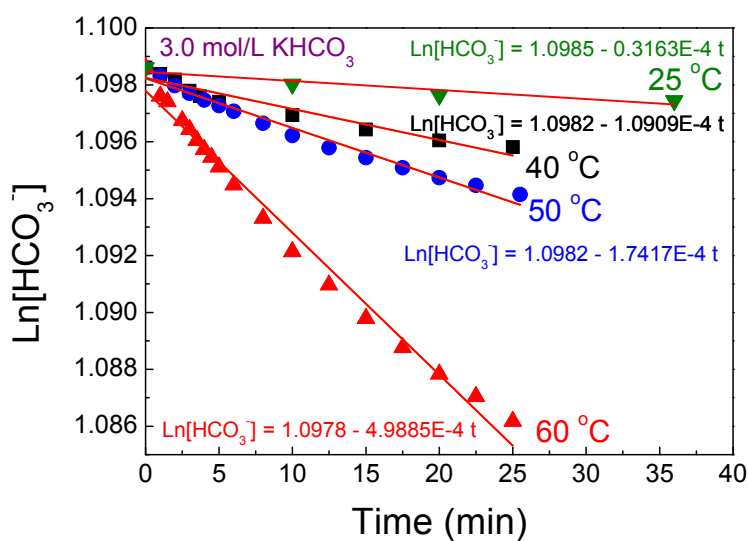
Fig. 4.6 $Ln[HCO_3^-]$ variations with time and their linear fittings obtained in 3.0 mol/L $KHCO_3$ at different temperatures (E–4 represents $\times10^{-4}$).

The rate constant k is defined as

$$k = Ae^{-E_a/RT} \qu\quad (4.13)$$

where,

A is the pre-exponential factor,

E_a is the activation energy,

R is the ideal gas constant,

T is the absolute temperature.

After taking the natural logarithm of both sides of Eq. 4.13, one can obtain

$$\ln k = \ln A - \frac{E_a}{R}\frac{1}{T} \tag{4.14}$$

Then, the activation energy of E_a can be solved from the slope of the ln k – 1/T curve. Fig 4.7 shows the ln k as function of 1/T and its linear fitting line. The slope of the linear fitting line is –7520.2, which represents the value of –E_a/R. Therefore, the activation energy of the decomposition of HCO_3^- into CO_2 (reaction 4.8) was 62.5 kJ/mol according to the experimental results.
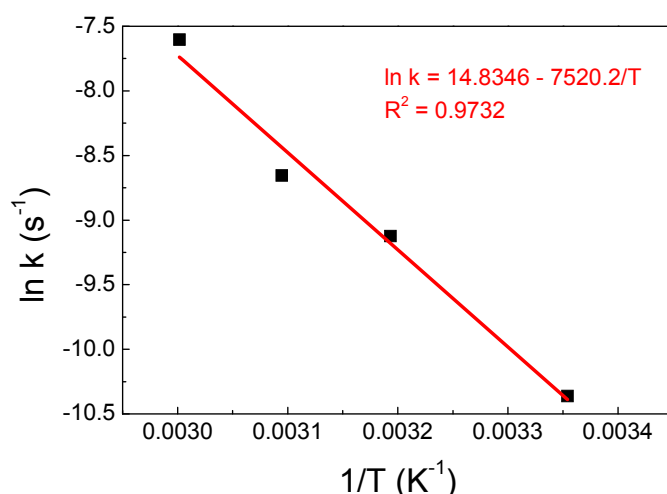
Fig. 4.7 *Ln* k variation as function of 1/T obtained in 3.0 mol/L $KHCO_3$.

It should be noted that in reaction 4.8, OH^- is generated in the decomposition of HCO_3^- into CO_2, which would lead to a pH increase in the solution. However, HCO_3^- is well known as a buffer solution, which can easily react with OH^- to produce CO_3^{2-} at high pH as shown below,

$$HCO_3^- \text{ (aq)} + OH^- \text{ (aq)} \rightleftarrows CO_3^{2-} \text{ (aq)} + H_2O \text{ (l)} \qquad (4.15)$$
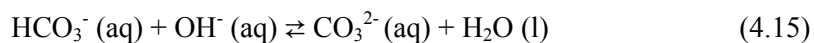
Combining reaction 4.8 and 4.15, the overall reaction in the decomposition of HCO_3^- into CO_2 should be

$$2HCO_3^- \text{ (aq)} \rightleftarrows CO_3^{2-} \text{ (aq)} + CO_2 \text{ (aq)} + H_2O \text{ (l)} \qquad (4.16)$$
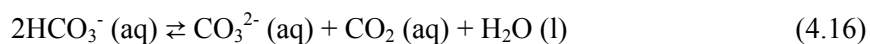
Fig. 4.8 shows the pH changes in 3.0 mol/L $KHCO_3$ solution with time at 60 ^{o}C. The $KHCO_3$ solution reached the required temperature of 60 ^{o}C within 10 min after being put into the water bath (60.1 ^{o}C) and remained stable thereafter. The initial pH of $KHCO_3$ was 8.59, which was caused by the reaction of HCO_3^- with H_2O, as shown in reaction 4.6. The equilibrium constant K_1 of reaction 4.6 is $10^{-7.65}$ at 25 ^{o}C [92]. As the temperature of $KHCO_3$ solution increased from room temperature to 60 ^{o}C, the pH of the $KHCO_3$ solution reduced from 8.59 to 8.37. This was caused by the decrease in the ion product of water (K_w) from 14.0 to about 13.1 when the temperature increased from 25 to 60 ^{o}C, which means both $[H^+]$ and $[OH^-]$ decreased with the increase in temperature [92]. When the temperature of the $KHCO_3$ solution remained at 60 ^{o}C, the pH of the solution gradually increased with time from 8.37 to 8.50 after 60 min.
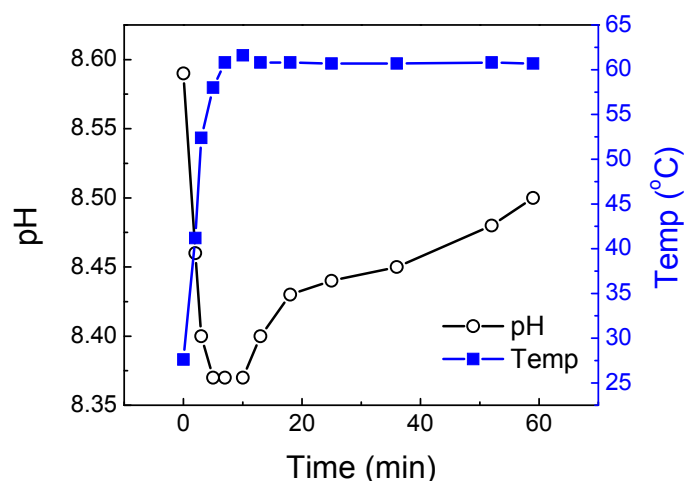
Fig. 4.8 pH and temperature changes of 3.0 mol/L $KHCO_3$ in 60°C water bath as function of time.

According to reaction 4.16, part of the HCO_3^- transformed into CO_3^{2-} during the decomposition of HCO_3^- into CO_2. The equilibrium constant K_2 of CO_3^{2-} reacting with H_2O (reaction 4.17) is $10^{-3.67}$ at 25 ^{o}C [92], which is more than 9500 times higher than K_1. This suggested that more OH^- was produced when HCO_3^- transformed into CO_3^{2-}, which then caused the pH of the $KHCO_3$ solution increase.

$$CO_3^{2-} \text{ (aq)} + H_2O \text{ (l)} \rightleftarrows HCO_3^- \text{ (aq)} + OH^- \text{ (aq)} \tag{4.17}$$

Therefore, the active species in the electrochemical reduction of $KHCO_3$ without CO_2 bubbling was probably CO_2, which was generated *in-situ* from the decomposition of HCO_3^-.

4.5 Summary

The electrochemical reduction of CO_2 in $KHCO_3$ solutions on a Cu working electrode at elevated temperatures without CO_2 bubbling was investigated in an H-type cell, and the gas products were analyzed. The activation energy of the decomposition of HCO_3^- into CO_2 was also calculated. Summaries of this chapter can be given as:

1. Although H_2 was the main product in all cases (faradaic efficiency over 90%), CO, CH_4, and C_2H_4 were detected in 3.0 mol/L $KHCO_3$ at 40 and 60 ^{o}C after 60 minutes' electrochemical reaction.

2. High $KHCO_3$ concentration and elevated temperature are necessary to obtain CO_2 reduction in the electrochemical reactions without CO_2 bubbling. This is because high $KHCO_3$ concentration and elevated temperature strongly promoted the CO_2 generation from the decomposition of HCO_3^-.

3. The decomposition of HCO_3^- into CO_2 provided the source of CO_2 reduction when no CO_2 bubbling was used. The reaction pathway of the HCO_3^- decomposition is probably

$$HCO_3^- \text{ (aq)} \rightleftarrows CO_2 \text{ (aq)} + OH^- \text{ (l)}$$

4. The reaction order of the decomposition of HCO_3^- into CO_2 was hard to be determined from the experimental results due to the HCO_3^- consumption was extremely low. If assuming
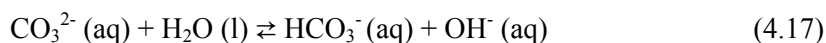
the decomposition of HCO_3^- was one order, the activation energy of this reaction was calculated to be 62.5 kJ/mol according to the experimental data.

5. The active species in the electrochemical reduction of $KHCO_3$ without CO_2 bubbling was probably the dissolved CO_2 rather than HCO_3^-.

Chapter 5

Electrochemical reduction of CO_2 in $KHCO_3$, KCl and KOH electrolytes under CO_2 bubbling

5.1 Introduction

Chapter 3 and 4 discussed the electrochemical reduction of CO_2 in $KHCO_3$ without CO_2 bubbling. Although CO, CH_4 and C_2H_4 were produced even without CO_2 bubbling, the faradaic efficiencies of these products were very low (<5%). Since CO_2 rather than HCO_3^- was the real active species in the electrochemical reduction of $KHCO_3$ solution, CO_2 bubbling was necessary to promote the CO_2 reduction. Therefore, the electrochemical reduction of CO_2 in different electrolytes, especially in $KHCO_3$, with CO_2 bubbling on Cu working electrode at various applied potentials were studied in this chapter.

Bicarbonate aqueous solutions, such as $KHCO_3$ and $NaHCO_3$, have been widely used as the supporting electrolytes in the electrochemical and photoelectrochemical reduction of CO_2 [54,83,90,98,99]. However, very few reports discussed the effect of bicarbonate ion concentration on the CO_2 reduction. Hori studied the effect of $KHCO_3$ concentration (ranging from 0.03 to 1.5 mol/L) on the electrochemical reduction of CO_2 at a Cu working electrode using galvanostatic method (current density = 5 mA/cm^2) [54]. It is reported that $KHCO_3$ concentration strongly affected the product selectivity and faradaic efficiency of CO_2 reduction [54]. The best faradaic efficiency of CO_2 reduction was obtained in 0.1 mol/L $KHCO_3$, higher or lower $KHCO_3$ concentration leads to a faradaic efficiency of CO_2 reduction decrease [54]. However, the electrolytes with lower $KHCO_3$ concentration have lower conductivity. If maintaining the current the same, the applied potentials should be much higher in low $KHCO_3$ concentration solution compared with that in higher $KHCO_3$ concentration solution. It is well known that the applied potential strongly affected the product selectivity in the electrochemical reduction of CO_2 [59,97]. Therefore, galvanostatic study, as reported by Hori [54], of the effect of $KHCO_3$ concentration on the electrochemical CO_2 reduction should be less appropriate than a potentiostatic method due to the potential effect. Hence, the effect of the $KHCO_3$ concentration on the CO_2 reduction was examined by comparing the optimum faradaic efficiency of CO_2 reduction in different $KHCO_3$ solutions using potentiostatic method at various potentials in this chapter.

5.2 Experimental

5.2.1 Materials.

The experimental materials used in this chapter were listed in Table 5.1. Copper wire (Φ 0.5 mm, 99.999%, Nilaco) and Pt wire (Φ 0.5 mm, 99.999%, Nilaco) were used as the working and counter electrode, respectively. Copper foil (99.9999%, 0.1×10×20 mm, Alfa Aesar) with a surface area of ca. 4.3 cm^2 was also used as a working electrode in some cases. The photograph of the Cu foil was shown in Fig. 5.1. If no specific announcement, the working electrode was always referred to the Cu wire working electrode. A standard Ag/AgCl (3.0 mol/L NaCl) electrode (RE-1B, ALS Co., Ltd) was used as the reference electrode. All the potentials in here were referred to this Ag/AgCl reference electrode unless otherwise specified. Chemicals of KHCO$_3$ (99.5%, Kanto chemical Co., Inc) and KCl (99.5%, Kanto chemical Co., Inc) were used directly without any purification to make the supporting electrolytes. The electrolytes were prepared by mixing the chemicals with deionized water (18.2 MΩ) made by Organo PRA-0015 deionized water maker. Carbon dioxide (CO$_2$) gas (99.995%, Taiyo Nippon Sanso Corporation) was used as the source of CO$_2$ during the experiment.

Table 5.1 Materials used in Chapter 5

| Entry	Item	Specification	Producer
1	Cu wire	99.999%, Φ 0.5 mm	The Nilaco Corporation
2	Cu foil	99.9999%, 0.1×10×20 mm	Alfa Aesar
3	Pt wire	99.999%, Φ 0.5 mm	The Nilaco Corporation
4	KHCO$_3$	99.5%	Kanto chemical Co., Inc
6	KCl	99.5%	Kanto chemical Co., Inc
7	KOH	0.1 mol/L	Kanto chemical Co., Inc
8	HCl	0.1 mol/L	Kanto chemical Co., Inc
9	Deionized water	18.2 MΩ,	Organo Corporation (PRA-0015)
10	CO$_2$ gas	99.995%	Taiyo Nippon Sanso Corporation
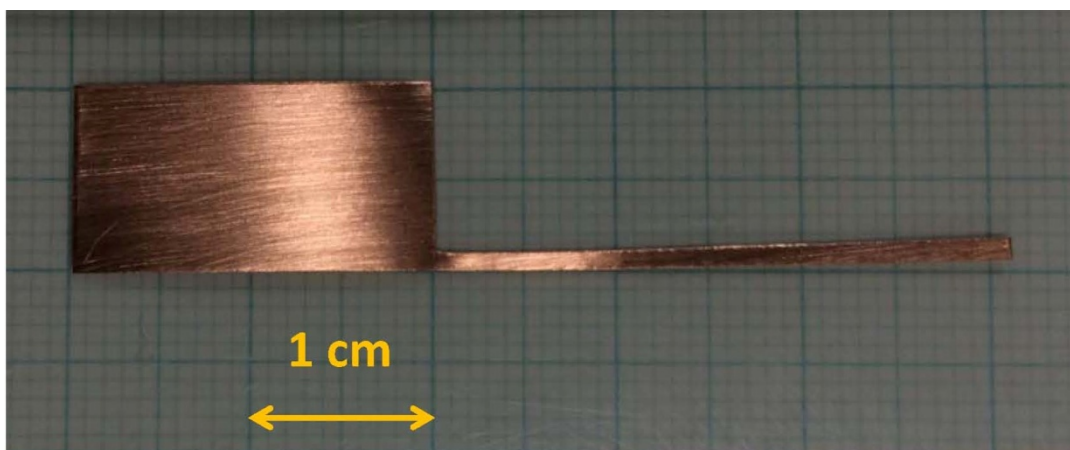
Fig 5.1 Photograph of Cu foil working electrode.

5.2.2 Methods

A home-made leak-tight H-type electrochemical cell was used in this chapter to analysis the effect of the electrolytes in the electrochemical reduction of CO_2. The schematic of this cell is shown in Fig. 5.2. A three electrodes system was used in this electrochemical cell. The working and reference electrodes were put in the same compartment and separated from the counter electrode by a Nafion film (DuPont: N117). The electrolytes in both compartments were identical unless otherwise specified. A Solartron 1280C electrochemical system was used to conduct all the electrochemical experiments. The details of the experimental conditions of the electrochemical reduction of CO_2 are listed in Table 5.2. The lengths of the working and counter electrode was 44 mm. Thus, the surface area of the working electrode was 0.69 cm^2. A typical experimental procedure is as follow. Same amount (35 mL) of electrolyte was added into both WE and CE chambers of the electrochemical cell. Then CO_2 was bubbled into the WE chamber for 30 min with a flow rate of 17.7 mL/min until saturation. The pH values of both chambers were measured then. After removing the native copper oxide from the working electrode (Cu wire or foil) by etching for 60 s in 0.1 mol/L aqueous HCl, the WE, CE and RE were placed in the electrochemical cell. The gas outlet tube was directly connected to an Agilent 7890A gas chromatographer equipped with a thermal conductivity detector (GC/TCD) for online gas analysis. A typical electrochemical reaction time was 60

min. The gas samples were analyzed at 5, 20, 40 and 60 min, respectively. The gas analysis method used in the GC/TCD is shown in Table 5.3. This online gas analyzing system allows the sample gas flow through five different columns and hence can analyze H_2, CO, CO_2, CH_4, C_2H_4, C_2H_6, O_2 and N_2 within one test. The liquid samples were analyzed by an ion chromatography (Tosoh IC-2001, Tosoh Corporation, Japan). The surface morphologies of the Cu wire before and after electrochemical reactions were examined by a Hitachi S-4300 scanning electron microscope (SEM).
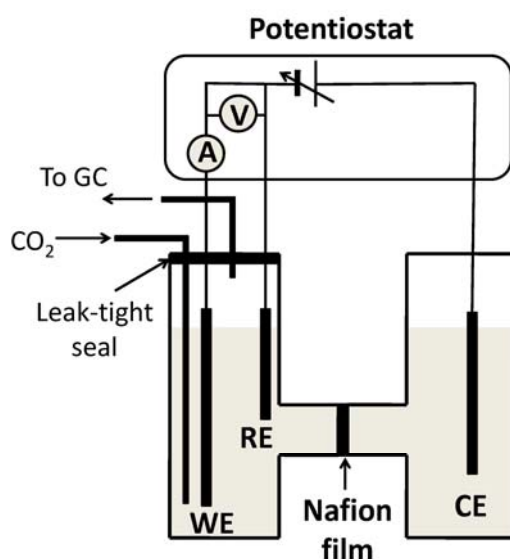
Fig. 5.2 Schematic of leak-tight H-type electrochemical reaction cell.

Table 5.2 Experimental conditions of chapter 5[a]

WE	Cu wire (Φ 0.5 mm, length: 44 mm)
	Cu foil (0.1×10×20 mm)
CE	Pt wire (Φ 0.5 mm, length: 44 mm)
RE	Ag/AgCl (3.0 mol/L NaCl)
Electrolyte	0.01 – 1.5 mol/L $KHCO_3$
	0.1 mol/L KCl
Potential	-1.35 – -2.7 V (*vs.* Ag/AgCl)
Reaction time	60 – 180 min
Temperature	23 – 60 °C
CO_2 flow rate	17.7 mL/min

[a]WE: working electrode, CE: counter electrode, RE: reference electrode.

Table 5.3 Analysis method of GC/TCD

Detectors	Thermal Conductivity Detector (TCD)
	(Back TCD & Side TCD)
	Column #1: MS5A 8ft
	Column #2: HAYASEP Q 3ft
Column	Column #3: HAYASEP Q 0.5m
	Column #4: HAYASEP Q 6ft
	Column #5: MS5A 8ft
	Side TCD: Ar (99.9999%) (for: H_2)
Carrier gas	Back TCD: He (99.99995%) (for: CO, CO_2, CH_4, C_2H_4, C_2H_6,)
Reference flow rate	Side TCD: 30 mL/min
	Back TCD: 45 mL/min
Inlet temperature	120 °C
Detector temperature	200 °C
Oven temperature	60 °C for 1 min
	then 20 °C/min to 150 °C for 0 min
	then 12 °C/min to 170 °C for 0 min
	then 30 °C/min to 190 °C for 2 min
Sample flow rate	17.7 mL/min

5.3 Effect of CO_2 bubbling on the product selectivity at various temperature

The electrochemical reduction of CO_2 in 0.1 and 3.0 mol/L $KHCO_3$ with CO_2 bubbling at 20 and 60 ^{o}C were conducted and the faradaic efficiencies of the gas products were calculated

and compared with those obtained without CO_2 bubbling (in Chapter 4) to study the effect of CO_2 bubbling. The results were shown in Fig 5.3. The applied potential in 0.1 and 3.0 mol/L $KHCO_3$ was -1.6 and -1.4 V, respectively. As discussed in Chapter 4, there was no CO_2 reduction observed in 0.1 mol/L $KHCO_3$ without CO_2 bubbling at 60 $^{\circ}$C, while CO and trace amount of C_2H_4 was found in 3.0 mol/L $KHCO_3$ without CO_2 bubbling at 60 $^{\circ}$C. When the CO_2 bubbling was introduced into the electrolytes, CO_2 reduction was found in 0.1 mol/L $KHCO_3$ and was promoted in 3.0 mol/L $KHCO_3$ at 60 $^{\circ}$C. This further proved that the CO_2 was the active species in the electrochemical reduction of CO_2 in $KHCO_3$ solutions.
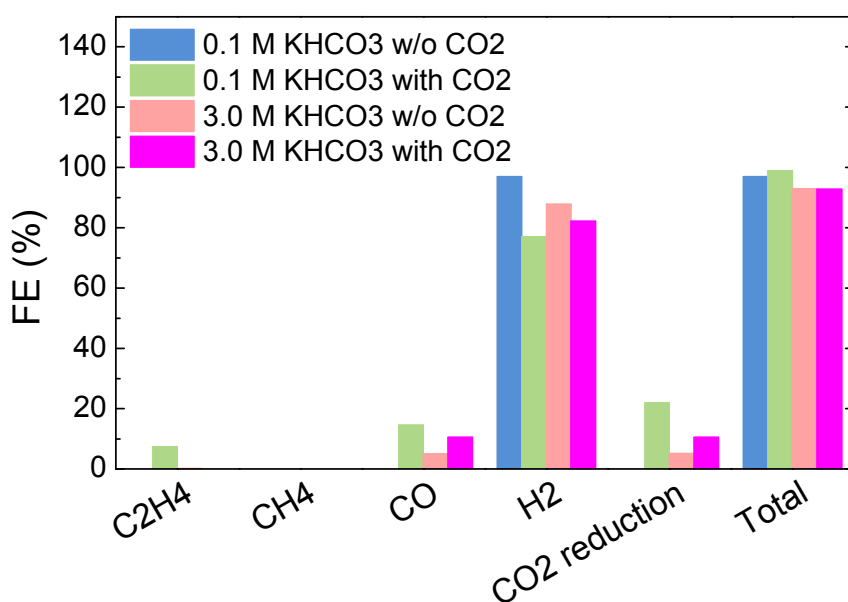
Fig. 5.3 Faradaic efficiencies (FE) of different gas products in the electrochemical reduction of CO_2 in 0.1 and 3.0 mol/L $KHCO_3$ with or without CO_2 bubbling (M: mol/L, reaction temperature: 60 $^{\circ}$C, reaction time: 60 min, CO_2 flow rate: 17.7 mL/min, applied potential: -1.6 V for 0.1 mol/L $KHCO_3$, -1.4 V for 3.0 mol/L $KHCO_3$).

As discussed in Chapter 3, most of the electrochemical CO_2 reduction reactions are exothermic, which suggests elevated temperature is not suitable for the CO_2 reduction. Therefore, the effect of temperature on the product selectivity was studied by carrying out the

experiments of electrochemical reduction of CO_2 in 0.1 mol/L $KHCO_3$ with CO_2 bubbling at -2.1 V for 60 min at 25 and 60 ^{o}C. The results were shown in Fig 5.4. It can be seen that, although CH_4, CO, and C_2H_4 were found in the reaction at 60 ^{o}C, H_2 evolution composed most of the faradaic efficiency. When the temperature decreased to 25 ^{o}C, faradaic efficiency of CO_2 reduction increased tremendously to 37.7% while the faradaic efficiency of H_2 evolution decreased to 44.0%. This result proved that elevated temperature could decrease the CO_2 reduction. Therefore, all the experiments of CO_2 reduction were studied in room temperature then. It also can be seen that the total faradaic efficiency of the gas products was 81.7% at 25 ^{o}C, which was possibly because some liquid products were generated when the temperature decreased. This will be discussed later.

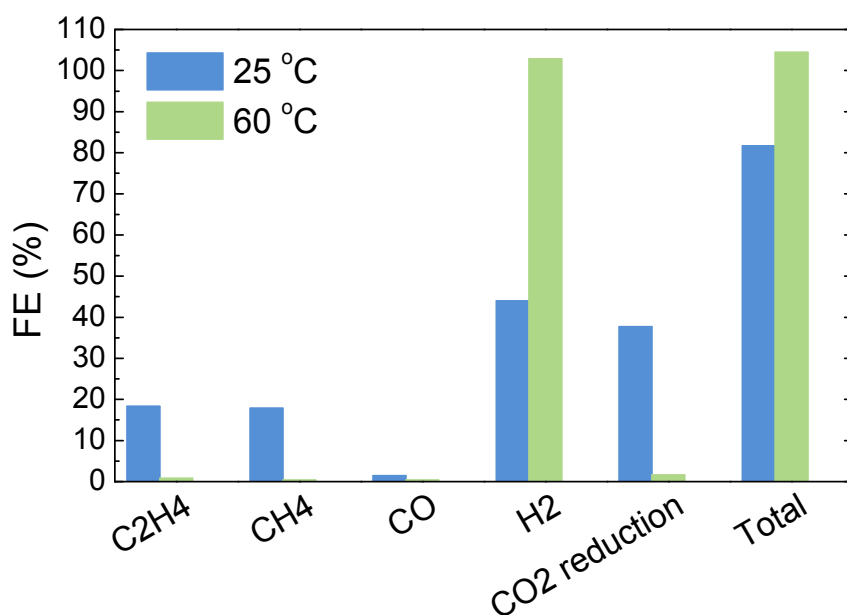**Fig. 5.4** Effect of temperature on the faradaic efficiencies (FE) of different gas products in the electrochemical reduction of CO_2 in 0.1 mol/L $KHCO_3$ with CO_2 bubbling (reaction condition: potential: -2.1 V, reaction time: 60 min, CO_2 flow rate: 17.7 mL/min).

5.4 Effect of different KHCO$_3$ concentrations with CO$_2$ bubbling

The effect of KHCO$_3$ concentration were studied by conducting the electrochemical reduction of CO$_2$ in 0.01, 0.1, 0.5, and 1.5 mol/L KHCO$_3$ electrolytes on a Cu working electrode at 25 ^{o}C for 60 min. The gas samples were measured at 5, 20, 40, and 60 min, respectively. The faradaic efficiencies of different gas products after the electrochemical reduction of CO$_2$ for 40 min in different KHCO$_3$ concentrations at various potentials were shown in Fig 5.5.

In 0.01 mol/L KHCO$_3$ (Fig. 5.5 (a)), H$_2$ was the main product when the applied potential ranged from -1.35 to -2.7 V (*vs.* Ag/AgCl). Besides H$_2$, CO, CH$_4$ and C$_2$H$_4$ were also generated during the reaction. When the applied potential increased negatively from -1.35 to -2.7 V, the faradaic efficiency of H$_2$ was decreased from 81% to 42% while the faradaic efficiency of CO$_2$ reduction (sum of CO, CH$_4$ and C$_2$H$_4$) increased from 20% to 32%. This suggested that more negative potential prohibited the H$_2$ evolution and promoted the CO$_2$ reduction in here. Meanwhile, CO was the only CO$_2$ reduction product at -1.35 V, and there was no CH$_4$ or C$_2$H$_4$ detected. When the potential negatively increased to -2.7 V, the faradaic efficiency of CO reduced to 5.6%, while the faradaic efficiencies of CH$_4$ and C$_2$H$_4$ increased to 4.1% and 22.4%, respectively. On the other hand the current density increased from 0.3 to 9.4 mA/cm^2 when the applied potential negatively increased from -1.35 to -2.7 V. These results suggested that the potential had a strongly effect on the product selectivity. This is because different reactions had different standard redox potential, which had been already introduced in Chapter 1 (Table 1.1). As a result, varying the potential leads to a product selectivity change.

In 0.1 mol/L KHCO$_3$ (Fig. 5.5 (b)), when the applied potential negatively increased from -1.7 to -2.2 V, the faradaic efficiency of H$_2$ first decreased from 34.2% to 27.1% and then increased to 44.6%, while the faradaic efficiency of CO$_2$ reduction first increased from 26.9% to 43.7% and then decreased to 36.0%. This suggested that potential strongly controlled the product selectivity, too low or too high potential is not suitable for the CO$_2$ reduction. This is probably because CO$_2$ reduction has a higher overpotential than the H$_2$ evolution on Cu

electrode. At lower potential, H_2 evolution was the dominant due to the high overpotential of CO_2 reduction. As the applied potential increasing, faradaic efficiency of CO_2 reduction was promoted because the inherent catalytic activity of Cu working electrode. However, when the potential further increased, the faradaic efficiency of CO_2 reduction decreased probably due to the limit of CO_2 concentration in the electrolyte. A suitable potential region for CO_2 reduction according to the experimental results ranges from -1.9 to -2.1 V in 0.1 mol/L $KHCO_3$. The optimum faradaic efficiency of CO_2 reduction of 43.7% was obtained at -2.1 V, in which the faradaic efficiencies of CO, CH_4, and C_2H_4 were 1.7%, 20.9%, and 21.0%, respectively.

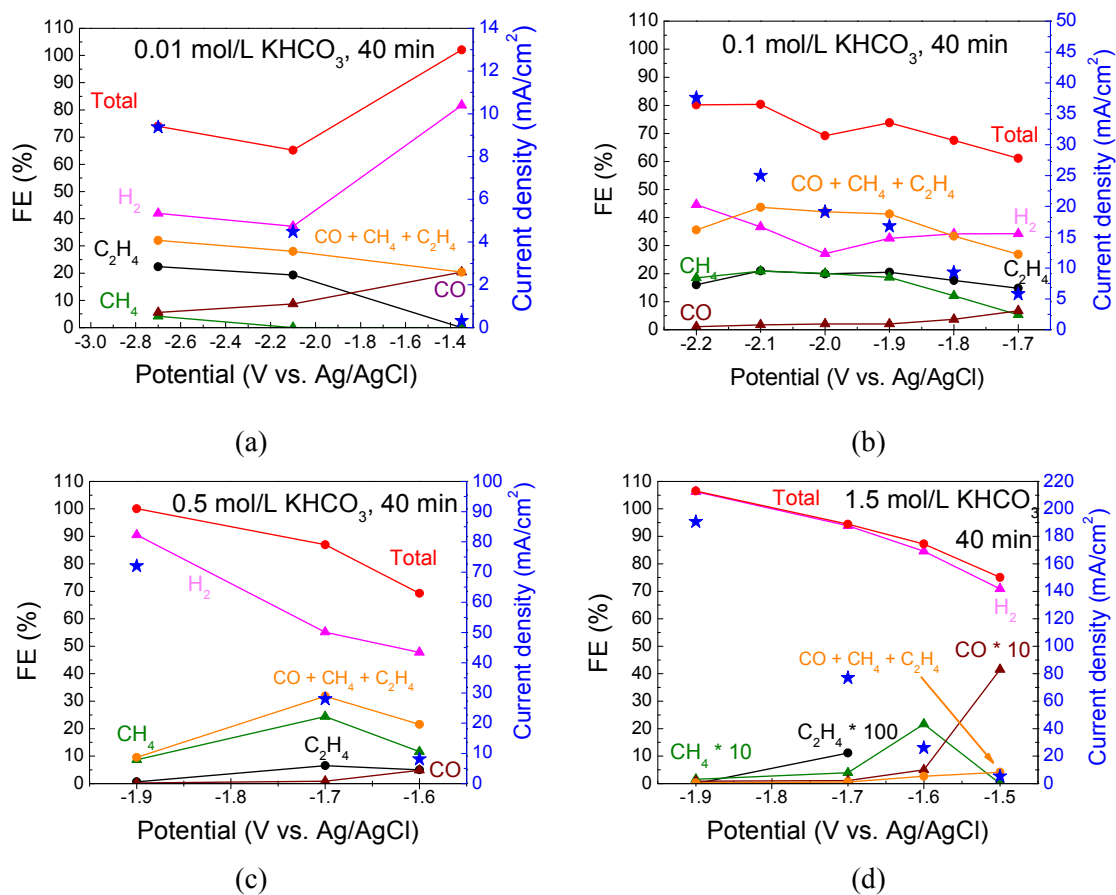**Fig. 5.5** Faradaic efficiencies (FE) of different gas products and current densities in the electrochemical reduction of CO_2 in different $KHCO_3$ concentration solutions at various applied potentials for 40 min (reaction temperature: 25 °C, reaction time: 40 min, CO_2 flow rate: 17.7 mL/min, $KHCO_3$ concentration: (a): 0.01 mol/L, (b): 0.1 mol/L, (c): 0.5 mol/L, (d) 1.5 mol/L).

In 0.5 mol/L $KHCO_3$ (Fig 5.5 (c)), H_2 was the main product. The faradaic efficiency of H_2 increased from 47.7% to 90.5% when the applied potential negatively increased from -1.6 to -1.9 V. The faradaic efficiency of CO_2 reduction first increased with the negative applied potential and then decreased. The best faradaic efficiency of CO_2 reduction in 0.5 mol/L $KHCO_3$ was obtained at -1.7 V, in which the faradaic efficiencies of CO, CH_4, and C_2H_4 were 0.8%, 24.4%, and 6.6%, respectively. It can be seen that CH_4 was the main CO_2 reduction product at -1.7 V.

In 1.5 mol/L $KHCO_3$ (Fig 5.5 (d)), the faradaic efficiency of CO_2 reduction reduced tremendously compared with that obtained in lower $KHCO_3$ concentration electrolytes. The optimum faradaic efficiency of CO_2 reduction was only 4.2% which was obtained at -1.5 V with a current density of 5.4 mA/cm^2. CO became the major product of CO_2 reduction, and there was no CH_4 and C_2H_4 detected at -1.5 V. Only trace amount of CH_4 and C_2H_4 were detected at -1.6 and -1.7 V. When the applied potential increased to -1.9 V, nearly all the gas product was H_2.

It can be seen that in Fig. 5.5 the product selectivity not only affected by the applied potential but also affected by the $KHCO_3$ concentration. In 0.01 mol/L $KHCO_3$ electrolyte, C_2H_4 was the main product of CO_2 reduction when the optimum faradaic efficiency of CO_2 reduction was achieved. When the $KHCO_3$ concentration increased to 0.1 mol/L, CH_4 and C_2H_4 were the main products of CO_2 reduction with almost the same faradaic efficiencies. In 0.5 mol/L $KHCO_3$, the faradaic efficiency of C_2H_4 decreased and CH_4 became the main product of CO_2 reduction. Although the faradic efficiency of CO_2 reduction was very low in 1.5 mol/L $KHCO_3$, the CO became the main product of CO_2 reduction instead of CH_4 and C_2H_4. As a result, lower $KHCO_3$ concentration promotes the C_2H_4 generation. This probably because low $KHCO_3$ concentration solutions has low pH after CO_2 bubbling, which promotes the most hydrogen consuming process of C_2H_4 production.

The faradaic efficiencies of CO_2 reduction and H_2 evolution at various potentials in Fig. 5.5 were summarized in Fig. 5.6, which can be used for comparing the CO_2 reduction and H_2 evolution more clearly. It can be seen that, the faradaic efficiency of CO_2 reduction was much higher in 0.1 mol/L $KHCO_3$ than others. Increasing or decreasing the $KHCO_3$ concentrations leads to a decrease in the CO_2 reduction.
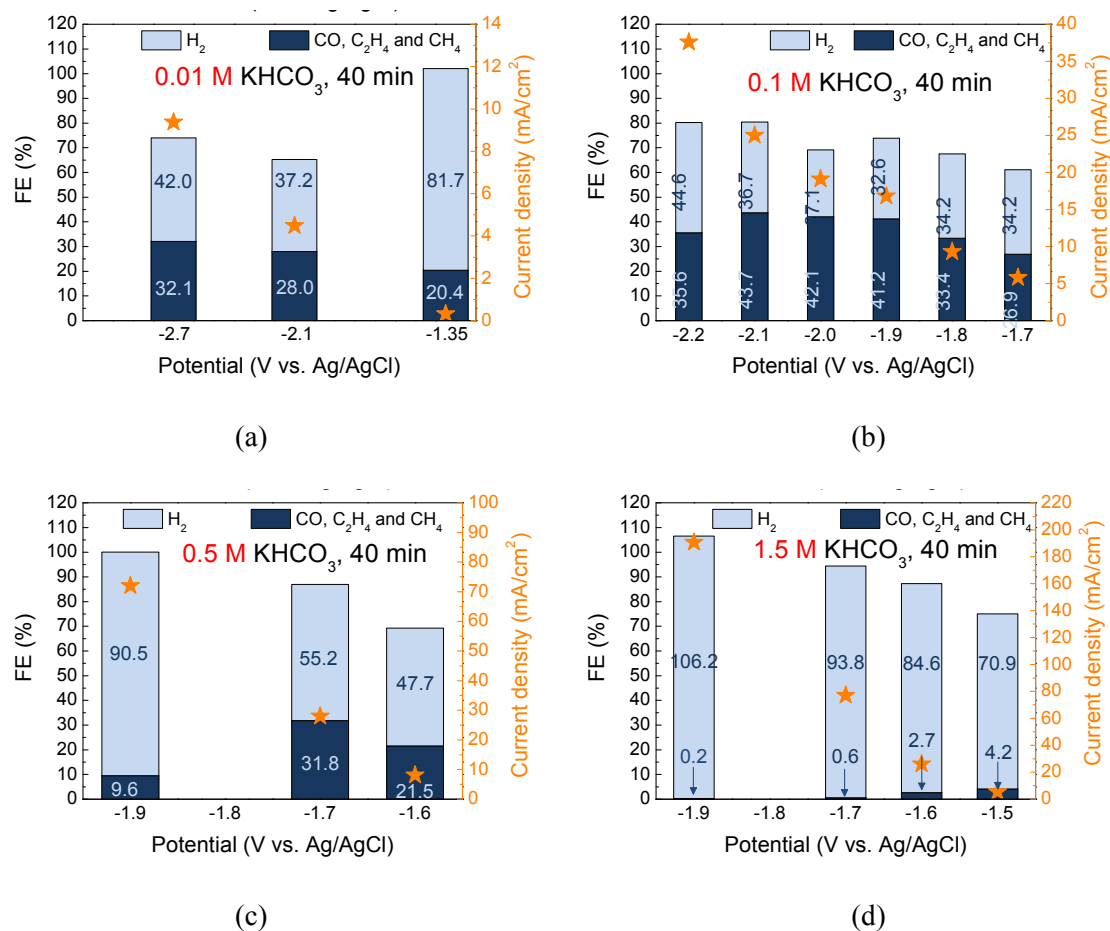
Fig. 5.6 Faradaic efficiencies (FE) of CO_2 reduction and H_2 evolution, and current densities in the electrochemical reduction of CO_2 in different $KHCO_3$ concentration solutions at various applied potentials for 40 min (M: mol/L; reaction temperature: 25 ^{o}C, reaction time: 40 min, CO_2 flow rate: 17.7 mL/min, $KHCO_3$ concentration: (a): 0.01 mol/L, (b): 0.1 mol/L, (c): 0.5 mol/L, (d) 1.5 mol/L).

The reaction conditions for obtaining the optimum faradaic efficiencies of CO_2 reduction in different concentrations of $KHCO_3$ solutions were summarized in Table 5.4. As the $KHCO_3$ concentration increasing from 0.01 to 1.5 mol/L, the applied potential for obtaining the optimum CO_2 reduction reduced from -2.7 to -1.5 V. This is probably because the conductivity of the electrolytes increased with $KHCO_3$ concentration. Therefore, less potential was needed to overcome the resistance of the electrolytes. The current density was relatively low in 0.01 and 1.5 mol/L $KHCO_3$ solutions. This could be attributed to the low conductivity

of 0.01 mol/L $KHCO_3$ and low potential applied in 1.5 mol/L KHCO. The optimum CO_2 reduction faradaic efficiency of 43.7% was obtained in 0.01 mol/L $KHCO_3$ electrolyte at -2.1 V. Although this conclusion was similar with Hori's report [54], this result should be more convincible because the effect of potential on the product selectivity was also considered in this research. In Hori's research, a galvanostatic study method with a constant current density of 5 mA/cm^2 was used. To compare with Hori's results, faradaic efficiencies of CO_2 reduction in different $KHCO_3$ concentrations at current density around 5 mA/cm^2 in this research were listed in Table 5.5. It can be seen that the best faradaic efficiency of CO_2 reduction of 28.0% was obtained in 0.01 mol/L $KHCO_3$ with a current density of 4.5 mA/cm^2, which was different from Hori's result. This further proved that galvanostatic method for studying the effect of $KHCO_3$ concentration was not suitable. This is because different concentrations of $KHCO_3$ solutions have different conductivity. Thus different potentials need to be applied to achieve the same current density. Therefore, the effect of the potential on the product selectivity should be considered.

Table 5.4 Optimum faradaic efficiencies of CO_2 reduction in different $KHCO_3$ concentration solutions[a]

C_{KHCO_3} (mol/L)	Potential (V vs Ag/AgCl)	Current density (mA/cm^2)	Faradaic efficiency (%)	
			CO_2 reduction	H_2
0.01	-2.7	9.4	32.1	42.0
0.1	-2.1	25.0	43.7	36.7
0.5	-1.7	28.0	31.8	55.2
1.5	-1.5	5.4	4.2	70.9

[a]Reaction condition: temperature: 25 °C, reaction time: 40 min, CO_2 flow rate: 17.7 mL/min.

Table 5.5 Faradaic efficiency of CO_2 reduction in different $KHCO_3$ concentration solutions at current density around 5 mA/cm^2 [a]

C_{KHCO_3} (mol/L)	Potential (V vs Ag/AgCl)	Current density (mA/cm^2)	Faradaic efficiency (%)	
			CO_2 reduction	H_2
0.01	-2.1	4.5	28.0	37.2
0.1	-1.7	5.8	26.9	34.2
0.5	-1.6	8.1	21.5	47.7
1.5	-1.5	5.4	4.2	70.9

[a]Reaction condition: temp: 25 °C, CO_2 flow rate: 17.7 mL/min.

Although 0.1 mol/L $KHCO_3$ was the most suitable concentration for the electrochemical reduction of CO_2, which was also reported by other groups [54,86], the reason why this specific concentration is the most suitable has not been reported yet. Therefore, this would be studied in the next chapter.

5.5 Effect of reaction time on the CO_2 reduction in different $KHCO_3$ concentrations

As introduced in the experimental section, the gas samples were directly connected to the GC-TCD and were online measured at 5, 20, 40 and 60 min. Therefore, the effect of the reaction time on the electrochemical reduction of CO_2 can be investigated. However, the faradaic efficiency of H_2 evolution and CO_2 reduction obtained in 5 min were abnormal which might because of the gas products were not well mixed in the beginning of the experiment. Therefore, results obtained only after 20 min were used. Fig. 5.7 shows the faradaic efficiencies of gas products, and current densities in the electrochemical reduction of CO_2 in 0.01mol/L $KHCO_3$ at -2.1 V as function of time. The faradaic efficiency of CO_2 reduction and H_2 evolution at 20 min were 28.0% and 40.1%, respectively. As the time increasing to 60 min,

the faradaic efficiency of CO_2 reduction slightly increased to 29.0% while the faradaic efficiency of H_2 evolution decreased to 38.8%. The product selectivity of CO, CH_4 and C_2H_4 was not affected by the time in 0.01 mol/L $KHCO_3$.

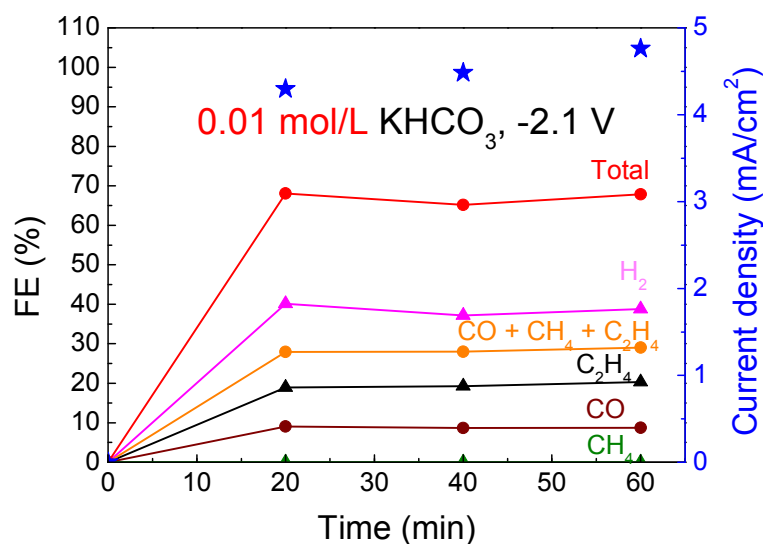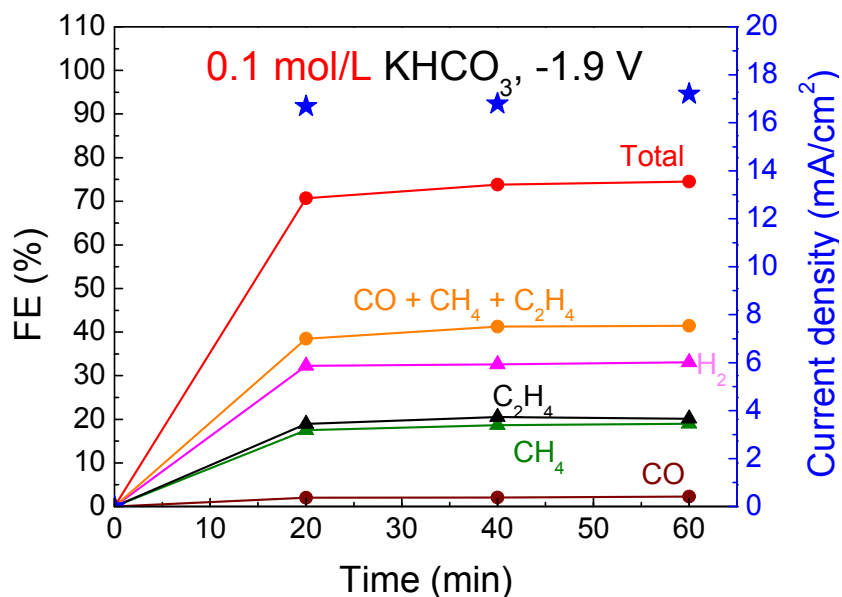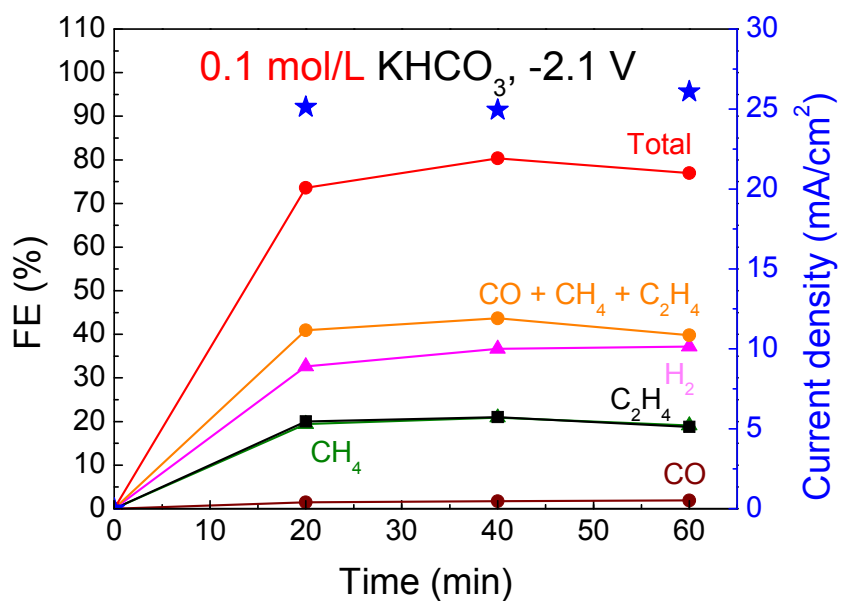**Fig. 5.7** Faradaic efficiencies (FE) of gas products and current densities in the electrochemical reduction of CO_2 in 0.01 mol/L $KHCO_3$ as function of time (reaction condition: temp: 25 $^{\circ}$C, potential: -2.1 V, CO_2 flow rate: 17.7 mL/min).

Fig. 5.8 depicted the faradaic efficiency of gas products, and current density in the electrochemical reduction of CO_2 in 0.1 mol/L $KHCO_3$ at various potentials as function of time. When the applied potential was -1.9 V, the faradaic efficiencies of CO_2 reduction and H_2 evolution did not change too much with the time. The faradaic efficiency of CO_2 reduction slightly increased from 38.5% to 41.4% as the time increased from 20 to 60 min. CH_4 and C_2H_4 were the main CO_2 reduction products. The faradaic efficiencies of CH_4 and C_2H_4 were 20.2% and 19.0% after 60 min, respectively. The faradaic efficiency of CO was 2.3% after 60 min. The current density slightly increased from 16.7 to 17.2 mA/cm^2. When the applied potential increased to -2.1 V (Fig. 5.8 (b)), the faradaic efficiency of CO_2 reduction first increased from 40.9% to 43.7% when the time increased from 20 to 40 min, and then decreased to 39.8% when the time further increased to 60 min. However, the faradaic efficiency of H_2 evolution increased from 32.7% to 37.2% as the CO_2 reduction decreasing,

which means the product selectivity was affected by the time in 0.1 mol/L $KHCO_3$ at a relatively high potential.
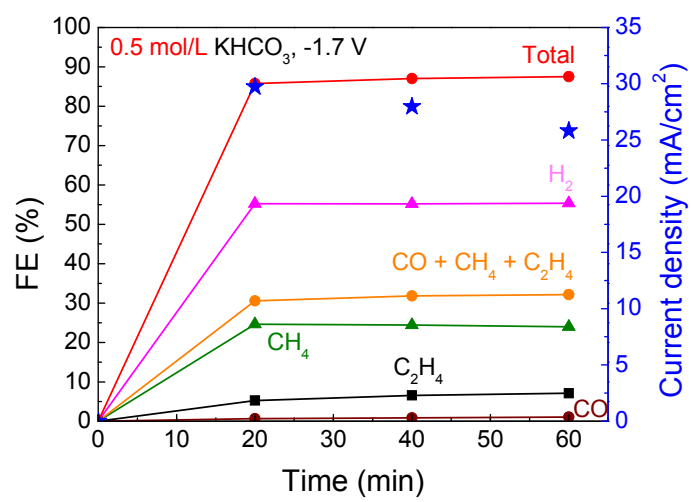

(a)

(b)

Fig. 5.8 Faradaic efficiencies (FE) of gas products and current densities in the electrochemical reduction of CO_2 in 0.1 mol/L $KHCO_3$ at different potentials as function of time (reaction condition: temp: 25 ^oC, CO_2 flow rate: 17.7 mL/min, potential: (a): -1.9 V, (b): -2.1 V).

There are two possible reasons for the decrease of faradaic efficiency of CO_2 reduction with time. One is that the adsorption of impurity heavy metals (mainly Fe and Zn) in the electrolyte on Cu working electrode caused the CO_2 reduction decrease. It is reported that the impurities in the electrolyte and working electrode could lead to a deactivation of the working electrode and affect the product selectivity [100,101]. Therefore, as the reaction time increasing, the impurity heavy metals in the electrolyte was reduced and covered on the surface of the working electrode, and then leaded to a decrease in the catalytic activity for CO_2 reduction of the working electrode. Another possible reason for the decrease in the faradaic efficiency of CO_2 reduction with time at higher potential could be the corrosion of the WE, which will be discussed later. Since the CO_2 reduction and H_2 evolution were competing reactions in this system, when the CO_2 reduction reduced, the H_2 evolution was promoted. As a result, the product selectivity was affected by the time when a more negative potential was applied.

Fig. 5.9 shows the faradaic efficiencies of gas products, and current densities in the electrochemical reduction of CO_2 in 0. 5 mol/L $KHCO_3$ at -1.7 V and -1.9 V as function of time. When the applied potential was -1.7 V, the faradaic efficiencies of CO_2 reduction and H_2 evolution were not affected by the time too much in 0.5 mol/L $KHCO_3$ electrolyte. The faradaic efficiency of CH_4 slightly decreased from 24.6% to 24.0%, while the faradaic efficiency of C_2H_4 slightly increased from 5.2% to 7.1% when the reaction time increased from 20 to 60 min. However, the current density decreased from 29.7 to 25.8 mA/cm^2 as the time increasing. This was probably because that the reduced intermediates covered the Cu surface and reduced the catalytic activity as discussed above. When the applied potential increased to -1.9 V (Fig. 5.9 (b)), an obvious decrease in the faradaic efficiency of CO_2 reduction was observed. Since the main product of CO_2 reduction was CH_4 at -1.9 V, the decrease of the faradaic efficiency of CO_2 reduction was mainly attributed to the decrease of CH_4 production. The faradaic efficiency of CH_4 reduced from 12.5% to 5.7% as the time increasing from 20 to 60 min. When the faradaic efficiency of CO_2 reduction decreased, the faradaic efficiency of H_2 evolution increased from 87.6% to 95.6%. The current density also decreased from 78.5 to 71.8 mA/cm^2 as the reaction time increasing. As discussed above, the current density represented the electrochemical reaction rate. The current density in 0.5 mol/L

KHCO$_3$ at -1.9 V was much higher than that in 0.1 and 0.01 mol/L KHCO$_3$. Therefore, much more reduced intermediates adsorbed on the surface of Cu and cause the faradaic efficiency of CO$_2$ reduction reducing tremendously. As a result, lower concentration and smaller potential should be used in the electrochemical reduction of CO$_2$ to achieve higher and more stable CO$_2$ reduction faradaic efficiency (for example: 0.1 mol/L KHCO$_3$ at -1.9 V).

(a)
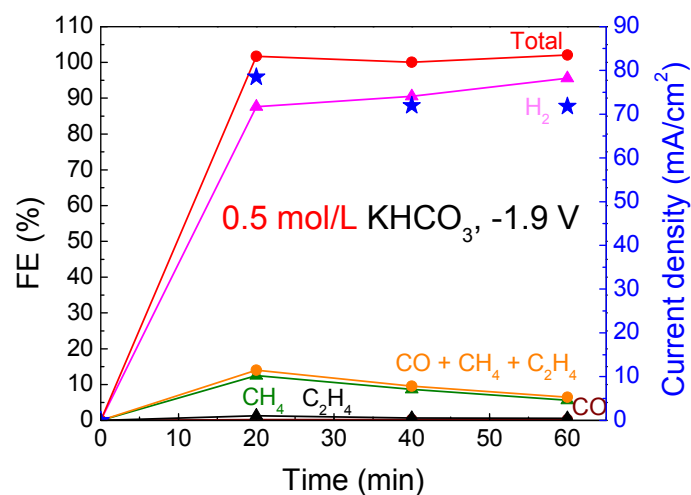
(b)

Fig. 5.9 Faradaic efficiencies (FE) of gas products and current densities in the electrochemical reduction of CO$_2$ in 0.5 mol/L KHCO$_3$ as function of time (reaction condition: temp: 25 ^{o}C, CO$_2$ flow rate: 17.7 mL/min, potential: (a): -1.7 V, (b): -1.9 V).

5.6 Electrochemical reduction of CO_2 in KCl solution

5.6.1 Effect of applied potential

KCl is another widely used supporting electrolyte in the electrochemical reduction of CO_2 in aqueous solutions. The effect of the KCl on the product selectivity was studied.   Fig. 5.10 shows the faradaic efficiencies of different gas products and current densities in the electrochemical reduction of CO_2 in 0.1 mol/L KCl as function of applied potential. H_2, CH_4, C_2H_4, and CO were detected in the gas phase which was the same as in $KHCO_3$. The product selectivity was also affected by the potential. The faradaic efficiency of H_2 evolution increased from 33.1% to 78.6% when the applied potential negatively increased from -1.7 to -2.1 V, which means more negative potential was favorable to the H_2 evolution. The faradaic efficiency of C_2H_4 first increased with the negative applied potential and reached the peak of 28.0% at -1.8 V, and then decreased with a further increase in the negative potential. The faradaic efficiency of CH_4 slowly increased with the negative potential. The optimum faradaic efficiency of CH_4 (9.9%) was obtained at -2.0 V. Further increasing the potential leaded to the decrease in the CH_4 faradaic efficiency. Similar as in the $KHCO_3$ solution, CO generation was also easier at lower applied potential in KCl solution. The faradaic efficiency of CO was 10.1% at -1.7 and reduced with the negative increase in applied potential. The overall faradaic efficiency of CO_2 reduction was first increased with the negative applied potential and then decreased, which was similar with the variation of C_2H_4 faradaic efficiency. This was because C_2H_4 was the main product of the CO_2 reduction. The optimum faradaic efficiency of CO_2 reduction in 0.1 mol/L KCl for 40 min was 35.7% at -1.8V.
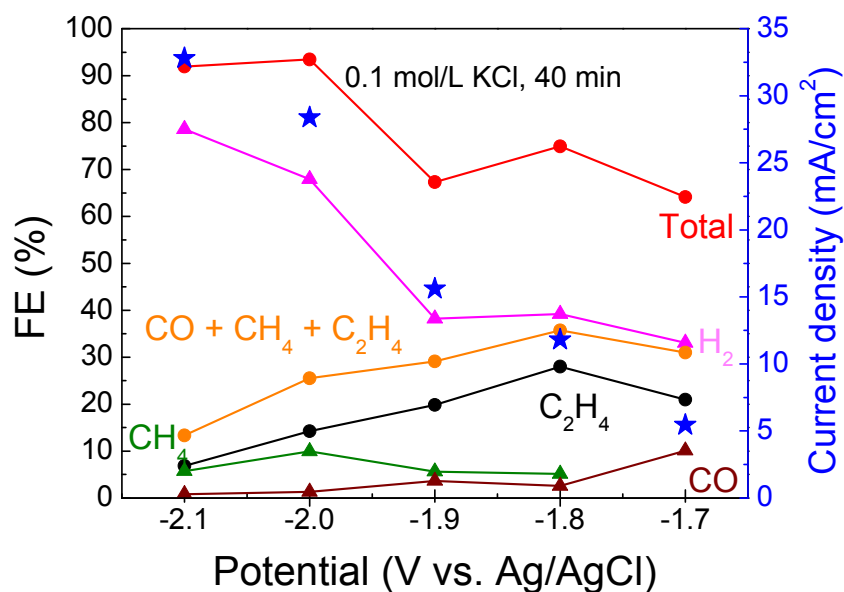
Fig. 5.10 Faradaic efficiencies (FE) of different gas products and current densities in the electrochemical reduction of CO_2 in 0.1 mol/L KCl at various applied potentials (reaction condition: temp: 25 ^{o}C, CO_2 flow rate: 17.7 mL/min, reaction time: 40 min).

5.6.2 Effect of reaction time on the faradaic efficiency

The effect of the reaction time on product selectivity in the electrochemical reduction of CO_2 in KCl solution was studied. The faradaic efficiencies of gas products and current densities in the electrochemical reduction of CO_2 in 0.1 mol/L KCl as function of time at -1.9 and -2.1 V were showed in Fig 5.11. When the applied potential was -1.9 V, the current density was about 16 mA/cm^2 and varied a little as the time increasing. The faradaic efficiency of H_2 slightly increased with time. The faradaic efficiencies of CH_4 and CO increased from 5.5% to 6.1% and 2.5% to 4.6% when the reaction time increased from 20 to 60 min, respectively. However, the faradaic efficiency of C_2H_4, which was the main product of CO_2 reduction, decreased from 22.0% to 18.0% as the reaction time increasing. The overall faradaic efficiency of CO_2 reduction was slightly decreased from 30.0% to 28.7% with the time. This decrease was possibly attributed to the adsorption of impurities and intermediates on the surface of Cu which caused the deactivation of the catalytic activity of the working

electrode and then leaded to a change of the product selectivity as discussed in section 5.5. When the applied potential increased to -2.1 V, the decrease of the faradaic efficiency of CO_2 reduction and increase of the faradaic efficiency of H_2 evolution with time was more obvious. The faradaic efficiency of CO_2 reduction decreased from 16.7% to 12.3% when the reaction time increased. This phenomenon was very similar with that in $KHCO_3$ solutions which was already discussed in section 5.5.
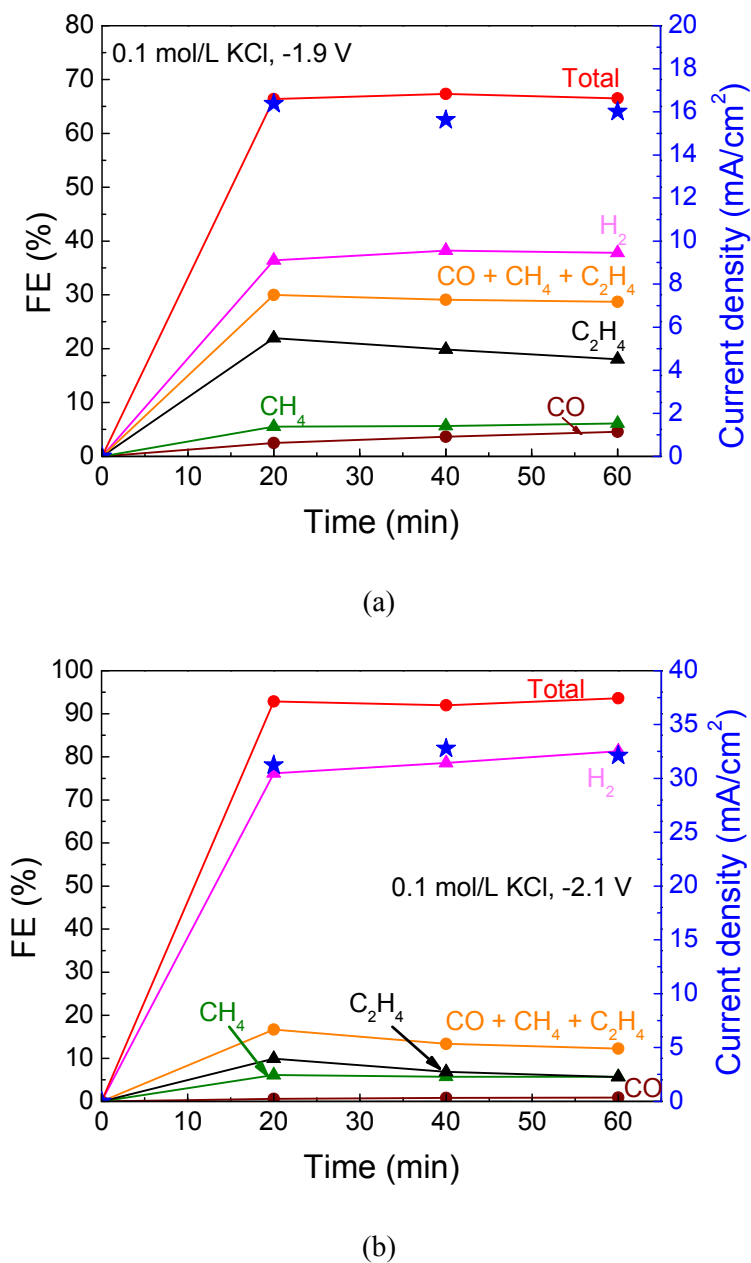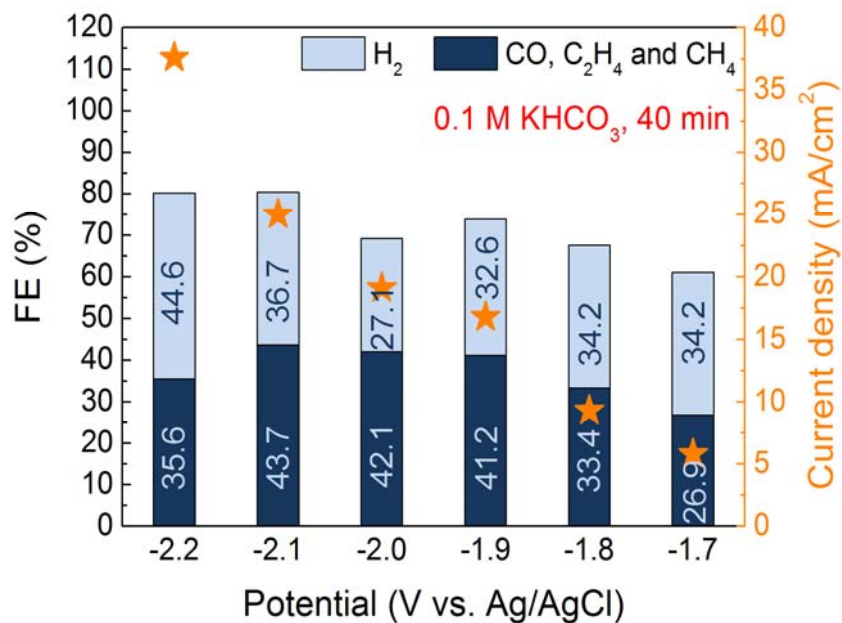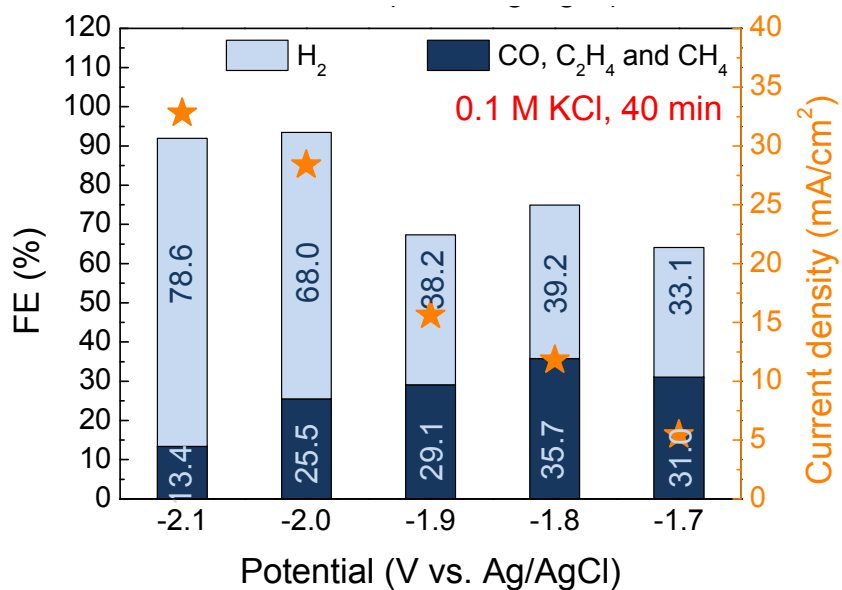

(a)

(b)

Fig. 5.11 Faradaic efficiencies (FE) of gas products and current densities in the electrochemical reduction of CO_2 in 0.1 mol/L KCl as function of time (reaction condition: temp: 25 ^{o}C, CO_2 flow rate: 17.7 mL/min, potential: (a): -1.9 V, (b): -2.1 V).

5.7 Comparison of KHCO$_3$ and KCl electrolytes

The effect of different electrolytes of KHCO$_3$ and KCl on the electrochemical reduction of CO$_2$ on Cu electrode at various potentials were studied and compared. Fig. 5.12 showed the faradaic efficiencies of H$_2$ evolution and CO$_2$ reduction, and the current density at applied potentials ranged from -1.7 and -2.2 V in 0.1 mol/L KHCO$_3$ and 0.1 mol/L KHCO$_3$ KCl. It can be seen that, faradaic efficiency of CO$_2$ reduction was higher in KCl solution than in KHCO$_3$ solution at -1.7 and -1.8 V. However, when the applied potential exceeded -1.8 V, the faradaic efficiency of CO$_2$ reduction was higher in KHCO$_3$ solution than that in KCl solution. The optimum faradaic efficiency of CO$_2$ reduction in 0.1 KHCO$_3$ was 43.7%, which was achieved at -2.1 V. The optimum faradaic efficiency of CO$_2$ reduction in 0.1 mol/L KCl was 35.7%, which was achieved at -1.8 V. These results suggested that KHCO$_3$ was a better electrolyte than KCl for obtaining high CO$_2$ reduction faradaic efficiency. The pH of 0.1 mol/L KHCO$_3$ saturated with CO$_2$ bubbling was measured to be 6.8 while the pH of 0.1 mol/L KCl saturated with CO$_2$ bubbling was 2.9. Therefore, much more H$^+$ (nealy 8000 times) was contained in KCl solution than in KHCO$_3$ solution. The huge amount of H$^+$ in the KCl solution possibly promoted the H$_2$ evolution and then reduced the faradaic efficiency of CO$_2$ reduction. As a result, higher faradaic efficiency of CO$_2$ reduction was obtained in KHCO$_3$ solution rather than in KCl solution.

(a)

(b)

Fig. 5.12 Faradaic efficiencies (FE) of CO_2 reduction and H_2 evolution, and current densities in the electrochemical reduction of CO_2 for 40 min in (a) 0.1 mol/L $KHCO_3$ and (b) 0.1 mol/L KCl at various applied potentials (M: mol/L, reaction temperature: 25 ^oC, reaction time: 40 min, CO_2 flow rate: 17.7 mL/min).

Possible reactions with the standard potentials in the electrochemical reduction of CO_2 in aqueous solutions (at 298.15K and pH = 0) are listed as follow [62].

$$CO_2 + 2H^+ + 2e^- \rightleftarrows CO + H_2O \qquad E_0 = \text{-0.103 V } vs. \text{ SHE} \qquad (5.1)$$

$$CO_2 + 8H^+ + 8e^- \rightleftarrows CH_4 + 2H_2O \qquad E_0 = \text{0.169 V } vs. \text{ SHE} \qquad (5.2)$$

$$2CO_2 + 12H^+ + 12e^- \rightleftarrows C_2H_4 + 4H_2O \qquad E_0 = \text{0.079 V } vs. \text{ SHE} \qquad (5.3)$$

$$2H^+ + 2e^- \rightleftarrows H_2 \qquad E_0 = \text{0.0 V } vs. \text{ SHE} \qquad (5.4)$$

The standard potentials of these equations are affected by the concentration of H^+, or in other words, affected by the pH of the solution. The relationship between the equilibrium potential and pH of reaction 5.1 − 5.4 can be calculated according to Eq. (5.5) based on the Nernst equation.

$$E = E_0 - \frac{RT}{nF} \ln \frac{1}{[H^+]^n} = E_0 - 0.059 \times pH \qquad (5.5)$$

where E_0 represents the standard potential in reaction 5.1 − 5.4, R is the ideal gas constant, T is the absolute temperature, n is the number of electrons transfer per molecule, F is the faradaic constant. Therefore, the relationship between the equilibrium potential of CO_2 reduction and H_2 evolution, and pH at 25°C can be plotted in Fig. 5.13. The equilibrium potential linearly decreased with the pH with a slope of -0.059 V/pH. Therefore, the pH difference of 3.9 between 0.1 mol/L $KHCO_3$ and KCl after saturated with CO_2 bubbling leads to a CO_2 reduction and H_2 evolution equilibrium potential difference of 0.23 V. The optimum CO_2 reduction potential in 0.1 mol/L $KHCO_3$ and KCl were -2.1 and -1.8, respectively. This difference of 0.3 V, which was close to 0.23 V, was probably caused by the pH difference of these two electrolytes.
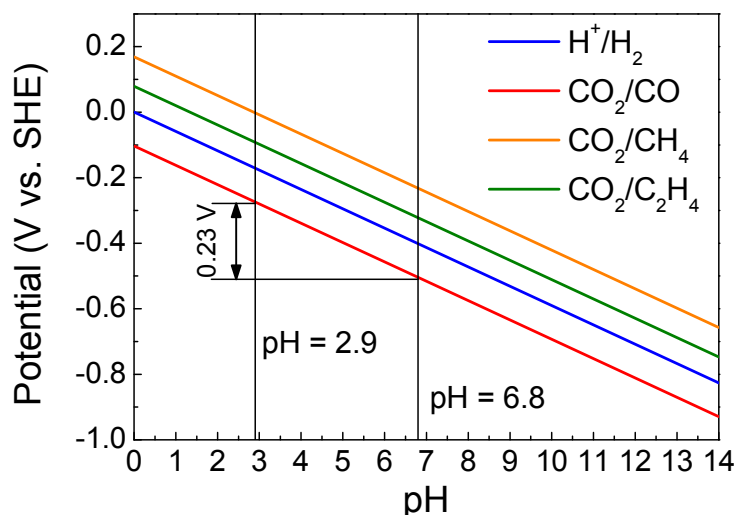
Fig. 5.13 The equilibrium potentials of CO_2 reduction reactions and H_2 evolution as a function of pH (at 25°C).

Fig. 5.14 (a) and (b) show the faradaic efficiencies of different products after electrochemical reduction of CO_2 in 0.1 mol/L $KHCO_3$ and KCl at various potentials, respectively. It is obvious that the major CO_2 reduction products in $KHCO_3$ solution were CH_4 and C_2H_4, while it was C_2H_4 in KCl solution at the potential for obtaining the optimum CO_2 reduction faradaic efficiency. This suggested that the electrolyte had the ability to affect the product selectivity. This was probably caused by the pH difference between the $KHCO_3$ and KCl electrolytes. It is reported that the pH can affect the product selectivity, especially for the CH_4 production, however, the detailed effect of the pH is still not clear [54,81].
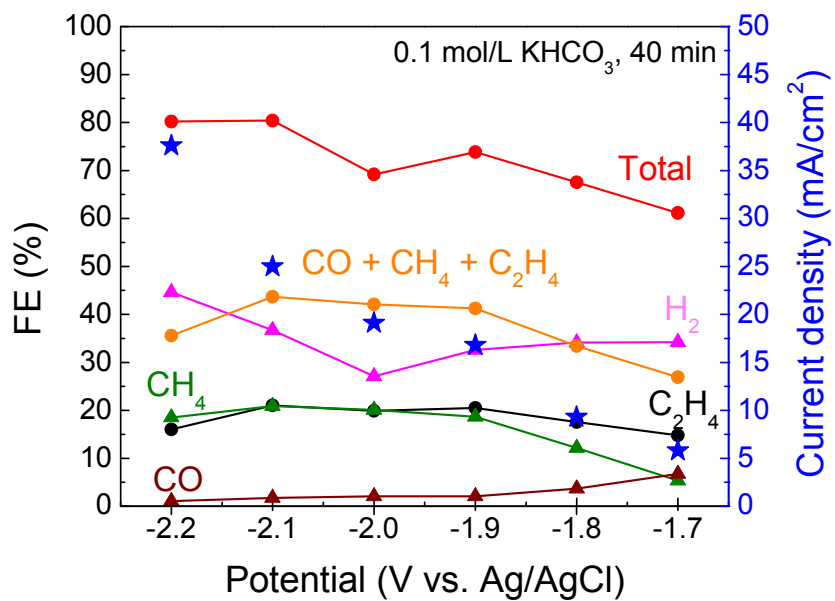
(a)
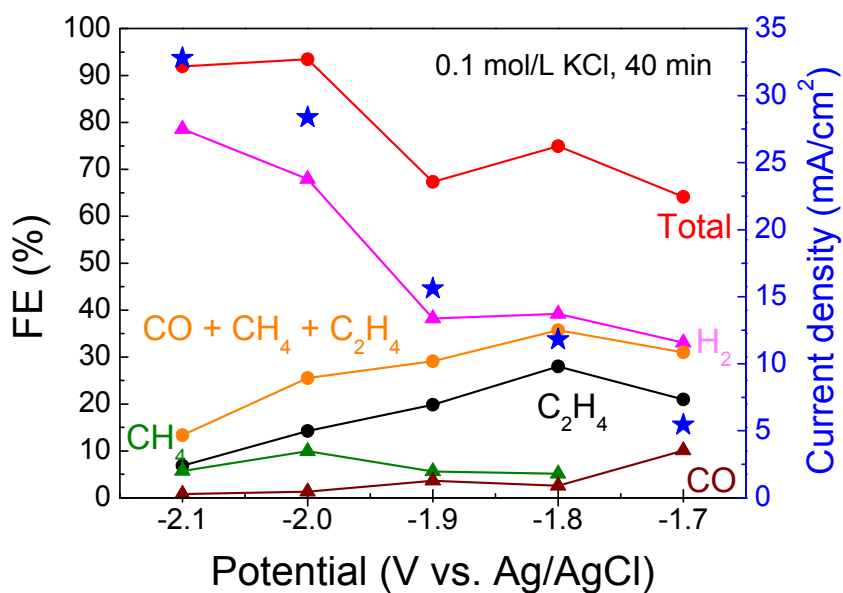
(b)

Fig. 5.14 Faradaic efficiencies (FE) of different products, and current densities in the electrochemical reduction of CO_2 in (a) 0.1 mol/L $KHCO_3$ and (b) 0.1 mol/L KCl for 40 min at various applied potentials (reaction temperature: 25 °C, reaction time: 40 min, CO_2 flow rate: 17.7 mL/min).

5.8 Effect of working electrode position and stirring

The position of the working electrode was accidentally found to be able to affect the faradaic efficiency of the products during the electrochemical reduction of CO_2 in $KHCO_3$. It was found that the CO_2 reduction efficiency was promoted by placing the working electrode in the CO_2 bubbling zone compared with placing in the normal position which was about 3 mm away from the bubbling zone. Fig. 5.15 shows the faradaic efficiencies of different products, and current densities in the electrochemical reduction of CO_2 in 0.1 mol/L $KHCO_3$ placing working electrode at different positions for 40 min at -2.1 V. The faradaic efficiencies of CH_4 and CO were not affected by the working electrode position too much. However, the faradaic efficiency of C_2H_4 was increased from 21.0% to 22.6%, while the faradaic efficiency of H_2 was reduced from 36.7% to 32.6% by placing the working electrode from normal position to the CO_2 bubbling zone. The faradaic efficiency of CO_2 reduction was increased from 43.7% to 44.4% after placing the working electrode in the bubbling zone. Moreover, the current density was also improved from 24.9 to 26.0 mA/cm^2 by placing the working electrode in the bubbling zone. Fig. 5.16 depicted the gas generation rate of different products during electrochemical reduction of CO_2 in $KHCO_3$. It is clear that the production of C_2H_4 and CO was enhanced while the H_2 generation was reduced after placing the working electrode in the bubbling zone. There are two possible reasons could be attributed to the enhancement of the CO_2 reduction by placing the working electrode in the bubbling zone. One is that CO_2 was much easier to adsorb and react on the Cu working electrode since the local CO_2 concentration was higher in the bubbling zone. Another reason could be the CO_2 bubbling improved the mass convection in the electrolyte. Since there is no stirring was used in the electrochemical reaction, the mass transfer was not good. Placing the working electrode in the bubbling zone somehow achieved the effect of stirring and then promoted the mass transfer. Therefore, the effect of stirring on the electrochemical reduction of CO_2 needs to be studied.
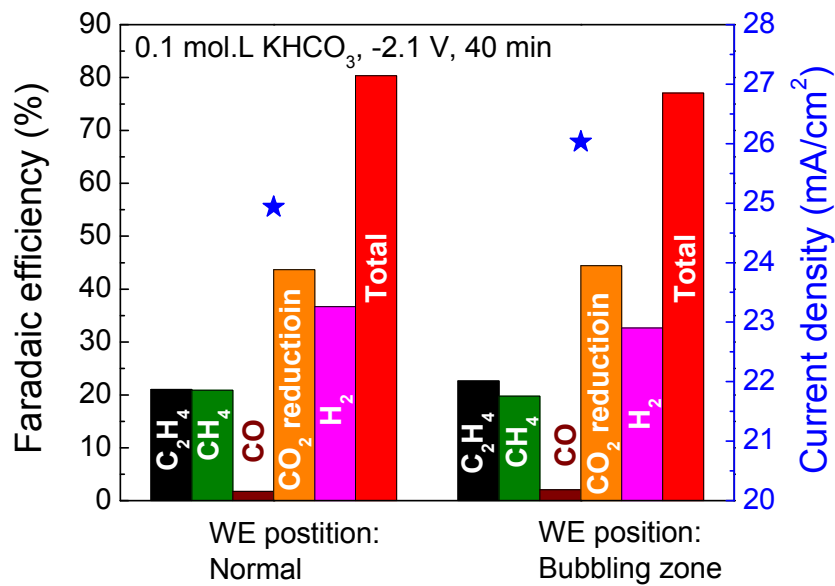
Fig. 5.15 Effect of working electrode position on the faradaic efficiencies (bars) of different products, and current densities (blue star) in the electrochemical reduction of CO_2 in 0.1 mol/L $KHCO_3$ for 40 min at -2.1 V (reaction temperature: 25 ^{o}C, CO_2 flow rate: 17.7 mL/min).

Fig. 5.16 Gas generation rate in the electrochemical reduction of CO_2 in 0.1 mol/L $KHCO_3$ after 40 min at -2.1 V (reaction condition: temp: 25°C, working electrode: Cu, CO_2 flow rate: 17.7 mL/min).

The effect of stirring on the electrochemical reduction of CO_2 was studied in 0.1 mol/L KHCO$_3$ at -2.1 V for 40 min by placing the working electrode in normal position and using a magnetic stirrer with a rotation rate of 1000 rpm. The faradaic efficiencies of different products were calculated and compared with those obtained without stirring, which were shown in Fig. 5.17. It has been discussed above that placing the working electrode in the CO_2 bubbling zone can promote the CO_2 reduction. The faradaic efficiency of H_2 evolution reduced to 22.1%, while the faradaic efficiency of CO_2 reduction further increased to 50.5% by stirring the electrolyte even when the working electrode was placed in normal position. Actually, when stirring was used, it was hard to determine the bubbling zone. These results prove that stirring of the electrolytes can improve the mass transfer and remove of the adsorbed CO_2 reduction products from the working electrode, and hence promote the faradaic efficiency of CO_2 reduction. Furthermore, the current density was also increased from 24.9 to 30.3 mA/cm^2 after stir was used. Considering that the faradaic efficiencies of CO_2 reduction were 43.7% and 50.5% with or without stirring, respectively, the partial current densities for CO_2 reduction was 10.9 and 15.3 mA/cm^2 with or without stirring. It should be noticed that the reported current density for the electrochemical CO_2 reduction in aqueous solutions without gas diffusion electrode (GDE) at pressure of 1 atm was generally lower than 10 mA/cm^2, although the faradaic efficiency for CO_2 reduction can be as high as 90% [54,78,79,87]. Therefore, results obtained in this research showed a very high current density for CO_2 reduction. However, the detailed reason was still not clear and need to be studied in the future.

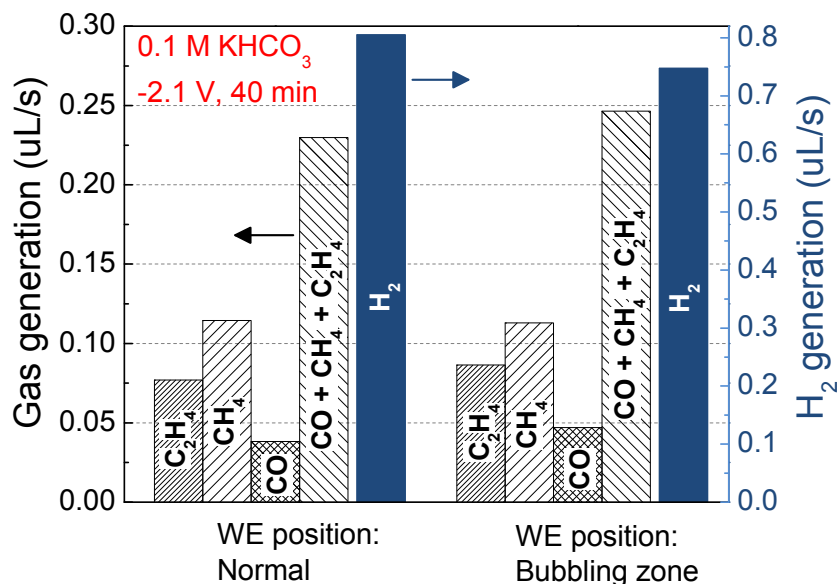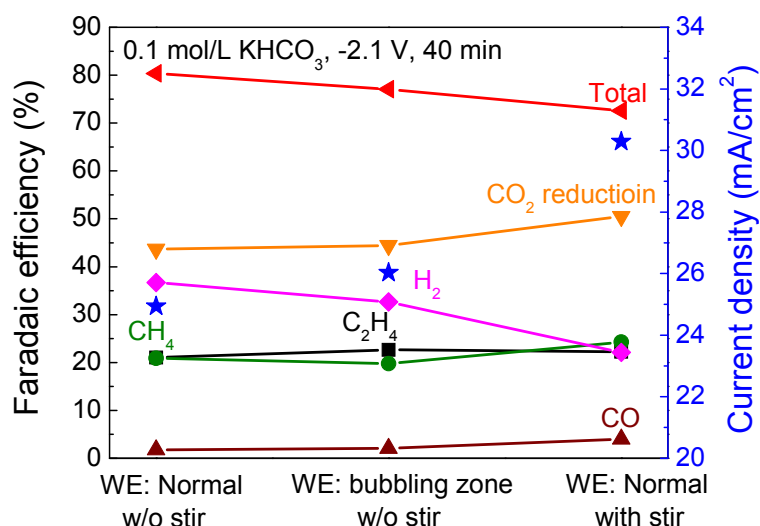**Fig. 5.17** Effect of stir on the faradaic efficiencies of different products, and current densities in the electrochemical reduction of CO_2 in 0.1 mol/L $KHCO_3$ for 40 min at -2.1 V (reaction temperature: 25 °C, CO_2 flow rate: 17.7 mL/min, stirring rate: 1000 rpm).

5.9 Reproducibility of CO_2 reduction in $KHCO_3$ solution

The reproducibility of CO_2 reduction in $KHCO_3$ solution were studied by repeating the experiments of electrochemical reduction of CO_2 in 0.1 mol/L $KHCO_3$ under CO_2 bubbling with or without stirring at -2.1 V for 60 min at room temperature for several times. These experiments were totally independent, the Cu working electrode, electrolyte, and Nafion film were all changed to new ones after each experiment. Fig.5.18 shows the faradaic efficiencies of different gas products obtained without stirring. It can be seen that the reproducibility of the electrochemical reduction of CO_2 is not very good. The highest faradaic efficiency of CO_2 reduction was 43.7%, however, the lowest faradaic efficiency of CO_2 reduction was only 31.4%. As the faradaic efficiency of CO_2 reduction decrease, the faradaic efficiency of H_2 evolution increased from 36.7% to 54.4%. The average faradaic efficiency of CO_2 reduction in 0.1 mol/L $KHCO_3$ without stirring at -2.1 V was 37.7%, while the average faradaic efficiency of H_2 evolution was 44.0%.
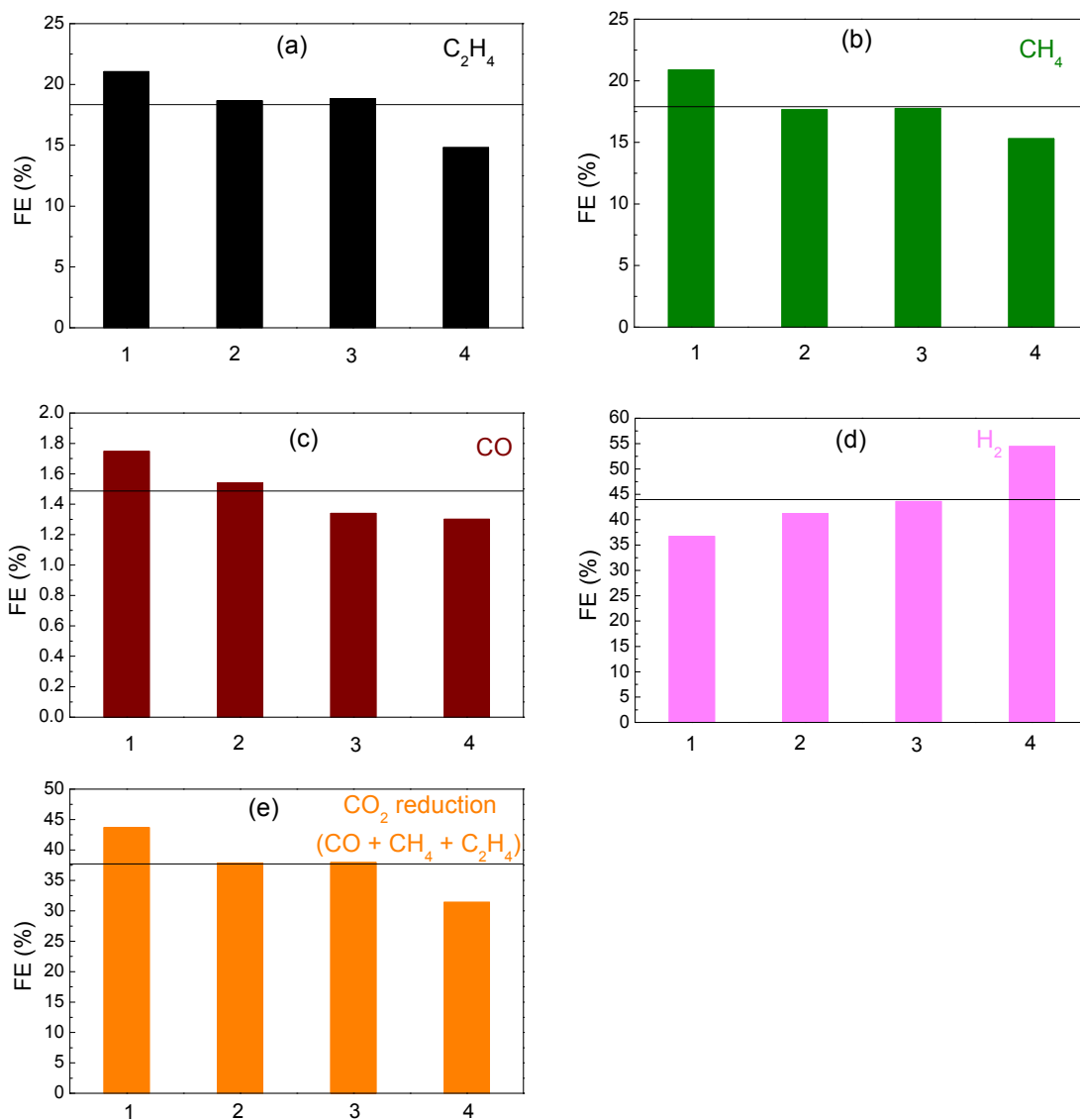
Fig. 5.18 Faradaic efficiencies (FE) of (a): C_2H_4, (b): CH_4, (c): CO, (d): H_2, and (e) CO_2 reduction (CO + CH_4 + C_2H_4) in four independent experiments of electrochemical reduction of CO_2 in 0.1 mol/L $KHCO_3$ without stirring at -2.1 V (reaction temperature: 25°C, reaction time: 40 min, CO_2 flow rate: 17.7 mL/min; the horizontal lines represent the average faradaic efficiencies calculated from the four different experiments).

Fig.5.19 shows the faradaic efficiencies of different gas products obtained in three independent experiments of electrochemical reduction of CO_2 in 0.1 mol/L $KHCO_3$ with stirring at -2.1 V for 60 min. It can be seen from the figure that the difference of the faradaic

efficiencies in each experiment is much smaller when stirring was used compared with those without stirring. The average faradaic efficiency of CO_2 reduction in 0.1 mol/L $KHCO_3$ with stirring at -2.1 V was 50.1%, while the average faradaic efficiency of H_2 evolution was 26.5%. These results suggested that stirring the electrolyte can improve the reproducibility. This is probably because the stirring helped the mass transfer of both CO_2 and generated gas products, and helped mixing the sample gas well before injecting into the GC analyzer. The fluctuation of the faradaic efficiencies in the electrochemical reduction of CO_2 without stirring probably because the dissolved CO_2 was not well mixed in the solution and sample gas injected into the GC were also not well mixed, which then caused the difference. Therefore, stirring the electrolyte is necessary in the electrochemical reduction of CO_2 to help the mass transfer, mixing the products, and promote the CO_2 reduction.
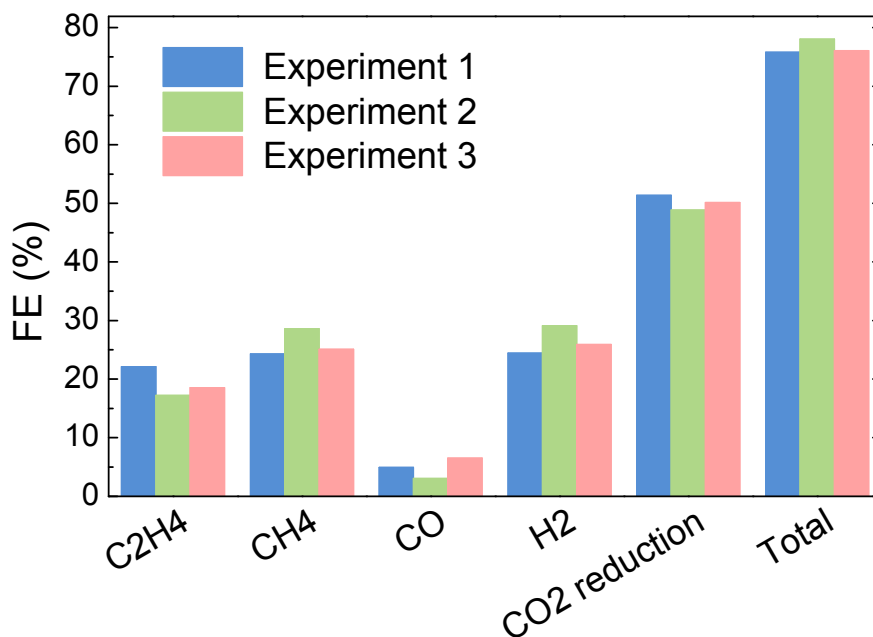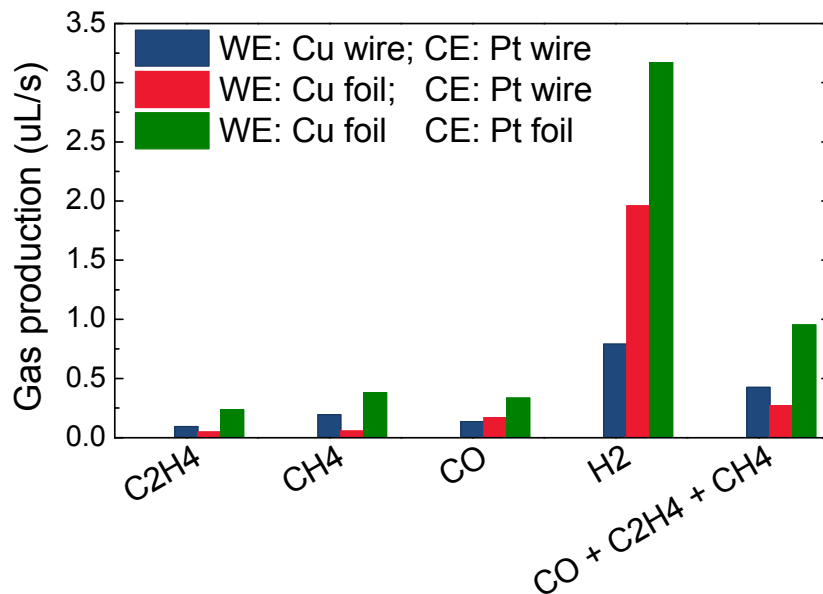

Fig. 5.19 Faradaic efficiencies (FE) of different gas products obtained in three independent experiments of electrochemical reduction of CO_2 in 0.1 mol/L $KHCO_3$ with stirring at -2.1 V for 60 min (CO_2 reduction = $CO + CH_4 + C_2H_4$, reaction temperature: 25 ^{o}C, reaction time: 60 min, CO_2 flow rate: 17.7 mL/min, stirring rate: 1000 rpm).

5.10 Effect of the geometrical shape of Cu working electrode on the CO_2 reduction

Cu wire was used as the working electrode (WE) in all the experiments above. However, the geometrical shape of the Cu working electrode might have an effect on the CO_2 reduction. Therefore, Cu foil (Fig 5.1) with a surface area of *ca.* 4.5 cm^2 was used as the working electrode to study the effect of geometrical shape of Cu working electrode. The counter electrode (CE) geometrical shape effects were also discussed by using Pt wire and Pt foil with a surface area of 0.68 and 5.2 cm^2, respectively. Faradaic efficiencies and production rate of different gas in the electrochemical reduction of CO_2 in 0.1 mol/L $KHCO_3$ under CO_2 bubbling at -2.1 V for 40 min with stirring using Cu wire or Cu foil WE and Pt wire or Pt foil CE were shown in Fig. 5.20. When the Cu foil was used as the WE instead of Cu wire, while keeping the CE as Pt wire, the sum of CH_4, C_2H_4, and CO production rate decreased from 0.43 to 0.27 μL/s, while the H_2 production strongly increased from 0.79 to 1.96 μL/s. As a result, the faradaic efficiency of CO_2 reduction decreased tremendously from 50.1% to 19.2% when Cu foil was used. However, when Pt foil was used as the CE instead of Pt wire, the production rates of all the products increased obviously. The faradaic efficiency of CO_2 reduction increased from 19.2% to 52.9% when replacing Pt wire with Pt foil on Cu foil WE. This CO_2 reduction faradaic efficiency was similar to that obtained on Cu wire WE with Pt wire CE. These results suggested that the CO_2 reduction was limited by the surface area of the CE when Cu foil was used as the WE instead of Cu wire. By changing the Pt wire CE to Pt foil CE (increasing the surface area of CE), the faradaic efficiencies of CO_2 reduction obtained on Cu wire and Cu foil WEs were similar.

It can be seen that in Fig. 5.20, the total faradaic efficiencies, which represent the sum H_2 evolution and CO_2 reduction, were much lower than 100% when Cu wire WE + Pt wire CE or Cu foil WE + Pt wire CE were used, while the total faradaic efficiency was almost 100% when Cu foil WE + Pt foil CE were used. This was possibly because some unknown liquid products existed in the liquid phase. HCOOH is widely reported as the main liquid product in the electrochemical reduction of CO_2 on Cu working electrode [54,78]. Therefore, the liquid

(a)
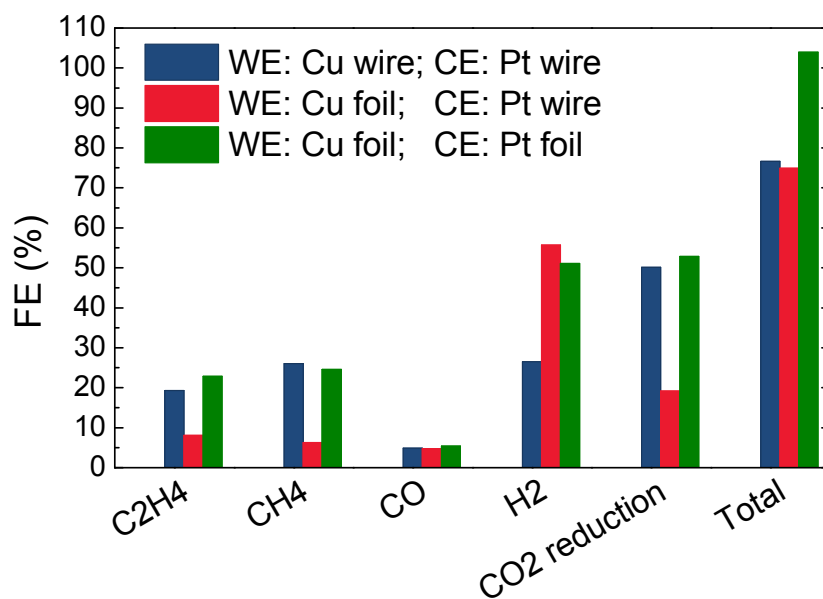
(b)

Fig. 5.20 Gas producing rate (a) and faradaic efficiencies (FE) (b) of different gas products obtained in the electrochemical reduction of CO_2 in 0.1 mol/L $KHCO_3$ with stirring at -2.1 V for 40 min using Cu wire or Cu foil working electrodes (WE), and Pt wire or Pt foil counter electrodes (CE) (reaction temperature: 25 ^{o}C, CO_2 flow rate: 17.7 mL/min, stirring rate: 1000 rpm).

samples after the electrochemical reactions on Cu wire or Cu foil WEs both with Pt wire CE were collected and analyzed by ion chromatography to examine the HCOOH production. Results showed that the faradaic efficiencies of HCOOH production were 5.0% and 14.0% on Cu wire and Cu foil WE, respectively, when using Pt wire CE. Combing the faradaic efficiency of HCOOH production, the total faradaic efficiencies obtained on Cu wire or Cu foil WEs both with Pt wire CE were 81.6% and 97.5%, respectively. The total faradaic efficiency obtained on the Cu wire WE + Pt wire CE was still less than 100%, which possibly caused by other unknown liquid products or some unknown back reactions. However, these are still not clear so far and will be studied in the future.

Fig. 5.21 shows the currents and current densities obtained in the electrochemical reduction of CO_2 in 0.1 mol/L $KHCO_3$ at -2.1 V using Cu wire or foil WE and Pt wire or foil CE. When the Cu foil was used as the WE instead of Cu wire while keeping Pt wire as the CE, the reaction current increased ca 5 mA. This was mainly attributed to the increasing surface area of WE promoting the H_2 evolution as discussed above. When substituting the Pt wire CE by Pt foil, the reaction current further increased. This was contributed by the enhancements of the production rates of all products. However, considering that Cu foil had a larger surface area than Cu wire, the current density was much higher in the case of using Cu wire WE (ca 30.9 mA/cm^2 at 40 min). The current density decreased to only ca 6.2 mA/cm^2 at 40 min when Cu foil WE and Pt wire CE were used. The CO_2 reduction currents and current densities on different WE and CE were summarized in Table 5.6. The CO_2 reduction current was 10.5 mA on Cu wire WE and Pt wire CE. However, it decreased to 5.3 mA when Cu foil WE was used while keeping Pt wire as the CE. When Pt foil CE was used (surface area increased ca 7.8 times compared with Pt wire), a much higher CO_2 reduction current of 25.8 mA was obtained. This suggested that the CO_2 reduction was limited by the surface area of Pt CE when Cu foil WE was used. However, the CO_2 reduction current density obtained on Cu foil WE and Pt foil CE (5.7 mA/cm^2) was still much lower than that obtained on Cu wire WE and Pt wire CE (15.4 mA/cm^2). Although the faradaic efficiencies of CO_2 reduction were similar in these two cases, the faradaic efficiency of H_2 was much higher when Cu foil WE and Pt foil CE were used. This indicated that there were some other factors limited the CO_2 reduction increase with the surface areas of WE and CE. One possible reason was that when Cu foil was

used as the WE, only one side was faced to the CE, the opposite side was much less active. Meanwhile, the mass transfer to the WE is effective from any direction when Cu wire WE was used, while it is less effective from a non-perpendicular direction when Cu foil WE was used. Furthermore, the diffusion constant of H^+ (9.311×10^{-5} cm^2s^{-1}) was much higher than that of CO_2 (1.91×10^{-5} cm^2s^{-1}) [92]. Hence, the CO_2 reduction current density decreased when Cu foil WE was used.
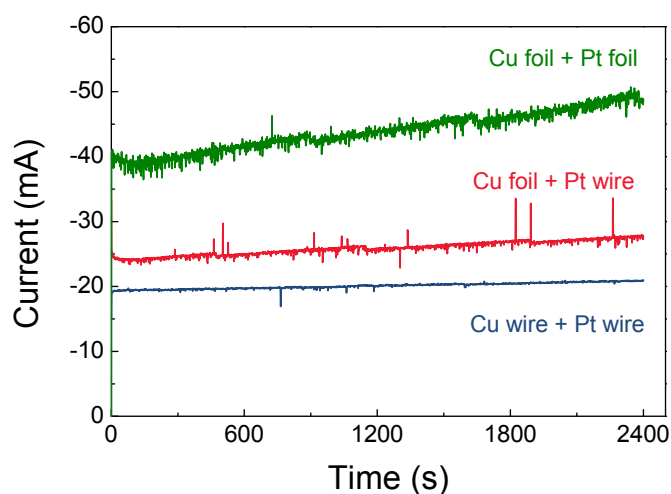
(a)
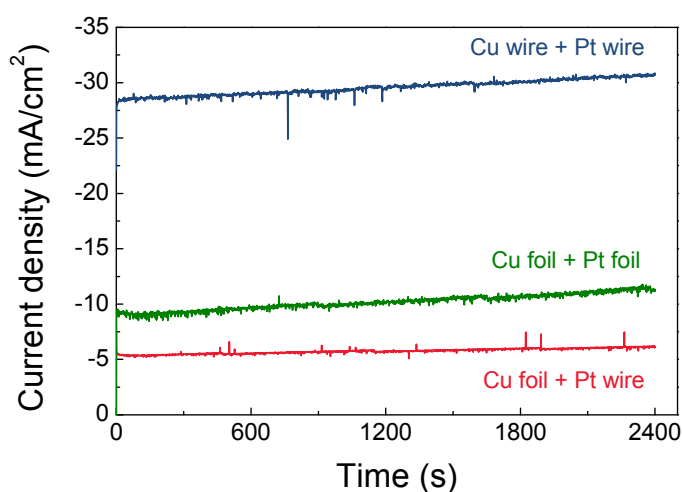
(b)

Fig. 5.21 Currents (a) and current densities (b) obtained in the electrochemical reduction of CO_2 in 0.1 mol/L $KHCO_3$ at -2.1 V using Cu wire or Cu foil WE and Pt wire or Pt foil CE (reaction temperature: 25 ^{o}C, CO_2 flow rate: 17.7 mL/min, stirring rate: 1000 rpm).

Table 5.6 CO_2 reduction current and current densities obtained in 0.1 mol/L $KHCO_3$ at -2.1V on different WE and CE[a]

WE	CE	CO_2 reduction current (mA)	CO_2 reduction current density (mA/cm^2)
Cu wire	Pt wire	10.5	15.4
Cu foil	Pt wire	5.3	1.2
Cu foil	Pt foil	25.8	5.7

[a]Reaction condition: temp: 25 ^{o}C, reaction time: 40 min, CO_2 flow rate: 17.7 mL/min, surface area of Cu wire and Pt wire: 0.68 cm^2, surface area of Cu foil: 4.5 cm^2, surface area of Pt foil: 5.2 cm^2.

The real applied voltage between WE and CE in the electrochemical reduction of 0.1 mol/L $KHCO_3$ at –2.1 V (vs Ag/AgCl) on Cu wire WE + Pt wire CE or Cu foil WE + Pt foil CE were measured by the voltmeter and showed in Fig. 5.22 as function of time. The average real applied voltage between WE and CE was *ca* 10.2 V when Cu wire WE and Pt wire CE were used at the applied potential of –2.1 V (*vs* Ag/AgCl). However, the real applied voltage between WE and CE was much higher when Cu foil WE and Pt foil CE were used. Although further studies are required, this possibly caused by the proton transfer limitation from the CE to WE. Much higher voltage was required to promote more protons transferring through the relatively small Nafion film between WE and CE when Cu foil WE and Pt foil CE were used. Moreover, it can be seen in Fig 5.22, the voltage kept increasing with time quickly on Cu foil WE, which exceeded the maximum voltage (30 V) that can be provided by the electrochemical workstation after 50 min. As a result, a current density decrease was observed after 50 min in the electrochemical reduction of CO_2 on Cu foil WE and Pt foil CE. The voltage increase was probably caused by the K^+ also passing through the Nafion film from the CE to WE side during the reaction, which leaded to a decrease in the conductivity of the electrolyte as reported by Murata [102]. Therefore, to improve the electrochemical CO_2 reduction, the area of the ion exchange membrane between WE and CE should be designed as large as possible and the distance between WE and CE should be as short as possible.
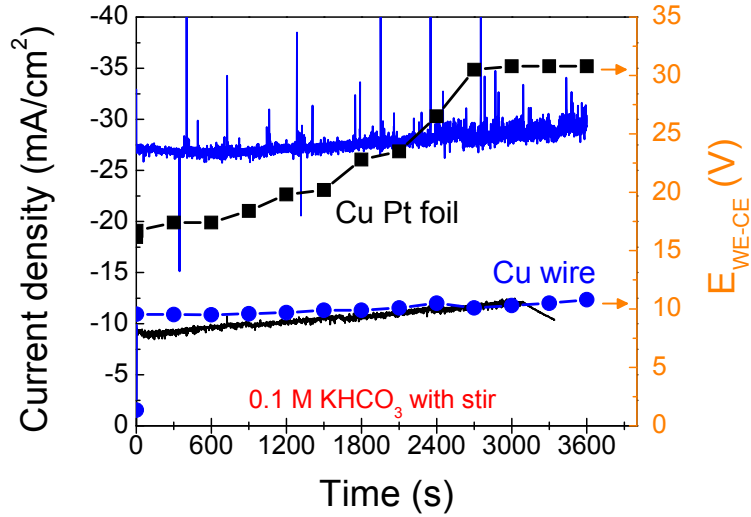
Fig. 5.22 Current density (lines) and real applied voltage between WE and CE (squares and circles) variations in the electrochemical reduction of CO_2 in 0.1 mol/L $KHCO_3$ on different WEs and CEs as function of time (Blue line and circles: data obtained on Cu wire WE and Pt wire CE, black line and squares: data obtained on Cu foil WE and Pt foil CE, applied potential between WE and RE: –2.1 V (*vs* Ag/AgCl), reaction temperature: 25 ℃, CO_2 flow rate: 17.7 mL/min, stirring rate: 1000 rpm).

5.11 Energy conversion efficiency

Since the real applied voltage between WE and CE was measured, the energy conversion efficiency of CO_2 reduction can be calculated by Eq. (5.6).

$$\eta_{CO_2} = \frac{1}{E_{appl}}[(E_{O_2/OH^-} - E_{CO/CO_2})FE_{CO} + (E_{O_2/OH^-} - E_{CH_4/CO_2})FE_{CH_4} + (E_{O_2/OH^-} -$$

$$E_{C_2H_4/CO_2})FE_{C_2H_4} + (E_{O_2/OH^-} - E_{HCOOH/CO_2})FE_{HCOOH}] \times 100\% \tag{5.6}$$

where,

η_{CO_2} is the energy conversion efficiency of CO_2 reduction, %,

E_{appl} is the real applied voltage between WE and CE, V,

E_{O_2/OH^-}, E_{CO/CO_2}, E_{CH_4/CO_2}, $E_{C_2H_4/CO_2}$, E_{HCOOH/CO_2} are the standard electrode potentials of different half reactions, V,

FE_{CO}, FE_{CH_4}, $FE_{C_2H_4}$, FE_{HCOOH} are the faradaic efficiencies of different products.

The measured voltage between Cu wire WE and Pt wire CE was *ca* 10.5 V at 40 min during the reaction. However, there was an initial voltage of 1.35 V between WE and CE before the reaction, which was probably caused by the pH difference of the electrolytes. Therefore the real applied voltage between WE and CE (E_{appl}) was 9.15 V. The relationship between the standard electrode potential and pH has been discussed in section 5.7. Table 5.7 summarized the calculated standard electrode potentials at the real experimental pH and the best faradaic efficiencies of different products obtained in this research. Therefore, the best energy conversion efficiency of CO_2 reduction was calculated to be 6.4%. If adding the energy conversion efficiency of H_2 production, the total energy conversion efficiency was 13.9%. However, these energy conversion efficiencies were not high, which was not only caused by the high over potential of CO_2 reduction and H_2 evolution but also caused by the high resistance of the electrochemical cell. Therefore, besides reducing the over potential of CO_2 reduction, decrease the cell resistance is also important to promote the energy conversion efficiency.

Table 5.7 Standard electrode potential of different products at 25 $^{\circ}$C and different pH[a]

	Standard electrode potential (V)		Faradaic efficiency (%)
	pH = 0	at real experimental pH	
CO/CO_2	–0.103	–0.504 (pH = 6.8)	4.8
CH_4/CO_2	0.169	–0.232 (pH = 6.8)	26.0
C_2H_4/CO_2	0.079	–0.322 (pH = 6.8)	19.3
$HCOOH/CO_2$	–0.225	–0.626 (pH = 6.8)	5.0
H^+/H_2	0	–0.401 (pH = 6.8)	26.5
O_2/OH^-	1.23	0.740 (pH = 8.3)	N/A

[a]reaction conditions: electrolyte: 0.1 mol/L $KHCO_3$, applied potential: -2.1 V, temperature: 25 $^{\circ}$C, reaction time: 40 min, CO_2 flow rate: 17.7 mL/min, stir rate: 1000 rpm.

5.12 Stability of Cu working electrode

The stability of the Cu wire working electrode was examined by conducting the electrochemical reduction of CO_2 in 0.1 mol/L $KHCO_3$ at -2.1 V for 3 hours with stir. Gases producing rates and their faradaic efficiencies during the electrochemical reactions as a function of time were shown in Fig 5.23. It can be seen that the producing rate of C_2H_4 slowly decreased with time while that of CH_4 slightly increased. The producing rate of CO did not change too much during the reaction. Although the overall producing rate of CO_2 reduction products (CO + CH_4 + C_2H_4) did not change too much as the reaction time increasing, the producing rate of H_2 increased more than two times after 3 hours' reaction. As a result, the faradaic efficiency of H_2 evolution increased from 23.4% to 41.6% while the faradaic efficiency of CO_2 reduction reduced from 50.8% to 42.8% when the reaction time increased from 20 min to 180 min. The current density slightly increased with the time from *ca.* 28 mA/cm^2 to *ca.* 37 mA/cm^2. Fig. 5.24 shows the SEM images of Cu wires before and after 1 and 3 hours' electrochemical reactions. The Cu wire was corroded after the electrochemical reaction according to the SEM images. Longer time caused more severe corrosion. Although further studies are needed, these corrosions probably caused by the local pH increase during the reaction and/or adsorption and desorption of the CO_2 and CO_2 reduction intermediates. These corrosions probably increased the surface area of WE, which then promoted the H_2 evolution as discussed above. Furthermore, the corrosion probably changed the crystal faces of the Cu WE. It is reported that the production of CH_4 and C_2H_4 on Cu WE is affected by the crystal face in the electrochemical reduction of CO_2 [62]. Therefore, the producing rate changes of CH_4 and C_2H_4 in Fig 5.22 (b) was possibly caused by the crystal faces change in the Cu WE during the corrosion.
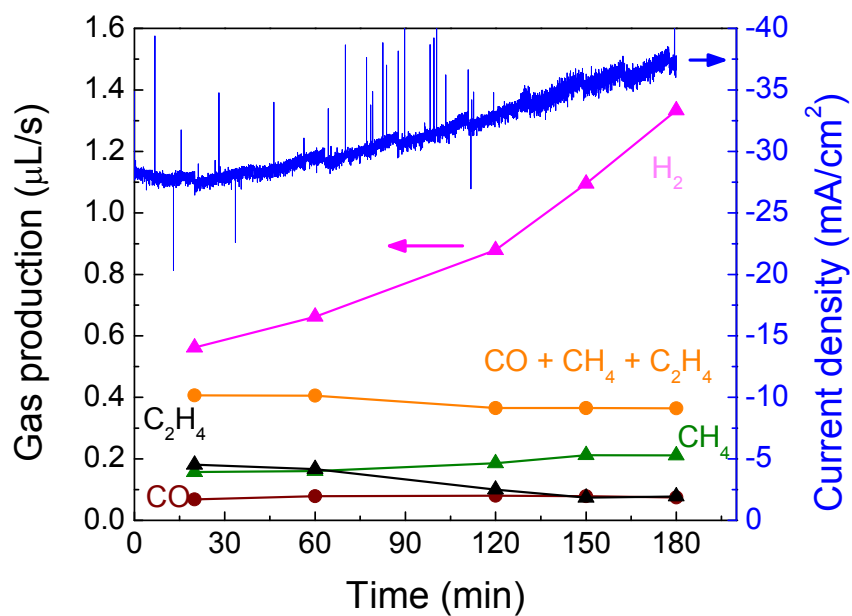
(a)
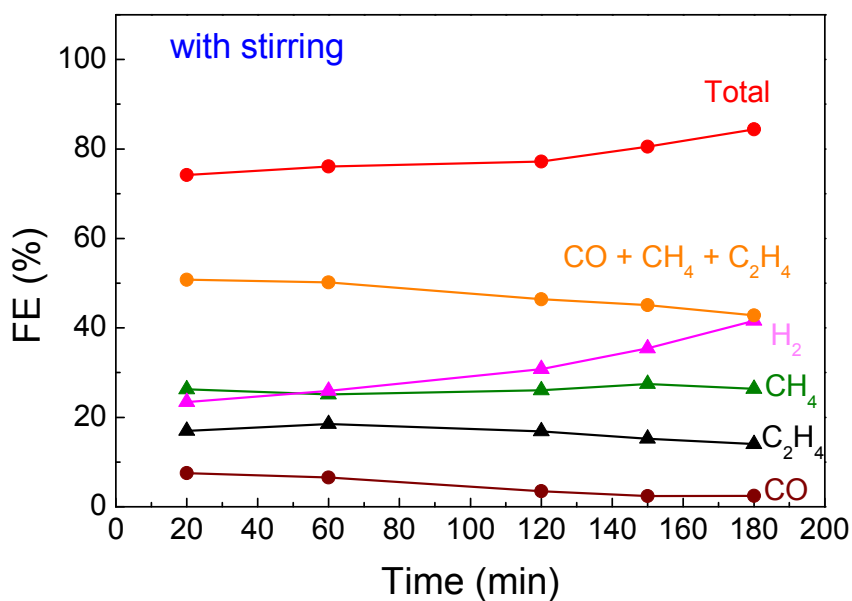
(b)

Fig. 5.23 Gas producing rates (a) and faradaic efficiencies (b) of different gas products as a function of time in the electrochemical reduction of CO_2 in 0.1 mol/L $KHCO_3$ at -2.1 V with stirring on a Cu wire working electrode (reaction temperature: 25 ^{o}C, CO_2 flow rate: 17.7 mL/min, stirring rate: 1000 rpm).
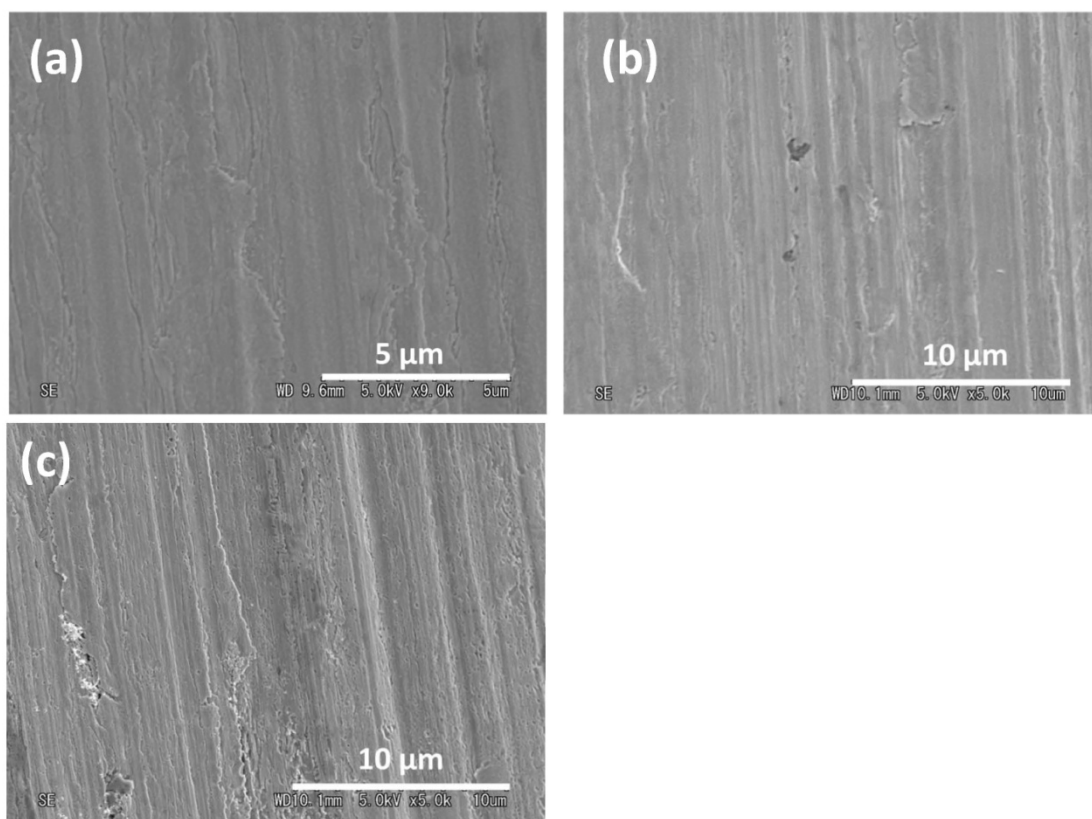
Fig. 5.24 SEM images of Cu wire before (a), after 1 hour (b), and 3 hours' (c) electrochemical reactions in 0.1 mol/L $KHCO_3$ at -2.1 V with stirring (reaction temperature: 25 ^{o}C, CO_2 flow rate: 17.7 mL/min, stirring rate: 1000 rpm).

5.13 Electrochemical reduction of CO_2 in KOH solution

Experiments for studying the effect of KOH solution on the CO_2 reduction were conducted in 0.1 mol/L KOH at -2.1 V for 60 min at room temperature under CO_2 bubbling. Faradaic efficiencies of different gas products obtained at 40 min were shown in Fig. 5.25. It can be seen that the faradaic efficiency of CO_2 reduction and H_2 evolution were very similar in KOH and $KHCO_3$ solutions with the same concentration. This suggested that there is no big difference between KOH and $KHCO_3$ solution in the electrochemical reduction of CO_2. This was because the OH^- transformed into HCO_3^- under the CO_2 bubbling. Therefore, the effect of the CO_2 bubbling on the electrolyte needs to be studied. Detailed studies of the effect of CO_2 bubbling will be discussed in the next chapter. Fig 5.26 showed the current density

obtained during the electrochemical reactions in 0.1 mol/L $KHCO_3$ and KOH. A higher current density was achieved in KOH solution. This probably caused by two reasons. The first is that the pH value in the CE chamber (chamber with counter electrode placed in) in KOH solution is higher than that in $KHCO_3$ solution due to the CO_2 bubbling was only performed in the WE chamber (chamber with working electrode placed in). OH^- remained unchanged in the CE chamber. Therefore, a pH difference made the pH voltage difference between WE and CE, which probably enhanced the current density. Another reason could be the electrical conductivity of 0.1 mol/L KOH solution (2.366 Ω^{-1} m^{-1}) was higher than that of 0.1 mol/L $KHCO_3$ solution (0.904 Ω^{-1} m^{-1}) which lead to the current density increase. Therefore, KOH should be a better electrolyte than $KHCO_3$ for obtaining higher current density while maintaining the product selectivity in the electrochemical CO_2 reduction.
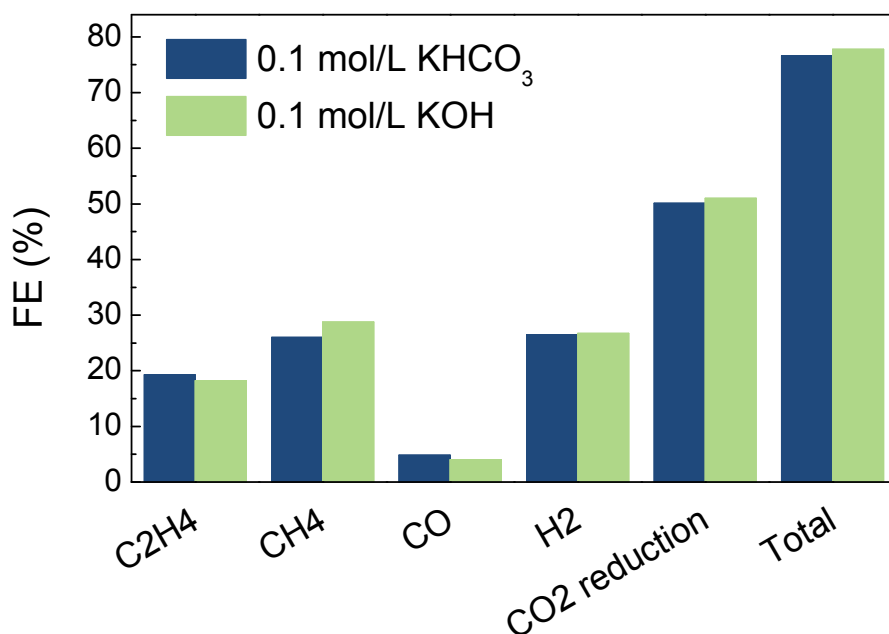

Fig. 5.25 Faradaic efficiencies (FE) of different gas products after the electrochemical reduction of CO_2 in 0.1 mol/L $KHCO_3$ and 0.1 mol/L KOH for 40 min at -2.1 V (reaction temperature: 25 ^oC, reaction time: 40 min, CO_2 flow rate: 17.7 mL/min, stir rate: 1000 rpm).
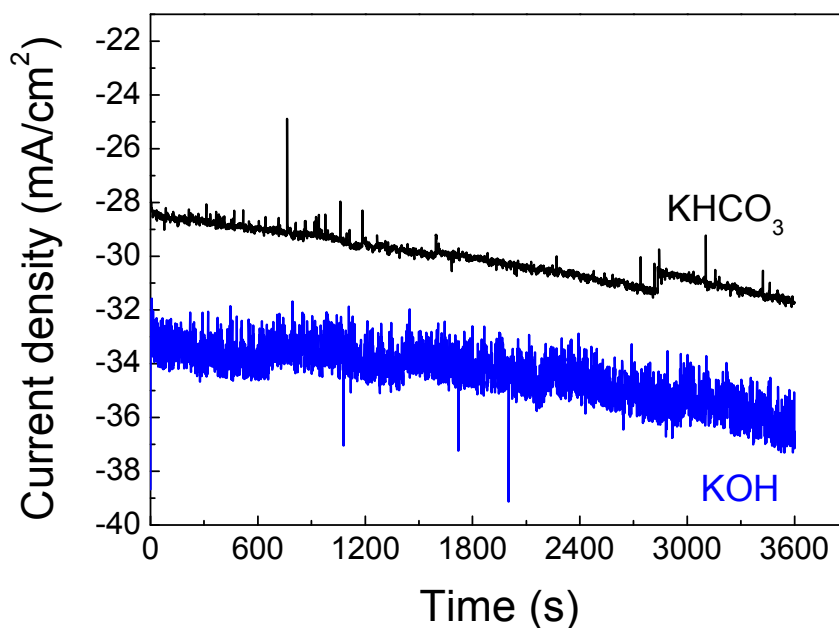
Fig. 5.26 Current densities obtained during the electrochemical reduction of CO_2 in 0.1 mol/L $KHCO_3$ or 0.1 mol/L KOH solutions at -2.1 V (reaction condition: temp: $25^{o}C$, working electrode: Cu, CO_2 flow rate: 17.7 mL/min).

5.14 Summary

The effect of CO_2 bubbling, temperature, electrolyte, applied potential, reaction time, stirring, and geometrical shape of the WE on the electrochemical reduction of CO_2 on Cu WE were studied in this chapter. The gas products after the electrochemical reaction were analyzed and their faradaic efficiencies were calculated. The best energy conversion efficiency of the CO_2 reduction was also calculated. Summaries of these results were given as follow:

1. Since the CO_2 is the active species in the electrochemical reduction of CO_2, the CO_2 bubbling is important and necessary for obtain high faradaic efficiency of the CO_2 reduction.

2. Elevated temperature is not suitable for the CO_2 reduction because the CO_2 reduction reactions are exothermic while the H_2 evolution is endothermic.

3. Concentration of $KHCO_3$ solution strongly affected the faradaic efficiencies of the CO_2 reduction and current density. The optimum faradaic efficiency of CO_2 reduction increased from 4.2% to 43.7% when the $KHCO_3$ concentration decreased from 1.5 to 0.1 mol/L without stir. However, further decreasing the $KHCO_3$ concentration to 0.01 mol/L caused the faradaic efficiency of CO_2 reduction reduced to 32.1%. The best $KHCO_3$ concentration for achieving highest CO_2 reduction was 0.1 mol/L. The reason will be discussed in chapter 6.

4. Product selectivity was also affected by the $KHCO_3$ concentration. C_2H_4 was the main CO_2 reduction product in 0.01 mol/L $KHCO_3$. When the $KHCO_3$ concentration increased to 0.5 mol/L, CH_4 became the dominant product of CO_2 reduction. CO becomes the main product of CO_2 reduction when $KHCO_3$ concentration further increased to 1.5 mol/L. This probably caused by the pH difference of the electrolytes.

5. Faradaic efficiency of CO_2 reduction was more stable with time at lower current density. This is because high current density increased the corrosion of Cu WE, which then promoted the H_2 evolution. The corrosion of Cu WE also caused a selectivity change in the CH_4 and C_2H_4 production, which could be attributed to the crystal faces changed during the corrosion.

6. The optimum faradaic efficiency of CO_2 reduction in 0.1 mol/L KCl without stir was 35.7% (at -1.8 V), which was lower than that in 0.1 mol/L $KHCO_3$ solution. The product selectivity was also different in $KHCO_3$ and KCl solutions. The main product of CO_2 reduction was CH_4 and C_2H_4 in $KHCO_3$, while C_2H_4 was the main product in KCl. These differences probably caused by the pH difference between $KHCO_3$ and KCl solution. KCl solution has much lower pH (2.9) which probably promoted the H_2 evolution while prohibited the CO_2 reduction compared with the $KHCO_3$ (pH 6.8).

7. Stirring the electrolyte can effectively improve the mass transfer, and help removing the adsorbed products on the working electrode and then promote the faradaic efficiency of CO_2 reduction. The reproducibility of CO_2 reduction faradaic efficiencies was much better when stirring was used. The best faradaic efficiency of CO_2 reduction of 55.1% was obtained in 0.1 mol/L $KHCO_3$ at -2.1 V with a current density of 30.9 mA/cm^2 at room temperature with a stir rate of 1000 rpm.

8. Increase the surface area of WE and CE did not promote the CO_2 reduction, but reduced the current density and enhanced H_2 evolution. This is probably because the mass transfer is less effective on the foil WE than wire WE.

9. Faradaic efficiencies of all the gas products in the $KHCO_3$ and KOH solutions were almost the same. However, the current density in KOH was slightly higher, which suggested that KOH could be a better electrolyte than $KHCO_3$ in the electrochemical reduction of CO_2.

10. The best energy conversion efficiency of CO_2 reduction achieved in $KHCO_3$ was only 6.4%, which was probably limited by the high resistance of the electrochemical cell as well as the high over potential of CO_2 reduction.
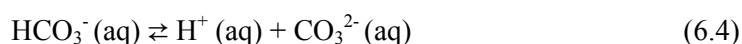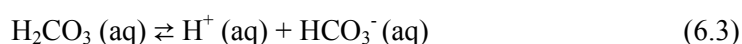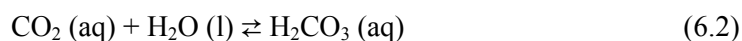
Chapter 6

Effect of CO_2 bubbling into typical aqueous solutions used for electrochemical CO_2 reduction

6.1 Introduction

CO_2 bubbling into the aqueous electrolytes is generally used as the carbon source in the electrochemical and photoelectrochemical reduction of CO_2 [36,37,48-50,56,61,62,85,103-110]. However, the effect of CO_2 bubbling on the electrolytes has been rarely studied. As discussed in chapter 5, bubbling CO_2 into the KOH can transform the KOH into $KHCO_3$, which led to the faradaic efficiencies of CO_2 reduction become almost the same in KOH and $KHCO_3$ solutions. Therefore, the effect of CO_2 bubbling into typical electrolytes used for electrochemical and photoelectrochemical reduction of CO_2 needs to be studied. Furthermore, the concentrations of the dissolved CO_2 in the different solutions probably limit the CO_2 reduction. However, the real amount of dissolved CO_2 in different solutions used in the electrochemical reduction of CO_2 under the CO_2 bubbling has not been reported before. Therefore, the amount of CO_2 in different aqueous solutions under CO_2 bubbling were studied in this chapter to help further study the mechanism of CO_2 reduction.

It is known that the CO_2 gas can dissolve into and react with H_2O to form H_2CO_3, which further decomposes into HCO_3^- and CO_3^{2-} as shown in reaction 6.1 to 6.4 [91].

$$CO_2\ (g) \rightleftarrows CO_2\ (aq) \tag{6.1}$$

$$CO_2\ (aq) + H_2O\ (l) \rightleftarrows H_2CO_3\ (aq) \tag{6.2}$$

$$H_2CO_3\ (aq) \rightleftarrows H^+\ (aq) + HCO_3^-\ (aq) \tag{6.3}$$

$$HCO_3^-\ (aq) \rightleftarrows H^+\ (aq) + CO_3^{2-}\ (aq) \tag{6.4}$$
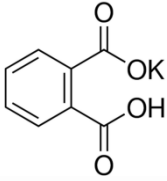
Thus, there are four different carbonaceous species (CO_2, H_2CO_3, HCO_3^-, and CO_3^{2-}) in the aqueous solutions. The concentrations and equilibrium of these different carbonaceous species in aqueous solutions without CO_2 bubbling have been widely studied [91]. However, the concentrations of these carbonaceous species after CO_2 bubbling have not yet been reported. Meanwhile, the pH, the ion composition and concentration, and the CO_2 absorption into the electrolyte are affected by the CO_2 bubbling according to reaction 6.1 to 6.4, which probably influences the CO_2 reduction. Therefore, the effects of the CO_2 bubbling into typical electrolytes used for the CO_2 reduction were studied in this chapter.

6.2. Experimental

6.2.1 Materials

The experimental materials used in this chapter were listed in Table 6.1. $KHCO_3$ (99.5%), K_2CO_3 (99.5%), KCl (99.5%), and KOH (flakes, 86.0%) (Kanto chemical Co., Inc., Japan) were used directly without any purification to make the aqueous solutions. Potassium hydrogen phthalate (99.8%, Sinopharm Chemical Reagent Co. Ltd, China) was used to make standard total organic carbon (TOC) solutions for calibration. Potassium hydrogen phthalate was baked in isothermal oven at $110^{\circ}C$ for 1 h and stored in desiccator before using. All the solutions were prepared by mixing the chemicals with deionized water (18.2 MΩ) made by Organo PRA-0015 deionized water maker. Carbon dioxide (CO_2) gas (99.995%, Taiyo Nippon Sanso Corporation, Japan) was used as the source of CO_2 bubbling during the experiment.

Table 6.1 Materials used in Chapter 6

Entry	Item	Specification	Producer
1	K_2CO_3	99.5%	Kanto chemical Co., Inc.
2	KOH	86.0%	Kanto chemical Co., Inc
3	$KHCO_3$	99.5%	Kanto chemical Co., Inc
4	KCl	99.5%	Kanto chemical Co., Inc
6	HCl	0.1 mol/L	Kanto chemical Co., Inc
7	Potassium hydrogen phthalate	99.8%	Sinopharm Chemical Reagent Co. Ltd, China.
8	Deionized water	18.2 MΩ,	Organo Corporation (PRA-0015)
9	CO_2 gas	99.995%	Taiyo Nippon Sanso

6.2.2 Methods

CO$_2$ was continuously bubbled into 30-mL sample solutions contained in a 40-mL TOC sample vial, and pHs of the solutions were measured online. The experiment setup was shown in Fig. 6.1. The CO$_2$ gas flow rate ranged from 50 to 100 mL/min. The total carbon concentrations (TC) of these solutions before and after bubbling with CO$_2$ until saturation (pH remained unchanged for 30 min) were analyzed by a Shimadzu TOC analyzer (TOC-V CPH).
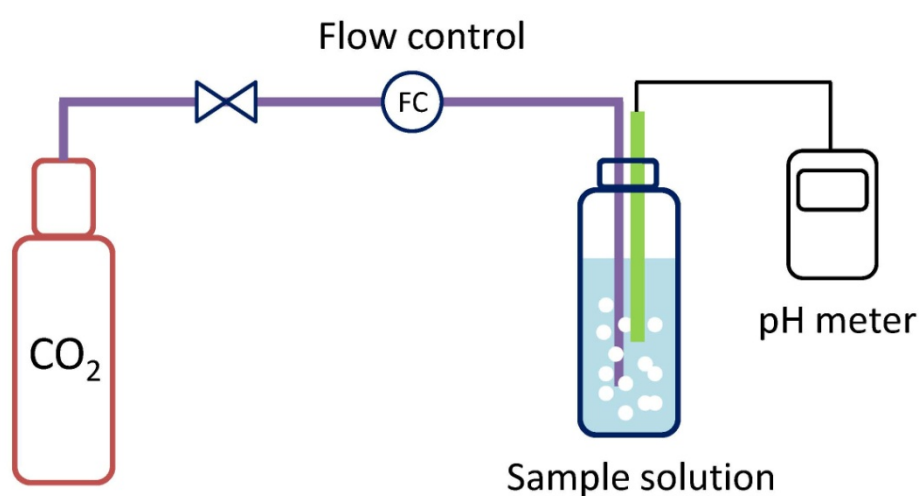
Fig. 6.1 Schematic of experiment setup in chapter 6.

6.3 Carbonate equilibrium in water solution

As shown in reaction 6.1 to 6.4, the CO$_2$ can dissolve into and react with H$_2$O to form H$_2$CO$_3$, HCO$_3^-$, and CO$_3^{2-}$. The concentration of the H$_2$CO$_3$ is, however, much smaller than that of the dissolved CO$_2$ (CO$_2$ (aq)) (≤ 0.3 %) [91]. The sum of the two electronic neutral forms are chemically inseparable [91]. Therefore, [H$_2$CO$_3^*$] is generally used to denote the sum of [H$_2$CO$_3$] and [CO$_2$ (aq)] in the aqueous solution. Note that the carbonate equilibrium in water solution is not denoted by the reaction path ways. It is generally denoted as follows [91]:

$$CO_2\ (aq) + H_2O\ (l) \overset{K_1}{\rightleftarrows} H^+\ (aq) + HCO_3^-\ (aq) \overset{K_2}{\rightleftarrows} 2H^+\ (aq) + CO_3^{2-}\ (aq) \tag{6.5}$$
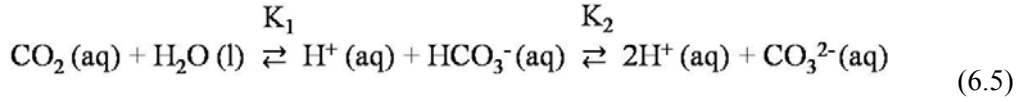
Then the equilibrium constants of K_1 and K_2 are given as:

$$K_1 = \frac{[H^+][HCO_3^-]}{[CO_2(aq)]} \approx \frac{[H^+][HCO_3^-]}{[H_2CO_3^*]} \tag{6.6}$$

$$K_2 = \frac{[H^+][CO_3^{2-}]}{[HCO_3^-]} \tag{6.7}$$

where $pK_1 = 6.35$ and $pK_2 = 10.33$ at 25 ^{o}C [95]. The total concentration of dissolved carbonaceous forms (TC) is expressed as follows:

$$TC = [H_2CO_3^*] + [HCO_3^-] + [CO_3^{2-}] \tag{6.8}$$

Then the $[CO_3^{2-}]$, $[HCO_3^-]$, and $[H_2CO_3^*]$ can be derived from Eqs (6.6) to (6.8) as follows:

$$[CO_3^{2-}] = \frac{K_1 K_2\ TC}{[H^+]^2 + K_1[H^+] + K_1 K_2} \tag{6.9}$$

$$[HCO_3^-] = \frac{K_1[H^+]TC}{[H^+]^2 + K_1[H^+] + K_1 K_2} \tag{6.10}$$

$$[H_2CO_3^*] = TC - [HCO_3^-] - [CO_3^{2-}] \tag{6.11}$$

Since the K_1 and K_2 are constants, the dependence of $[HCO_3^-]$, $[CO_3^{2-}]$, and $[H_2CO_3^*]$ on the $[H^+]$ at given TC in aqueous solution can be plotted in accordance with Eqs. (6.9) to (6.11) as shown in Fig. 6.2. The composition of carbonaceous species is dependent on $[H^+]$ and independent of TC. The TC affects the maximum concentration of each species. The $H_2CO_3^*$ is the dominant species at pH below 5. The HCO_3^- becomes the major anion when the pH ranges from 7.5 to 9. There is only CO_3^{2-} when the pH is above 12. When $[HCO_3^-]$ is the same as $[H_2CO_3^*]$, it can be derived immediately from Eq. (6.6) that the pH is equal to pK_1, which is 6.35. This is indicated by the intersection A in Fig. 6.2. A similar reasoning holds for

intersection B in Fig. 6.2, where the pH is equal to pK_2 (10.33) and $[HCO_3^-]$ is equal to $[CO_3^{2-}]$.
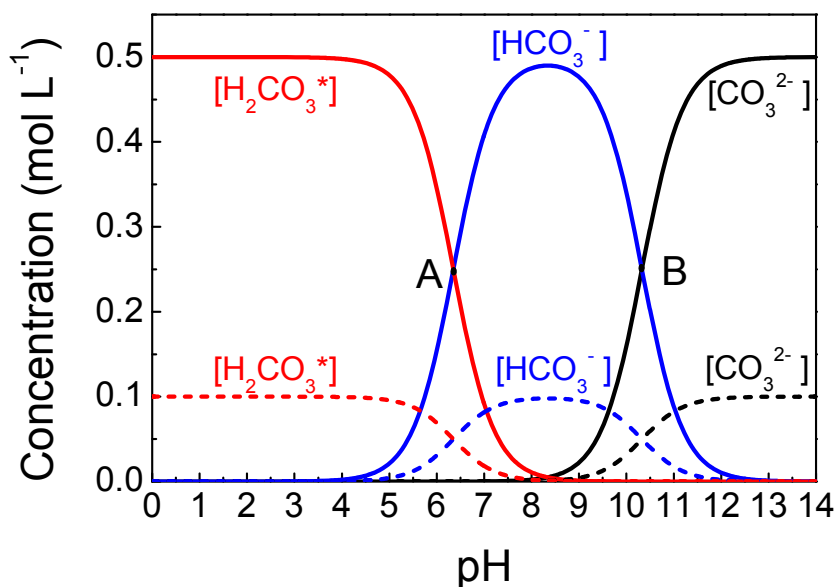
Fig. 6.2 Variations of the compositions of the carbonaceous species in water solution with the pH at different total dissolved carbon concentrations (TC) (TC: solid line: 0.5 mol L^{-1}; dashed line: 0.1 mol L^{-1}).

6.4 Effect of CO_2 bubbling on the pH changes of different solutions

As shown in reactions 6.1 to 6.4, the dissolved CO_2 in the aqueous solutions decomposes into HCO_3^- and CO_3^{2-} and produces H^+, which probably leads to a pH decrease in the solutions. The time dependences of the pH changes in different solutions were investigated by measuring the pH under a constant CO_2 bubbling rate of 50 mL min^{-1} to study the effect of CO_2 bubbling on the pH. The results are shown in Fig. 6.3. The pHs of the solutions obviously decrease after bubbling with CO_2 in all cases except for 0.1 mol L^{-1} HCl, in which the pH remains almost the same during the experiment. As shown in reaction 6.5, the pK_1 and

pK_2 of the H^+ generation from the reaction of CO_2 with H_2O are 6.35 and 10.33, respectively. This suggests that the H^+ generated from the decomposition of the absorbed CO_2 is extremely lower than the concentration of the H^+ contained in 0.1 mol L^{-1} HCl. Therefore, no significant change is observed in the pH of 0.1 mol L^{-1} HCl.
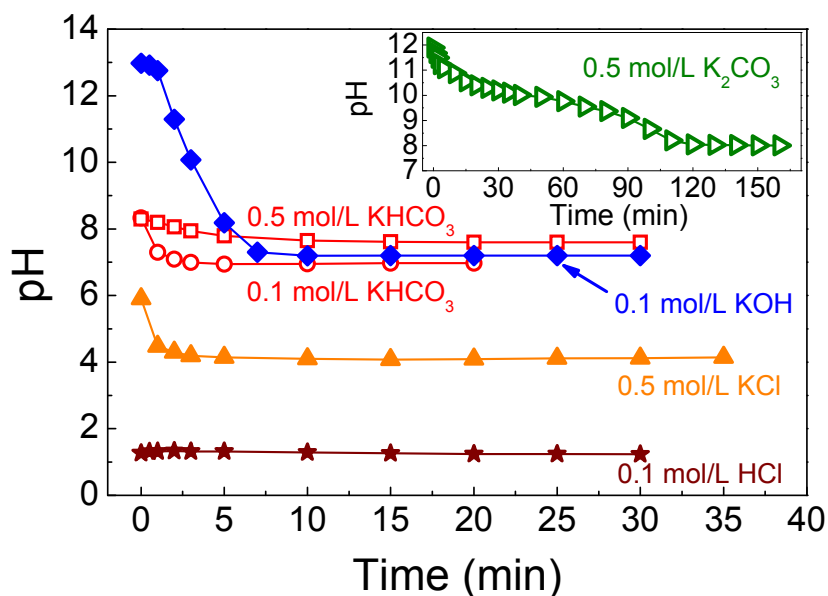
Fig. 6.3 pHs as functions of time in different electrolytes under the bubbling of CO_2 (CO_2 flow rate: 50 mL min^{-1}, temperature: room temperature (23 ^oC)).

In solutions of KOH, $KHCO_3$, and KCl, the pH dropped quickly in the first 10 min but kept stable after that. This means the CO_2 absorptions in these electrolytes were reached a steady state after bubbling of CO_2 for 10 min. In 0.1 mol L^{-1} KOH, the pH dropped from 13.0 to 7.2 after CO_2 bubbling. This can be attributed to the reaction of $H_2CO_3^*$ (dissolved CO_2) with the OH^- contained in the KOH solution as shown in reaction 6.12.

$$H_2CO_3^* \text{ (aq)} + OH^- \text{ (aq)} \rightleftarrows HCO_3^- \text{ (aq)} + H_2O \text{ (l)} \qquad (6.12)$$
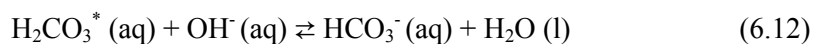
This reaction can be derived from reaction 6.1 to 6.4. As a result, the KOH solution changed into $KHCO_3$ solution after bubbling with CO_2 until saturation. The pH of 0.1 mol L^{-1} KOH after the CO_2 bubbling (pH = 7.2) was very similar to that of 0.1 mol L^{-1} $KHCO_3$ after the CO_2 bubbling (pH = 7.1). This suggests that the final solutions of 0.1 mol L^{-1} KOH and 0.1 mol L^{-1} $KHCO_3$ are similar after the CO_2 bubbling.

In the $KHCO_3$ solution, the CO_2 bubbling did not affect the pH much. Both pHs were *ca.* 8.3 in 0.1 and 0.5 mol L^{-1} $KHCO_3$ before the CO_2 bubbling. The basicity before bubbling was caused by the OH^- generated from the reaction of HCO_3^- with H_2O as shown in reaction 6.13.

$$HCO_3^- \text{ (aq)} + H_2O \text{ (l)} \rightleftarrows H_2CO_3^* \text{ (aq)} + OH^- \text{ (aq)} \qquad pK_3 = 7.65 \qquad (6.13)$$
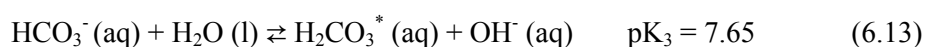
The equilibrium constant K_3 of this equation can be derived as:

$$K_3 = \frac{[H_2CO_3^*] \times [OH^-]}{[HCO_3^-]} = \frac{[H_2CO_3^*] \times K_w}{[HCO_3^-] \times [H^+]} = \frac{K_w}{K_1} \qquad (6.14)$$

Therefore,

$$pK_3 = pK_w - pK_1 = 7.65 \qquad (6.15)$$

The reaction 6.13 is actually the reverse reaction of reaction 6.12. In the $KHCO_3$ solutions before CO_2 bubbling, reaction 6.13 was the dominant reaction. During the bubbling of CO_2, the dissolved CO_2 increased the concentration of $H_2CO_3^*$ and then made reaction 6.13 shift to the left, which means reaction 6.12 became the dominant. As a result, the OH^- was consumed by $H_2CO_3^*$ and leaded to the pH decrease and $[HCO_3^-]$ increase. This suggested that reaction 6.12 was the dominant reaction under CO_2 bubbling. The pHs in 0.1 and 0.5 mol L^{-1} $KHCO_3$ after bubbling with CO_2 were 7.0 and 7.6, respectively. Less pH drop was observed in higher concentration $KHCO_3$ solution. This is because increasing the HCO_3^- concentration can prevent the $H_2CO_3^*$ from reacting with OH^- as shown in reaction 6.12, and then prohibit the pH drop.

In 0.5 mol L^{-1} K_2CO_3, it took over 2 h for the pH drop to reach the steady state than other solutions under CO_2 bubbling as shown in the inset of Fig. 6.3. The pH decrease under the CO_2 bubbling can be roughly separated into three parts: a quick drop in the first 30 min, a slow drop between 30 to 90 min, and a relatively quick drop from 90 to 120 min. In the

K_2CO_3 solution before the CO_2 bubbling, OH^- were generated from the reaction of CO_3^{2-} with H_2O as shown in reaction 6.16.

$$CO_3^{2-} \text{ (aq)} + H_2O \text{ (l)} \rightleftarrows HCO_3^- \text{ (aq)} + OH^- \text{ (aq)} \qquad pK_4 = 3.67 \qquad (6.16)$$
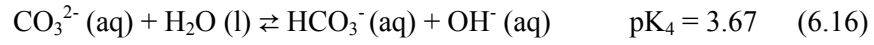
The equilibrium constant K_4 of this equation can be derived as:

$$K_4 = \frac{[HCO_3^-] \times [OH^-]}{[CO_3^{2-}]} = \frac{[HCO_3^-] \times K_w}{[CO_3^{2-}] \times [H^+]} = \frac{K_w}{K_2} \qquad (6.17)$$

Therefore,

$$pK_4 = pK_w - pK_2 = 3.67 \qquad (6.18)$$

This leads to the basicity of the K_2CO_3 solution before bubbling. Although the generated HCO_3^- from reaction 6.16 can further react with H_2O to form OH^- as shown in reaction 6.13, pK_3 of reaction 6.13 is much bigger than pK_4 of reaction 6.16. The effect of reaction 6.13 in K_2CO_3 solution can be omitted. Therefore, reaction 6.16 was the dominant reaction in K_2CO_3 solution without CO_2 bubbling. In the beginning of CO_2 bubbling into K_2CO_3, the absorbed CO_2 reacted with the OH^- and produced HCO_3^- in accordance with reaction 6.12. This leaded to the quick pH drop in the first 30 min. The decrease of OH^- caused the reaction 6.16 shifted to the right side and then leaded to the CO_3^{2-} transforming into HCO_3^-. Although both reaction 6.12 and reaction 6.16 produced HCO_3^-, the concentration of HCO_3^- was very low in the starting state, which was not able to affect reaction 6.12 and 6.16 obviously. However, as the reactions processed, the increased concentration of HCO_3^- prohibited the reaction 6.12 and 6.16. Since the CO_2 was keep bubbling into the solution, reaction 6.12 should still dominate in the system. As a result, the pH drop slowed down from 30 min. After all the CO_3^{2-} transformed into HCO_3^-, situations became the same as bubbling of CO_2 into $KHCO_3$ solutions. The pH drop speeded up again from 90 min. Therefore, the pH drop pattern of CO_2 bubbling into K_2CO_3 showed three different parts. The detailed mechanism should be controlled by the reaction kinetics which needs to be studied in the future. By combining reactions 6.12 and 6.16, the total reaction of CO_2 bubbling into K_2CO_3 solution can be derived as follows:

$$CO_3^{2-} \text{ (aq)} + H_2CO_3^* \text{ (aq)} \rightleftarrows 2HCO_3^- \text{ (aq)} \qquad (6.19)$$
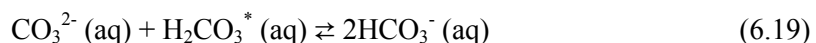
As a result, the 0.5 mol L^{-1} K$_2$CO$_3$ became 1.0 mol L^{-1} KHCO$_3$ after bubbling with CO$_2$ until saturation. The reaction 6.12 should be the dominant reaction to drive the pH decrease in all the solutions under CO$_2$ bubbling.

6.5 Total carbon concentrations of different solutions before and after CO$_2$ bubbling

The concentrations of different carbonaceous species (H$_2$CO$_3$*, HCO$_3$$^-$, and CO$_3$$^{2-}$) can be calculated through Eqs. 6.9 − 6.11 if the TC is known. Then the TCs of different solutions before and after bubbling with CO$_2$ were measured by TOC and the results are shown in Figure 6.4. The TCs in 0.1, 0.5 and 1.5 mol L^{-1} KHCO$_3$ were 0.105, 0.523 and 1.575 mol L^{-1} before bubbling and 0.141, 0.549 and 1.599 mol L^{-1} after bubbling, respectively. Therefore, the TCs increased 0.036, 0.026, and 0.024 mol L^{-1} in 0.1, 0.5, and 1.5 mol L^{-1} KHCO$_3$ after bubbling with CO$_2$, respectively. These TC increases were caused by the absorption of CO$_2$ into the solutions. However, the absolute increases in TC reduced from 0.036 to 0.024 mol L^{-1} as the KHCO$_3$ concentration increased from 0.1 to 1.5 mol L^{-1}. Hence, more CO$_2$ was absorbed in lower concentration of KHCO$_3$, which suggested that the lower concentration of KHCO$_3$ promoted the absorption of CO$_2$ into the solution. This can be also explained from reaction 6.12. Decreasing the HCO$_3$$^-$ concentration caused the reaction 6.12 shifted to the right, which led to a decrease of H$_2$CO$_3$* concentration. As the H$_2$CO$_3$* concentration decrease, more CO$_2$ was absorbed into the solution to maintain the H$_2$CO$_3$* concentration which was controlled by the Henry's law. Results in chapter 5 showed that the optimum CO$_2$ reduction was obtained in 0.1 mol/L KHCO$_3$. Hori et al. also reported similar results [54]. This was probably because more CO$_2$ was absorbed in the lower concentration KHCO$_3$ electrolytes and hence promoted the CO$_2$ reduction.
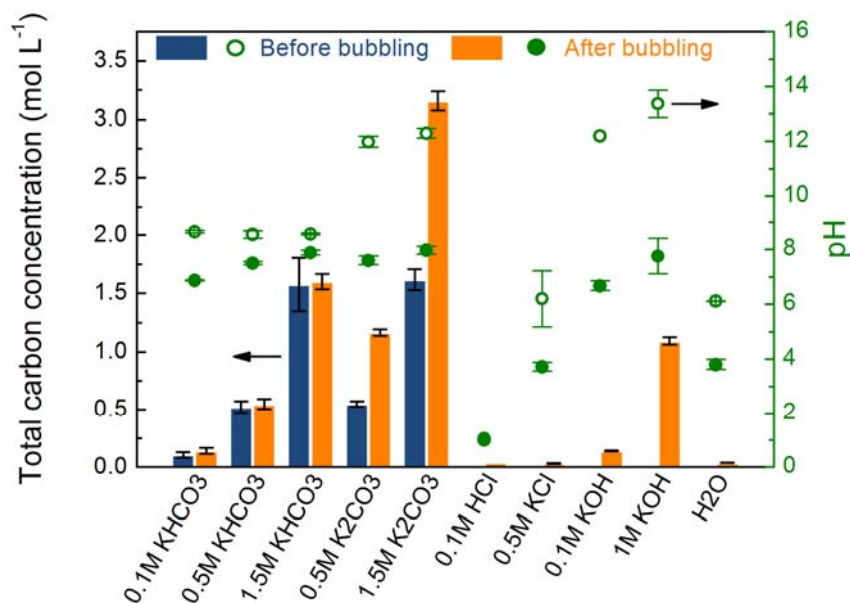
Fig. 6.4 Total dissolved carbon concentration (TC) and pH changes in different solutions before and after bubbling with CO_2 until saturation (blue bar: TC before bubbling, orange bar: TC after bubbling, open green circle: pH before bubbling, solid green circle: pH after bubbling, M: mol L^{-1}, CO_2 flow rate: 100 mL min^{-1}, temperature: room temperature (23^oC)).

In the case of K_2CO_3, the TC doubled after the CO_2 bubbling. The TCs increased from 0.55 to 1.17 and 1.61 to 3.16 mol L^{-1} in 0.5 and 1.5 mol L^{-1} K_2CO_3 after CO_2 bubbling, respectively. This proved that all the original CO_3^{2-} was transformed into HCO_3^- after bubbling with CO_2, and the same amount of HCO_3^- was generated from the absorbed CO_2 depending on the electroneutrality of the solution as discussed in the former section. As a result, the 0.5 and 1.5 mol L^{-1} K_2CO_3 solutions change into 1.0 and 3.0 mol L^{-1} $KHCO_3$ solutions after the CO_2 bubbling, respectively, which can be explained by reaction 6.19.

In the solutions of 0.1 mol L^{-1} HCl, 0.5 mol L^{-1} KCl, and pure H_2O, the TCs were almost zero before CO_2 bubbling. The TCs were very similar in these solutions after bubbling with CO_2, ranging from 0.03 to 0.04 mol L^{-1}. This suggests that the major ions such as K^+ and Cl^- in these solutions have no obvious effect on the absorption of the CO_2.

The TC increased from zero to 1.1 mol L^{-1} after the CO_2 bubbling in the OH^- abundant solution of 1.0 mol L^{-1} KOH. Considering that the pH of the KOH solution after bubbling

with CO_2 was *ca.* 7.8, the dominant anion changed into HCO_3^- in accordance with the reaction of OH^- with $H_2CO_3^*$ in reaction 6.12. As a result, the solutions of 1.0 mol L^{-1} KOH, 1.0 mol L^{-1} $KHCO_3$, and 0.5 mol L^{-1} K_2CO_3 probably change into 1.0 mol L^{-1} CO_2 saturated $KHCO_3$ after the CO_2 bubbling.

If we assume the CO_2 is a simple gas and can be applied to Henry's law, which describes the equilibrium between vapor and liquid as below:

$$c_{H_2CO_3*} = \kappa p_{CO_2} \tag{6.20}$$

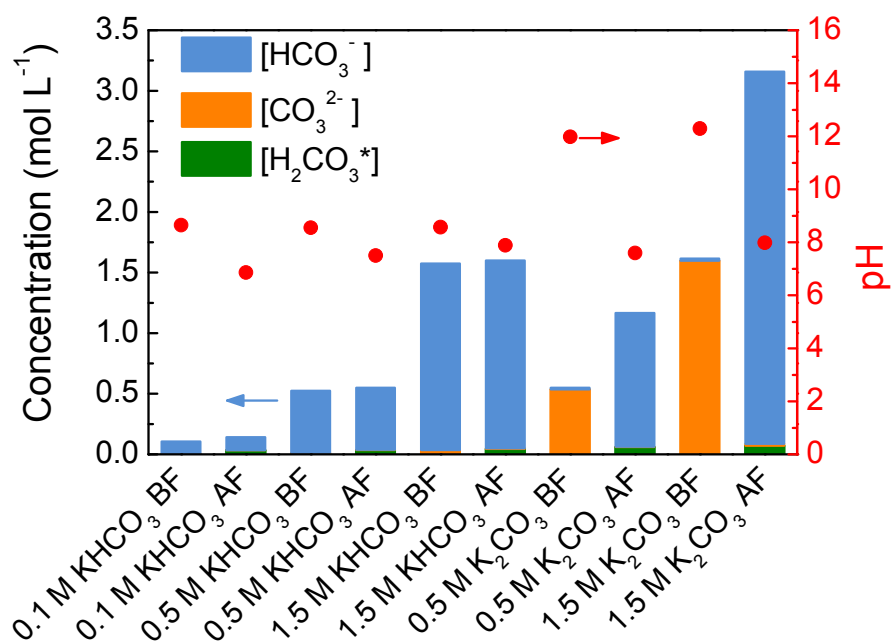where the p_{CO_2} is the partial pressure of the CO_2 in the bulk atmosphere, κ is the Henry's law constant for CO_2 ($\kappa = 0.035$ mol L^{-1} atm^{-1}, at 25 ^{o}C) [111], and $c_{H_2CO_3*}$ is the concentration of dissolved CO_2. Therefore, the concentration of $H_2CO_3^*$ is calculated to be 2.46×10^{-4} mmol/mol (1.38×10^{-5} mol L^{-1}) and 0.622 mmol/mol (0.035 mol L^{-1}) in water under CO_2 partial pressure of *ca.* 3.95×10^{-4} atm (the real partial pressure of CO_2 in the atmosphere) and 1 atm at 25°C, respectively. Our experiment results showed that the TC in pure H_2O was observed to be *ca.* 0.036 mol L^{-1} after bubbling with CO_2 until saturated in comparison that the TC was almost zero before CO_2 bubbling. These results were very close to the theoretic results. According to Henry's law, this suggests that the CO_2 bubbling increased the CO_2 partial pressure into about 1 atm and then lead to the concentration of CO_2 in water increased over 2500 times.

6.6. $[H_2CO_3^*]$, $[HCO_3^-]$, and $[CO_3^{2-}]$ in different solutions before and bubbling with CO_2.

The concentration of each carbonaceous species ($H_2CO_3^*$, HCO_3^-, and CO_3^{2-}) can be calculated by Eqs. 6.9 to 6.11 from the measured TC and pH of different solutions before and after CO_2 bubbling as discussed. Fig. 6.5 shows the composition and concentrations of $H_2CO_3^*$, HCO_3^-, and CO_3^{2-} in different solutions before and after bubbling with CO_2 until saturation. The major anion in the $KHCO_3$ solutions is always HCO_3^- before and after CO_2 bubbling. It is not affected by the $KHCO_3$ concentration. However, the major anion changed

from CO_3^{2-} into HCO_3^- after bubbling in K_2CO_3 solutions, as already discussed. A small amount of $H_2CO_3^*$ was also found in both $KHCO_3$ and K_2CO_3 solutions after CO_2 bubbling. This was caused by the pH decrease that affected the distribution of carbonaceous species, which could be explained by Fig. 6.2. In the case of 0.1 mol L^{-1} HCl, 0.5 mol L^{-1} KCl, and pure H_2O, the dissolved carbonaceous forms are $H_2CO_3^*$ after CO_2 bubbling. In the case of 1.0 mol L^{-1} KOH, the dominant anion is the HCO_3^- after bubbling, which holds *ca.* 96% of the TC. Therefore, the major anion in $KHCO_3$, K_2CO_3, and KOH is HCO_3^-, while $H_2CO_3^*$ is the dominant species in HCl, KCl, and pure H_2O after bubbling with CO_2.

Since the active species in the electrochemical reduction of CO_2 is dissolved CO_2, the concentration of $H_2CO_3^*$ (represents the active species) and the ratio of $[H_2CO_3^*]$/TC were calculated and shown in Fig. 6.6 to clarify the amount of the active species in different solutions. The $[H_2CO_3^*]$ increased from 33 to 45 mmol L^{-1} in the CO_2 saturated $KHCO_3$ solutions with the concentration from 0.1 to 1.5 mol L^{-1}. The ratio of $[H_2CO_3^*]$/TC was 23.6% in 0.1 mol L^{-1} $KHCO_3$, while it was only 2.8% in 1.5 mol L^{-1} $KHCO_3$, after CO_2 bubbling. The relationship between $[H_2CO_3^*]$/TC ratio and the optimum faradaic efficiency of CO_2 reduction in different concentration $KHCO_3$ solutions (data from chapter 5) were showed in Fig. 6.7. It can be seen that, the optimum faradaic efficiency of CO_2 reduction increased with the $[H_2CO_3^*]$/TC ratio. Therefore, the promotion of CO_2 reduction in low concentration $KHCO_3$ solution probably caused by the high $[H_2CO_3^*]$/TC ratio. Although further evidences are needed, a possible explanation of why high $[H_2CO_3^*]$/TC ratio in low concentration $KHCO_3$ solutions promotes the CO_2 reduction could be suggested as follow. Low concentration $KHCO_3$ solution also contains low concentration of K^+. Although K^+ cannot be reduced at the operation potential (redox potential of K^+/K is -2.925 V vs NHE @ 25^oC), it should be attracted around or even adsorbed on the Cu electrode which might prevent the CO_2 adsorption and/or reduction. As a result, the prevention effect of K^+ was smaller in low concentration $KHCO_3$ solution with high $[H_2CO_3^*]$/TC ratio.

(a)

(b)

Fig. 6.5 Concentrations of $H_2CO_3^*$ (green bar), HCO_3^- (blue bar), and CO_3^{2-} (orange bar) calculated from TC and pHs (orange circle) in different solutions before and after bubbling with CO_2 until saturation ((a): in solutions of $KHCO_3$ and K_2CO_3; (b) in solutions of HCl, KCl, KOH, and deionized H_2O. BF: before bubbling, AF: after bubbling, M: mol L^{-1}, temperature: room temperature (23°C)).

Fig. 6.6 $H_2CO_3^*$ concentrations and molar ratios of $H_2CO_3^*$ to TC in different solutions before and after bubbling with CO_2 until saturation (orange bar: $[H_2CO_3^*]$ before bubbling, blue bar: $[H_2CO_3^*]$ after bubbling, solid green circle: $[H_2CO_3^*]$/TC ratio after bubbling, temperature: room temperature (23°C)).

Fig. 6.7 Optimum faradaic efficiency of CO_2 reduction obtained in chapter 5 as function of $[H_2CO_3^*]$/TC ratio (reaction condition: temp: 25°C; potential: -2.1 V, -1.7V and -1.5 V for 0.1, 0,5 and 1.5 mol/L KHCO3 respectively; reaction time: 40 min).

The concentration of $H_2CO_3^*$ in the K_2CO_3 solution is generally higher than that in the $KHCO_3$ solution. A 62 and 72 mmol L^{-1} of $H_2CO_3^*$ were obtained in 0.5 and 1.5 mol L^{-1} K_2CO_3, respectively, after the CO_2 bubbling. However, the ratio of $[H_2CO_3^*]/TC$ is still very low: only 5% of the TC is in the form of $H_2CO_3^*$ in 1.5 mol L^{-1} K_2CO_3. In the case of 0.1 mol L^{-1} HCl, 0.5 mol L^{-1} KCl, and pure H_2O, almost 100% of the TC is $H_2CO_3^*$, and the concentrations of $H_2CO_3^*$ are around 30 to 40 mmol L^{-1}, which is close to that in the 0.1 mol L^{-1} $KHCO_3$ (33 mmol L^{-1}). This suggests that the HCl, KCl, and H_2O could be good electrolytes for the electrochemical reduction of CO_2 from the viewpoint of a high active species ratio. However, considering the low pH of HCl with a large amount of H^+ and the poor conductivity 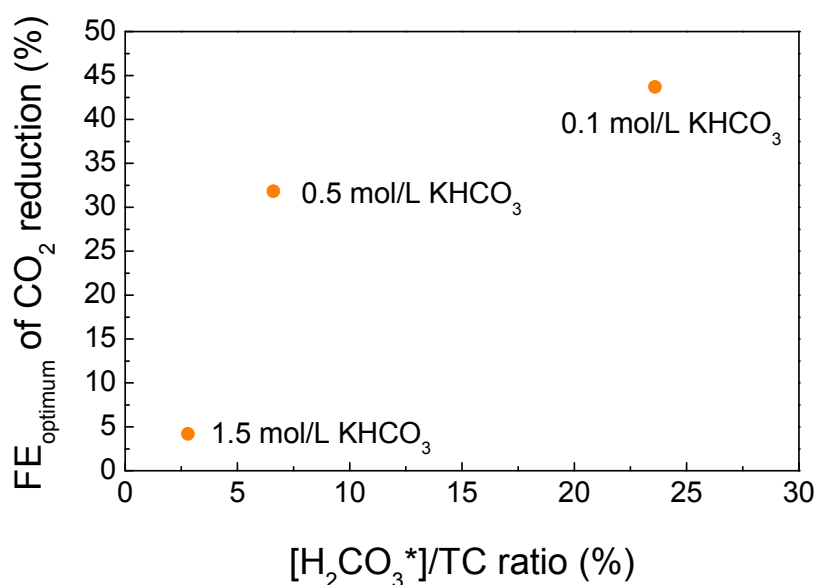of pure H_2O, they are not suitable for CO_2 reduction. Only KCl is appropriate for the electrochemical reduction of CO_2. Therefore, the $KHCO_3$ and KCl solutions are two of the most widely used electrolytes in the electrochemical and photoelectrochemical reduction of CO_2 in aqueous solutions probably because they have a high ratio of the active species ($H_2CO_3^*$) according to our results [37,54,86,87,112]. Note that in the electrochemical reduction of CO_2, H^+ was consumed and the local pH around the electrode was increased, which was not good for the CO_2 reduction because the standard redox potential of the CO_2 reduction shifted negatively as the pH increased (Fig. 5.13). Therefore, the $KHCO_3$ solution is probably better than KCl solution because the existence of HCO_3^- in $KHCO_3$ solution has a buffer effect to maintain the pH of the solution. In the case of 0.1 mol L^{-1} KOH, the ratio of $[H_2CO_3^*]/TC$ was similar to that obtained in 0.1 mol L^{-1} $KHCO_3$. Therefore, the faradaic efficiencies of CO_2 reduction obtained in KOH and $KHCO_3$ solutions were no big difference as discussed in chapter 5.

6.7 Thermodynamic calculation

Thermodynamic study suggested that the pH of H_2O under CO_2 bubbling was decided by the carbonate equilibrium as shown in reaction 6.5. Since the equilibrium constants K_2 is much smaller than K_1, the pH was mainly decided by the decomposition of H_2CO_3 into H^+ and HCO_3^- as shown in reaction 6.3. According to the definition of K_1 as shown in Eq. 6.6, the pH can be obtained as:

$$pH = pK_1 + \log[HCO_3^-] \; - \; \log[H_2CO_3^*] \qquad (6.21)$$

Replacing the $[H_2CO_3^*]$ with $P(CO_2)$ using Henry's law as shown in Eq. 6.20, and using pK_1 = 6.35, κ = 0.035, the pH can be calculated as:

$$pH = 7.81 + \log[HCO_3^-] \; - \; \log P(CO_2) \qquad (6.22)$$

If started calculating the pH from reaction 6.12 or 6.13, which represented the equilibrium of $KHCO_3$ solutions under or without CO_2 bubbling, the same equation was derived. Assuming the pressure of CO_2 was 3.95×10^{-4} and 1 atm before and under bubbling, respectively, and using the experimental data of $[HCO_3^-]$ shown in Fig. 6.5, the pHs of 0.1 and 0.5 mol L^{-1} $KHCO_3$ under bubbling can be calculated to be 6.84 and 7.52, respectively. These were very close to our measured pHs (6.97 and 7.60), which suggested that a thermodynamic equilibrium was almost achieved under the CO_2 bubbling until the pH remained unchanged. However, the calculated pHs of 0.1 and 0.5 mol L^{-1} $KHCO_3$ before bubbling should be 10.24 and 10.92 respectively, which were totally disagree with the experiment results (both about 8.3). This suggested that the fresh made $KHCO_3$ solution was far from equilibrium. OH^- would generate to increase the pH according to reaction 6.13.

6.8 Summary

The effect of the CO_2 bubbling into different solutions, such as $KHCO_3$, KCl and K_2CO_3, on the pH, TC and carbonaceous equilibrium in the aqueous solutions were studied. The concentration of different carbonaceous species (CO_2, H_2CO_3, HCO_3^-, CO_3^{2-}) in typical solutions before and after bubbling with CO_2 were examined and calculated. The reason why low concentration $KHCO_3$ solution could promote the CO_2 reduction was also discussed. Summaries of these results were given as follow:

1. CO_2 bubbling decreased the pH of all the electrolytes except HCl, in which the pH remained unchanged. The CO_2 bubbling induced pH decrease in $KHCO_3$, KCl and KOH was much faster than in K_2CO_3. The pH drop quickly saturated within 10 min in $KHCO_3$, KCl and KOH, while it took 120 min in K_2CO_3. This was probably because the reaction between CO_2

and CO_3^{2-} was a slow process.

2. The existence of the dissolved carbonaceous species changes as $CO_3^{2-} \rightarrow HCO_3^- \rightarrow H_2CO_3^*$ with decreasing pH. The CO_3^{2-} is the dominant species at pH above 12. The HCO_3^- becomes the major anion when the pH ranges from 7.5 to 9. There is only $H_2CO_3^*$ when the pH is below 5.

3. The $[H_2CO_3^*]$ increased from 33 to 45 mmol L^{-1} in the CO_2 saturated $KHCO_3$ solutions with the concentration from 0.1 to 1.5 mol L^{-1}. However, the $[H_2CO_3^*]$/TC ratio decreased from 23.6% to 2.8% as the $KHCO_3$ concentration increasing from 0.1 to 1.5 mol/L. This probably because high concentration of HCO_3^- contained in high concentration $KHCO_3$ solution before bubbling reduces the CO_2 absorption ability.

4. Experimental results suggested that low concentration (0.1 mol/L) $KHCO_3$ electrolyte promoting the CO_2 reduction was probably because low concentration (0.1 mol/L) $KHCO_3$ contained high $[H_2CO_3^*]$/TC ratio.

5. CO_2 bubbling changes the anion composition and concentration in the electrolytes. The solutions of KOH and K_2CO_3 changed into CO_2 saturated $KHCO_3$ after CO_2 bubbling.

6. Solubility of CO_2 in water was improved tremendously from 0.0135 to 36 mmol/L under CO_2 bubbling due to the increased CO_2 partial pressure, which is in accordance with Henry's law.

7. $KHCO_3$, KOH and KCl solutions are suitable electrolytes for the electrochemical reduction of CO_2 from the viewpoint of a high ratio of active reactant.

8 Thermodynamic study showed that the $KHCO_3$ solution reached the equilibrium when pH remained steady under CO_2 bubbling. However, fresh made $KHCO_3$ is far from equilibrium.

Chapter 7

Conclusions

7.1 Purpose of this research

This study was set out to confirm the active species in the electrochemical reduction of CO_2, and examine the effect of CO_2 bubbling into different aqueous solutions on the electrochemical CO_2 reduction. The reasons and motivations for this research are trying to help understanding the reaction mechanism of electrochemical CO_2 reduction and then improve the CO_2 reduction efficiency. To fulfill these targets, this dissertation mainly aimed to solve three questions as below:

1. Is HCO_3^- or CO_2 the active species in the electrochemical reduction of HCO_3^- solutions without CO_2 bubbling?

2. What is the best electrolyte for electrochemical CO_2 reduction and why?

3. How much active species exist in different electrolytes and how does CO_2 bubbling affect it?

7.2 Summary of the main findings

The experiments in this dissertation were carried out step by step to solve the questions above. Question 1 was solved in chapter 3 and 4 by examining the I-V characteristics, gas and liquid products during the electrochemical reactions, and gas production from the decomposition of HCO_3^-. Chapter 5 worked out the first half of question 2 (What is the best electrolyte for electrochemical CO_2 reduction) by analyzing the gas products under various experimental conditions. The second half of question 2 and question 3 were together solved in chapter 6 by determining the dissolved CO_2 concentration in different solutions using total carbon concentration (TOC) analyzer. The answers to the questions and main findings in this dissertation are summarized as below:

1. Is HCO_3^- or CO_2 the active species in the electrochemical reduction of HCO_3^- solutions without CO_2 bubbling?

a. The active species in the electrochemical reduction of HCO_3^- solutions is probably CO_2, which comes from the decomposition of HCO_3^- as: HCO_3^- (aq) $\rightleftarrows CO_2$ (aq) $+$ OH^- (aq).

Although the reaction order cannot be determined from the experimental data, if assuming this reaction is a one order reaction, the activation energy of this reaction is calculated to be 62.5 kJ/mol according to the experimental data.

b. CO, CH_4, and C_2H_4 were the main CO_2 reduction products found in the gas phase, however, H_2 production was much higher than the CO, CH_4, and C_2H_4 production. There was no HCOOH detected in the liquid sample.

c. Elevated temperature (60 ^{o}C) strongly promoted the decomposition of HCO_3^- into CO_2. Although increasing HCO_3^- concentration also enhanced the HCO_3^- decomposition, it was much less effective than elevating the temperature.

2. What is the best electrolyte for electrochemical CO_2 reduction and why?

a. 0.1 mol/L KOH should be the best electrolyte for electrochemical CO_2 reduction.

b. The reason is probably the high ratio of dissolved CO_2 to total carbon concentration ($[H_2CO_3^*]$/TC) in 0.1 mol/L KOH promoted the CO_2 reduction and inhibited the H_2 evolution.

c. 0.1 mol/L KOH actually transformed to 0.1 mol/L $KHCO_3$ after CO_2 bubbling. Although the faradaic efficiencies of CO_2 reduction were similar in 0.1 mol/L $KHCO_3$ and KOH, the current density obtained in KOH was *ca* 1.1 times higher than that obtained in $KHCO_3$. This is probably caused by the pH difference between WE and CE chambers after CO_2 bubbling.

d. The highest CO_2 reduction faradaic efficiency obtained in this research was 55.1% with a current density of 30.9 mA/cm^2. The energy conversion efficiency of CO_2 reduction was 6.4%, and the total energy conversion efficiency of CO_2 reduction and H_2 evolution was 13.9%.

e. The optimum reaction condition for obtaining the highest CO_2 reduction faradaic efficiency in $KHCO_3$ was: electrochemical reduction of CO_2 in 0.1 mol/L $KHCO_3$ at 25 ^{o}C and -2.1 V for 40 min with CO_2 bubbling rate of 17.7 mL/min and stirring rate of 1000 rpm.

3. How much active species exist in different electrolytes and how does CO_2 bubbling affect it?

a. $[H_2CO_3^*]$ in 0.1 mol/L $KHCO_3$ was 0.51 and 33.24 mmol/L before and after CO_2 bubbling, respectively. $[H_2CO_3^*]/TC$ in 0.1 mol/L $KHCO_3$ was 23.6%, and it decreased with the increase in $KHCO_3$ concentration.

b. The dissolved CO_2 concentration ($[H_2CO_3^*]$) in different solutions was controlled by the Henry's law and pH of the solutions.

c. CO_2 bubbling increased the partial pressure of CO_2 and then promoted the solubility of CO_2. CO_2 bubbling also decreased the pH of the solutions and then affected the carbonate equilibrium in the solutions.

7.3 Achievements compared with others' works

As discussed in the introduction chapter, Hori el al. reported that the CO_2 generated from the decomposition of HCO_3^- should be the active species in the electrochemical reduction of HCO_3^- without CO_2 bubbling [83]. This dissertation confirmed this statement, and further observed the CO_2 generation from the decomposition of HCO_3^- and calculated the activation energy of this reaction. CO, CH_4, and C_2H_4 were generated in this dissertation, which haven't been reported before. However, HCOOH was not observed in this research. The possibility of HCOOH (or formate) directly reduced from HCO_3^- as reported by Koper [84] and Kokoh [67] cannot be excluded from this research.

Hori et al reported that the electrolyte concentration had an important effect on the CO_2 reduction, but did not explain the detailed reason [54]. This dissertation further studied the effect of electrolyte concentration on the CO_2 reduction in more details and explained the possible reason.

Although the CO_2 reduction faradaic efficiency in this dissertation (55.1%) was lower than the reported data (81.1%) [54], a much higher CO_2 reduction current density of 17.0 mA/cm^2 was achieved, which was rarely reported before in the electrochemical reduction of CO_2 on metal electrodes in aqueous solutions under atmospheric pressure.

This dissertation also determined the concentration of the dissolved CO_2 in different solutions after CO_2 bubbling, which haven't been reported before. These data can be used for further study of the CO_2 conversion efficiency and reaction rate calculation.

7.4 Limitations in this dissertation and recommendations for future research

The CO_2 reduction faradaic efficiency and energy conversion efficiency obtained in this dissertation were not high. This was probably caused by high over potential of CO_2 reduction and high resistance of the electrochemical cell, the detailed reason needs to be studied. The total faradaic efficiency of CO_2 reduction and H_2 evolution obtained in the optimum conditions for yielding the highest CO_2 reduction faradaic efficiency was only *ca* 77%, which was less than 100%. The reason should be further examined. When Cu foil used as the working electrode instead of Cu wire, although the CO_2 reduction faradaic efficiency did not vary too much, the H_2 evolution faradaic efficiency increased and the current density decreased. It possibly caused by the CO_2 mass transfer limitation, however, detailed studies should be further conducted.

7.5 Conclusion

Ratio of dissolved CO_2 concentration to total carbon concentration ($[H_2CO_3^*]$/TC) in aqueous solutions is a more important factor than the dissolved CO_2 concentration ($[H_2CO_3^*]$) to affect CO_2 reduction. High $[H_2CO_3^*]$/TC can promote the CO_2 reduction. Decrease the pH can effectively increase the $[H_2CO_3^*]$/TC. However, low pH would lead to a high H_2 evolution. Therefore, the balance between the pH and $[H_2CO_3^*]$/TC in the aqueous solutions needs to be carefully controlled to promote the CO_2 reduction.

References

1. BP, BP Statistical review of world energy 2014, *Availabe at:* *http://www.bp.com/en/global/corporate/about-bp/energy-economics/statistical-review-of-world-energy.html*.

2. P. Mann, L. Gahagan and M. B. Gordon. Tectonic setting of the world's giant oil and gas fields. In *Giant Oil and Gas Fields of the Decade, 1990-1999*; M. T. Halbouty, Ed.; American Association of Petroleum Geologists, 2003.

3. G. W. Team, *Global Energy Assessment: Toward a Sustainable Future* (Cambridge University Press, Cambridge, UK & New York, NY, USA and IIASA, Laxenburg, Austria, 2012).

4. G. Bala, K. Caldeira, A. Mirin, M. Wickett and C. Delire, Multiceutury Changes to the Global Climate and Carbon Cycle: Results from a Coupled Climate and Carbon Cycle Model, *J. Clim.* **18**, 4531-4544 (2005).

5. S. Solomon, G. K. Plattner, R. Knutti and P. Friedlingstein, Irreversible Climate Change Due to Carbon Dioxide Emissions, *Proc. Natl. Acad. Sci. U. S. A.* **106**, 1704-1709 (2009).

6. F. R. Pazheri, M. F. Othman and N. H. Malik, A review on global renewable electricity scenario, *Renew. Sust. Energ. Rev.* **31**, 835-845 (2014).

7. P. Forster, V. Ramaswamy, P. Artaxo, T. Berntsen, R. Betts, D. W. Fahey, J. Haywood, J. Lean, D. C. Lowe, G. Myhre, J. Nganga, R. Prinn, G. Raga, M. Schulz and R. V. Dorland, in *Climate Change 2007: The Physical Science Basis. Contribution of Working Group I to the Fourth Assessment Report of the Intergovernmental Panel on Climate Change*, edited by S. Solomon, D. Qin, M. Manning, Z. Chen, M. Marquis, K. B. Averyt, M. Tignor and H. L. Miller (Cambridge University Press, Cambridge, United Kingdom and New York, NY, USA, 2007).

8. U. Cubasch, D. Wuebbles, D. Chen, M. C. Facchini, D. Frame, N. Mahowald and J.-G. Winther, in *Climate Change 2013: The Physical Science Basis. Contribution of Working Group I to the Fifth Assessment Report of the Intergovernmental Panel on Climate Change*, edited by T. F. Stocker, D. Qin, G.-K. Plattner, M. Tignor, S. K. Allen, J. Boschung, A. Nauels, Y. Xia, V. Bex and P. M. Midgley (Cambridge University Press, Cambridge, United Kingdom and New York, NY, USA, 2013).

9. M. M. Abu-Khader, Recent advances in nuclear power: A review, *Prog. Nucl. Energy* **51**, 225-235 (2009).

10. P. Moriarty and D. Honnery, What is the global potential for renewable energy?, *Renew. Sust. Energ. Rev.* **16**, 244-252 (2012).

11. in *Popular Mechanics* (1952), Vol. 97, pp. 105.

12. A. Demirbas, Progress and recent trends in biofuels, *Prog. Energy Combust. Sci.* **33**, 1-18 (2007).

13. S. Akhtari, T. Sowlati and K. Day, Economic feasibility of utilizing forest biomass in district energy systems - A review, *Renew. Sust. Energ. Rev.* **33**, 117-127 (2014).

14. P. Kalyani and A. Anitha, Biomass carbon & its prospects in electrochemical energy systems, *Int. J. Hydrog. Energy* **38**, 4034-4045 (2013).

15. R. Sternberg, Hydropower's future, the environment, and global electricity systems, *Renew. Sust. Energ. Rev.* **14**, 713-723 (2010).

16. R. Sternberg, Hydropower: Dimensions of social and environmental coexistence, *Renew. Sust. Energ. Rev.* **12**, 1588-1621 (2008).

17. M. Z. Jacobson and M. A. Delucchi, A Plan to Power 100 per cent of the Planet with Renewables, *Scientific American*, (2009).

18. REN21, *Renewables 2012 Global Status Report*. (REN21 Secretariat, Paris, 2012).

19. X. J. Sun, D. G. Huang and G. Q. Wu, The current state of offshore wind energy technology development, *Energy* **41**, 298-312 (2012).

20. G. R. Timilsina, L. Kurdgelashvili and P. A. Narbel, Solar energy: Markets, economics and policies, *Renew. Sust. Energ. Rev.* **16**, 449-465 (2012).

21. K. F. Fong, C. K. Lee, T. T. Chow, Z. Lin and L. S. Chan, Solar hybrid air-conditioning system for high temperature cooling in subtropical city, *Renew. Energy* **35**, 2439-2451 (2010).

22. S. Sadhishkumar and T. Balusamy, Performance improvement in solar water heating systems-A review, *Renew. Sust. Energ. Rev.* **37**, 191-198 (2014).

23. REN21, *Renewables 2014 Global Status Report - Key Findings*. (2014).

24. V. V. Tyagi, N. A. A. Rahim, N. A. Rahim and J. A. L. Selvaraj, Progress in solar PV technology: Research and achievement, *Renewable and Sustainable Energy Reviews* **20**, 443-461 (2013).

25. B. J. M. de Vries, D. P. van Vuuren and M. M. Hoogwijk, Renewable energy sources: Their global potential for the first-half of the 21st century at a global level: An integrated approach, *Energy Policy* **35**, 2590-2610 (2007).

26. B. Dunn, H. Kamath and J. M. Tarascon, Electrical Energy Storage for the Grid: A Battery of Choices, *Science* **334**, 928-935 (2011).

27. A. Poullikkas, A comparative overview of large-scale battery systems for electricity storage, *Renew. Sust. Energ. Rev.* **27**, 778-788 (2013).

28. A. Midilli, M. Ay, I. Dincer and M. A. Rosen, On hydrogen and hydrogen energy strategies: I: current status and needs, *Renewable and Sustainable Energy Reviews* **9**, 255-271 (2005).

29. http://en.wikipedia.org/wiki/Electrolysis_of_water.

30. M. Carmo, D. L. Fritz, J. Merge and D. Stolten, A Comprehensive Review on PEM Water Electrolysis, *Int. J. Hydrog. Energy* **38**, 4901-4934 (2013).

31. K. Mazloomi, N. B. Sulaiman and H. Moayedi, Electrical Efficiency of Electrolytic Hydrogen Production, *Int. J. Electrochem. Sci.* **7**, 3314-3326 (2012).

32. K. Fujii, S. Nakamura, M. Sugiyama, K. Watanabe, B. Bagheri and Y. Nakano, Characteristics of hydrogen generation from water splitting by polymer electrolyte electrochemical cell directly connected with concentrated photovoltaic cell, *Int. J. Hydrog. Energy* **38**, 14424-14432 (2013).

33. A. Fujishima and K. Honda, Electrochemical photolysis of water at a semiconductor electrode, *Nature* **238**, 37-+ (1972).

34. O. Khaselev and J. A. Turner, A Monolithic Photovoltaic-Photoelectrochemical Device for Hydrogen Production via Water Splitting, *Science* **280**, 425-427 (1998).

35. A. Kudo and Y. Miseki, Heterogeneous photocatalyst materials for water splitting, *Chem.*

Soc. Rev. **38**, 253-278 (2009).

36. N. S. Spinner, J. A. Vega and W. E. Mustain, Recent progress in the electrochemical conversion and utilization of CO2, *Catal. Sci. Technol.* **2**, 19-28 (2012).

37. B. Kumar, M. Llorente, J. Froehlich, T. Dang, A. Sathrum and C. P. Kubiak, Photochemical and Photoelectrochemical Reduction of CO_2, *Annu. Rev. Phys. Chem.* **63**, 541-569 (2012).

38. J. L. Qiao, Y. Y. Liu, F. Hong and J. J. Zhang, A Review of Catalysts for the Electroreduction of Carbon Dioxide to Produce Low-Carbon Fuels, *Chem. Soc. Rev.* **43**, 631-675 (2014).

39. I. Taniguchi, B. Aurian-Blajeni and J. O. M. Bockris, The reduction of carbon dioxide at illuminated p-type semiconductor electrodes in nonaqueous media, *Electrochimica Acta* **29**, 923-932 (1984).

40. K. Hirota, D. A. Tryk, T. Yamamoto, K. Hashimoto, M. Okawa and A. Fujishima, Photoelectrochemical reduction of CO_2 in a high-pressure CO_2 plus methanol medium at p-type semiconductor electrodes, *J. Phys. Chem. B* **102**, 9834-9843 (1998).

41. K. Hirota, D. A. Tryk, T. Yamamoto, K. Hashimoto, M. Okawa and A. Fujishima, Photoelectrochemical Reduction of CO_2 in a High-Pressure CO_2 + Methanol Medium at p-Type Semiconductor Electrodes, *The Journal of Physical Chemistry B* **102**, 9834-9843 (1998).

42. Y. Taniguchi, H. Yoneyama and H. Tamura, Photo-electrochemical reduction of carbon-dioxide at para-type gallium-phosphide electrodes in the presence of crown ether, *Bulletin of the Chemical Society of Japan* **55**, 2034-2039 (1982).

43. S. Ikeda, A. Yamamoto, H. Noda, M. Maeda and K. Ito, Influence of surface-treatment of the p-GaP photocathode on the photoelectrochemical reduction of carbon-dioxide, *Bulletin of the Chemical Society of Japan* **66**, 2473-2477 (1993).

44. S. Kaneco, H. Katsumata, T. Suzuki and K. Ohta, Photoelectrochemical reduction of carbon dioxide at p-type gallium arsenide and p-type indium phosphide electrodes in methanol, *Chemical Engineering Journal* **116**, 227-231 (2006).

45. S. Kaneco, H. Katsumata, T. Suzuki and K. Ohta, Photoelectrocatalytic reduction of CO_2 in LiOH/methanol at metal-modified p-InP electrodes, *Applied Catalysis B: Environmental* **64**, 139-145 (2006).

46. J. O. M. Bockris and J. C. Wass, On the photoelectrocatalytic reduction of carbon dioxide, *Materials Chemistry and Physics* **22**, 249-280 (1989).

47. J. Hawecker, J.-M. Lehn and R. Ziessel, Photochemical and Electrochemical Reduction of Carbon Dioxide to Carbon Monoxide Mediated by (2,2′-Bipyridine)tricarbonylchlororhenium(I) and Related Complexes as Homogeneous Catalysts, *Helvetica Chimica Acta* **69**, 1990-2012 (1986).

48. B. Kumar, J. M. Smieja and C. P. Kubiak, Photoreduction of CO_2 on p-type Silicon Using Re(bipy-Bu')(CO)$_3$Cl: Photovoltages Exceeding 600 mV for the Selective Reduction of CO_2 to CO, *J. Phys. Chem. C* **114**, 14220-14223 (2010).

49. E. E. Barton, D. M. Rampulla and A. B. Bocarsly, Selective Solar-Driven Reduction Of CO_2 to Methanol Using a Catalyzed P-Gap Based Photoelectrochemical Cell, *J. Am. Chem. Soc.* **130**, 6342-6344 (2008).

50. J. L. Yuan and C. J. Hao, Solar-driven photoelectrochemical reduction of carbon dioxide

to methanol at CuInS2 thin film photocathode, *Solar Energy Materials and Solar Cells* **108**, 170-174 (2013).

51. M. E. Royer, *C.R. Acad. Sci.* **70**, 731 (1870).

52. http://en.wikipedia.org/wiki/Electrochemical_reduction_of_carbon_dioxide.

53. J. P. Collin and J. P. Sauvage, Electrochemical reduction of carbon-dioxide mediated by molecular catalysts, *Coordination Chemistry Reviews* **93**, 245-268 (1989).

54. Y. Hori, A. Murata and R. Takahashi, Formation of Hydrocarbons in the Electrochemical Reduction of Carbon Dioxide at a Copper Electrode in Aqueous Solution, *J. Chem. Soc., Faraday Trans. 1* **85**, 2309-2326 (1989).

55. Y. Hori and S. Suzuki, Electrolytic Reduction of Carbon Dioxide at Mercury Electrode in Aqueous Solution, *B Chem. Soc. Jpn.* **55**, 660-665 (1982).

56. K. W. Frese and S. Leach, Electrochemical Reduction of Carbon Dioxide to Methane, Methanol, and CO on Ru Electrodes, *J. Electrochem. Soc.* **132**, 259-260 (1985).

57. K. W. Frese and D. Canfield, Reduction of CO_2 on n-GaAs electrodes and selective methanol synthesis, *J. Electrochem. Soc.* **131**, 2518-2522 (1984).

58. J. Ryu, T. N. Andersen and H. Eyring, Electrode reduction kinetics of carbon dioxide in aqueous solution, *The Journal of Physical Chemistry* **76**, 3278-3286 (1972).

59. Y. Hori. Electrochemical CO_2 Reduction on Metal Electrodes. In *Modern Aspects of Electrochemistry*; C. Vayenas, R. White and M. Gamboa-Aldeco, Eds.; Springer New York, 2008; Vol. 42; pp 89-189.

60. R. J. Lim, M. S. Xie, M. A. Sk, J. M. Lee, A. Fisher, X. Wang and K. H. Lim, A review on the electrochemical reduction of CO2 in fuel cells, metal electrodes and molecular catalysts, *Catalysis Today* **233**, 169-180 (2014).

61. M. Mikkelsen, M. Jorgensen and F. C. Krebs, The teraton challenge. A review of fixation and transformation of carbon dioxide, *Energ Environ. Sci.* **3**, 43-81 (2010).

62. M. Gattrell, N. Gupta and A. Co, A Review of the Aqueous Electrochemical Reduction of CO_2 to Hydrocarbons at Copper, *J Electroanal. Chem.* **594**, 1-19 (2006).

63. W. Wang, S. P. Wang, X. B. Ma and J. L. Gong, Recent advances in catalytic hydrogenation of carbon dioxide, *Chem. Soc. Rev.* **40**, 3703-3727 (2011).

64. G. Centi and S. Perathoner, Opportunities and prospects in the chemical recycling of carbon dioxide to fuels, *Catalysis Today* **148**, 191-205 (2009).

65. J. L. Qiao, P. Jiang, J. S. Liu and J. J. Zhang, Formation of Cu nanostructured electrode surfaces by an annealing-electroreduction procedure to achieve high-efficiency CO2 electroreduction, *Electrochem. Commun.* **38**, 8-11 (2014).

66. D. P. Summers, S. Leach and K. W. Frese, The electrochemical reduction of aqueous carbon-dioxide to methanol at molybdenum electrodes with low overpotentials, *Journal of Electroanalytical Chemistry* **205**, 219-232 (1986).

67. B. Innocent, D. Pasquier, F. Ropital, F. Hahn, J. M. Leger and K. B. Kokoh, FTIR spectroscopy study of the reduction of carbon dioxide on lead electrode in aqueous medium, *Appl. Catal. B-Environ.* **94**, 219-224 (2010).

68. M. R. Thorson, K. I. Siil and P. J. A. Kenis, Effect of Cations on the Electrochemical Conversion of CO2 to CO, *J. Electrochem. Soc.* **160**, F69-F74 (2013).

69. A. Schizodimou and G. Kyriacou, Acceleration of the reduction of carbon dioxide in the presence of multivalent cations, *Electrochimica Acta* **78**, 171-176 (2012).

70. S. Ikeda, T. Takagi and K. Ito, Selective formation of formic-acid, oxalic-acid, and carbon-monoxide by electrochemical reduction of carbon-dioxide, *Bulletin of the Chemical Society of Japan* **60**, 2517-2522 (1987).

71. G. Y. Zhao, T. Jiang, B. X. Han, Z. H. Li, J. M. Zhang, Z. M. Liu, J. He and W. Z. Wu, Electrochemical reduction of supercritical carbon dioxide in ionic liquid 1-n-butyl-3-methylimidazolium hexafluorophosphate, *J. Supercrit. Fluids* **32**, 287-291 (2004).

72. S. Kaneco, K. Iiba, H. Katsumata, T. Suzuki and K. Ohta, Electrochemical reduction of high pressure carbon dioxide at a Cu electrode in cold methanol with CsOH supporting salt, *Chemical Engineering Journal* **128**, 47-50 (2007).

73. S. Kaneco, K. Iiba, H. Katsumata, T. Suzuki and K. Ohta, Electrochemical reduction of high pressure CO2 at a Cu electrode in cold methanol, *Electrochimica Acta* **51**, 4880-4885 (2006).

74. T. Saeki, K. Hashimoto, N. Kimura, K. Omata and A. Fujishima, Electrochemical reduction of CO2 with high current density in a CO_2 + methanol medium II. CO formation promoted by tetrabutylammonium cation, *Journal of Electroanalytical Chemistry* **390**, 77-82 (1995).

75. J. P. Jones, G. K. S. Prakash and G. A. Olah, Electrochemical CO_2 Reduction: Recent Advances and Current Trends, *Isr. J. Chem.* **54**, 1451-1466 (2014).

76. I. Ganesh, Conversion of carbon dioxide into methanol - a potential liquid fuel: Fundamental challenges and opportunities (a review), *Renew. Sust. Energ. Rev.* **31**, 221-257 (2014).

77. Y. Chen, C. W. Li and M. W. Kanan, Aqueous CO_2 Reduction at Very Low Overpotential on Oxide-Derived Au Nanoparticles, *J. Am. Chem. Soc.* **134**, 19969-19972 (2012).

78. C. W. Li and M. W. Kanan, CO_2 Reduction at Low Overpotential on Cu Electrodes Resulting from the Reduction of Thick Cu_2O Films, *J. Am. Chem. Soc.* **134**, 7231-7234 (2012).

79. S. Zhang, P. Kang and T. J. Meyer, Nanostructured Tin Catalysts for Selective Electrochemical Reduction of Carbon Dioxide to Formate, *J. Am. Chem. Soc.* **136**, 1734-1737 (2014).

80. K. J. P. Schouten, Y. Kwon, C. J. M. van der Ham, Z. Qin and M. T. M. Koper, A new mechanism for the selectivity to C1 and C2 species in the electrochemical reduction of carbon dioxide on copper electrodes, *Chemical Science* **2**, 1902-1909 (2011).

81. K. J. P. Schouten, E. P. Gallent and M. T. M. Koper, The influence of pH on the reduction of CO and CO2 to hydrocarbons on copper electrodes, *Journal of Electroanalytical Chemistry* **716**, 53-57 (2014).

82. R. P. S. Chaplin and A. A. Wragg, Effects of process conditions and electrode material on reaction pathways for carbon dioxide electroreduction with particular reference to formate formation, *J. Appl. Electrochem.* **33**, 1107-1123 (2003).

83. Y. Hori and S. Suzuki, Electrolytic Reduction of Bicarbonate Ion at a Mercury-Electrode, *J. Electrochem. Soc.* **130**, 2387-2390 (1983).

84. R. Kortlever, K. H. Tan, Y. Kwon and M. T. M. Koper, Electrochemical carbon dioxide and bicarbonate reduction on copper in weakly alkaline media, *J Solid State Electrochem* **17**, 1843-1849 (2013).

85. Y. H. Chen and M. W. Kanan, Tin Oxide Dependence of the CO_2 Reduction Efficiency on Tin Electrodes and Enhanced Activity for Tin/Tin Oxide Thin-Film Catalysts, *J. Am. Chem. Soc.* **134**, 1986-1989 (2012).

86. M. R. Goncalves, A. Gomes, J. Condeco, T. R. C. Fernandes, T. Pardal, C. A. C. Sequeira and J. B. Branco, Electrochemical Conversion of CO_2 to C_2 Hydrocarbons Using Different ex situ Copper Electrodeposits, *Electrochim. Acta* **102**, 388-392 (2013).

87. M. Le, M. Ren, Z. Zhang, P. T. Sprunger, R. L. Kurtz and J. C. Flake, Electrochemical Reduction of CO_2 to CH_3OH at Copper Oxide Surfaces, *J. Electrochem. Soc.* **158**, E45-E49 (2011).

88. S. Kaneco, H. Hiei, Y. Xing, H. Katsumata, H. Ohnishi, T. Suzuki and K. Ohta, Electrochemical conversion of carbon dioxide to methane in aqueous NaHCO3 solution at less than 273 K, *Electrochimica Acta* **48**, 51-55 (2002).

89. J. J. Kim, D. P. Summers and K. W. Frese, Reduction of CO_2 and CO to methane on Cu foil electrodes, *Journal of Electroanalytical Chemistry* **245**, 223-244 (1988).

90. J. Qu, X. Zhang, Y. Wang and C. Xie, Electrochemical reduction of CO_2 on RuO_2/TiO_2 nanotubes composite modified Pt electrode, *Electrochimica Acta* **50**, 3576-3580 (2005).

91. R. Zeebe and D. Wolf-Gladrow, *CO_2 in Seawater: Equilibrium, Kinetics, Isotopes.* (Elsevier Science, Amsterdam, Netherlands, 2001).

92. D. R. Lide. CRC Handbook of Chemistry and Physics (90th Edition); D. R. Lide, Ed.; CRC Press: Boca Raton, Florida, 2009.

93. A. J. Bard and L. R. Faulkner, *Electrochemical Methods: Fundamentals and Applications.* (Wiley, 2000).

94. P. Atkins and J. de Paula, *Physical Chemistry.* (Oxford University Press, Great Britain, 2010).

95. J. A. Dean, *Lange's Handbook of Chemistry.* (McGraw-Hill, Inc., New York, USA, 1998).

96. M. Binnewies and E. Milke, *Thermochemical Data of Elements and Compounds.* (Wiley-VCH Verlag GmbH, Weinheim, Germany, 2002).

97. K. P. Kuhl, E. R. Cave, D. N. Abram and T. F. Jaramillo, New insights into the electrochemical reduction of carbon dioxide on metallic copper surfaces, *Energ Environ. Sci.* **5**, 7050-7059 (2012).

98. Y. H. Chen, C. W. Li and M. W. Kanan, Aqueous CO_2 Reduction at Very Low Overpotential on Oxide-Derived Au Nanoparticles, *J. Am. Chem. Soc.* **134**, 19969-19972 (2012).

99. J. P. Popic, M. L. AvramovIvic and N. B. Vukovic, Reduction of carbon dioxide on ruthenium oxide and modified ruthenium oxide electrodes in 0.5 M $NaHCO_3$, *Journal of Electroanalytical Chemistry* **421**, 105-110 (1997).

100. Y. Hori, H. Konishi, T. Futamura, A. Murata, O. Koga, H. Sakurai and K. Oguma, "Deactivation of copper electrode" in electrochemical reduction of CO_2, *Electrochimica Acta* **50**, 5354-5369 (2005).

101. S. Ikeda, K. Ito and H. Noda, Electrochemical Reduction Of Carbon Dioxide Using Gas Diffusion Electrodes Loaded With Fine Catalysts, *AIP Conference Proceedings* **1136**, 108-113 (2009).

102. 村田 暁, 二酸化炭素の電気化学還元, 千葉大学, 1991 (in Japanese).

103. H. Li, P. H. Opgenorth, D. G. Wernick, S. Rogers, T.-Y. Wu, W. Higashide, P. Malati, Y.-X. Huo, K. M. Cho and J. C. Liao, Integrated Electromicrobial Conversion of CO_2 to Higher Alcohols, *Science* **335**, 1596 (2012).

104. Y. Chen and M. W. Kanan, Tin Oxide Dependence of the CO_2 Reduction Efficiency on Tin Electrodes and Enhanced Activity for Tin/Tin Oxide Thin-Film Catalysts, *J. Am. Chem. Soc.* **134**, 1986-1989 (2012).

105. B. A. Rosen, A. Salehi-Khojin, M. R. Thorson, W. Zhu, D. T. Whipple, P. J. A. Kenis and R. I. Masel, Ionic Liquid–Mediated Selective Conversion of CO_2 to CO at Low Overpotentials, *Science* **334**, 643-644 (2011).

106. Y. Izumi, Recent Advances in the Photocatalytic Conversion of Carbon Dioxide to Fuels with Water and/or Hydrogen Using Solar Energy and Beyond, *Coord. Chem. Rev.* **257**, 171-186 (2013).

107. S. Bensaid, G. Centi, E. Garrone, S. Perathoner and G. Saracco, Towards Artificial Leaves for Solar Hydrogen and Fuels from Carbon Dioxide, *ChemSusChem* **5**, 500-521 (2012).

108. M. R. Hoffmann, J. A. Moss and M. M. Baum, Artificial photosynthesis: semiconductor photocatalytic fixation of CO_2 to afford higher organic compounds, *Dalton Transactions* **40**, 5151-5158 (2011).

109. R. Beranek, (Photo)electrochemical Methods for the Determination of the Band Edge Positions of TiO_2-Based Nanomaterials, *Advances in Physical Chemistry* **2011**, 20 (2011).

110. S. C. Roy, O. K. Varghese, M. Paulose and C. A. Grimes, Toward Solar Fuels: Photocatalytic Conversion of Carbon Dioxide to Hydrocarbons, *ACS Nano* **4**, 1259-1278 (2010).

111. J. J. Carroll, J. D. Slupsky and A. E. Mather, The Solubility of Carbon Dioxide in Water at Low Pressure, *J. Phys. Chem. Ref. Data* **20**, 1201-1209 (1991).

112. W. L. Zhu, R. Michalsky, O. Metin, H. F. Lv, S. J. Guo, C. J. Wright, X. L. Sun, A. A. Peterson and S. H. Sun, Monodisperse Au Nanoparticles for Selective Electrocatalytic Reduction of CO_2 to CO, *J. Am. Chem. Soc.* **135**, 16833-16836 (2013).

List of publications and conference presentations

Journal papers:

1. <u>Heng Zhong</u>, Katsushi Fujii, Yoshiaki Nakano and Fangming Jin. Effect of CO_2 bubbling into aqueous solutions used for electrochemical reduction of CO_2 for energy conversion and storage, *J. Phys. Chem. C*, **2015**, 119 (1), 55–61.

2. <u>Heng Zhong</u>, Katsushi Fujii, and Yoshiaki Nakano. Study of the active reactant in the electrochemical reduction of $KHCO_3$ without CO_2 bubbling, submitted.

3. <u>Heng Zhong,</u> Ying Gao, Guodong Yao, Xu Zeng, Qiuju Li, Zhibao Huo, Fangming Jin. Highly efficient hydrothermal water splitting and CO_2 reduction into formic acid with common Fe and Cu powder, Submitted.

Conference proceedings:

1. <u>Heng Zhong</u>, Katsushi Fujii and Yoshiaki Nakano. Effect of $KHCO_3$, K_2CO_3 and CO_2 on the electrochemical reduction of CO_2 into organics on a Cu electrode for the solar energy conversion and storage. *MRS Proceedings*, 2014, 1640, DOI: http://dx.doi.org/10.1557/opl.2014.404.

Conference presentations:

1. <u>Heng Zhong</u>, Fangming Jin, Xu Zeng, Ying Gao and Katsushi Fujii. Highly efficient reduction of $NaHCO_3$ and water into HCOOH with the use of Fe reductant and Cu catalyst under hydrothermal conditions. International Workshop "SolChES 2012", W-1-5, July 2012, Sendai, Japan.

2. <u>Heng Zhong</u>, Katsushi Fujii and Yoshiaki Nakano. Electrochemical reduction of $KHCO_3$ and $NaHCO_3$ using Cu electrode for the energy conversion and storage. The 74th JSAP Autumn Meeting, 17a-P4-5, September **2013**, Kyoto, Japan.

3. <u>Heng Zhong</u>, Katsushi Fujii, Masakazu Sugiyama and Yoshiaki Nakano. Effect of Carbonate and Bicarbonate on the Electrochemical Reduction of CO_2 into Organics for the Solar Energy Conversion and Storage. NMS-IX & FCFP-XXIII, P11, October **2013**, Shanghai, China.

4. <u>Heng Zhong</u>, Katsushi Fujii, and Yoshiaki Nakano. Effect of $KHCO_3$, K_2CO_3 and CO_2 on the Electrochemical Reduction of CO_2 into Organics on a Cu Electrode for the Solar Energy Conversion and Storage. *2013 MRS Fall Meeting*, Z10.52, December **2013**, Boston, USA.

5. <u>Heng Zhong</u>, Katsushi Fujii, Yoshiaki Nakano, and Fangming Jin. Study of the active reactant in the electrochemical reduction of CO_2 in bicarbonate aqueous solutions. *20th International Conference on Photochemical Conversion and Storage of Solar*

Energy, C2-4, July **2014**, Berlin, Germany.

6. <u>Heng Zhong</u>, Katsushi Fujii, and Yoshiaki Nakano. Study of the Active Species in the Electrochemical Reduction of CO_2 at Elevated Temperatures on a Cu Electrode for the Solar Energy Conversion and Storage. *2014 MRS Fall Meeting*, V5.33, December **2014**, Boston, USA.